I. THEORETICAL STUDIES OF PHOTOIONIZATION

II. THE ELECTRONIC STRUCTURE OF LINEAR POLYENES

Thesis by

Marco Antonio Chaer Nascimento

In Partial Fulfillment of the Requirements

For the Degree of

Doctor of Philosophy

California Institute of Technology

Pasadena, California

1978

(Submitted May 1, 1978)

"The man who is certain he is right is almost sure to be wrong, and he has the additional misfortune of inevitably remaining so."

Michael Faraday (1791-1867)

"Attempts to direct research toward results of possible applicability cannot lead to growth in science which is of much value...We shall see the authorities recoiling at various points from the destruction of wealth and culture caused by their attempts at total planning...Unless we fully reestablish man's right to pursue truth regardless of social interests...This generation will find, too late, that it has opened wide the pass to the barbarians."

Michael Polanyi (1891-1976)

I dedicate this work to my wife, Regina, and to my children Ricardo and Monica. Their love, support, understanding, and respect were a source of constant reassurance that I am something more than a simple part of a cold machine that has to be kept on going at any cost. For me, the best machines still are warm with a beating heart and full of sensitiveness.

ACKNOWLEDGMENTS

I would like to thank my family in Brasil for their constant moral and financial support. Without their help this work would never be completed.

I would like to thank my supervisor, Bill Goddard, for giving me the opportunity of working on projects of my own interest even if not directly related to his interests. Of course, his guidance during the course of these projects was essential for their completion. My interaction with him was almost always very stimulating and I learned a great deal from him.

My appreciation to all the members of our research group is also acknowledged, particularly to Barry Olafson and Marvin Goodgame.

ABSTRACT

Part I

The photoionization cross section is shown to be directly related to the imaginary part of the frequency dependent polarizability.

Using this relation, an approximate representation of the frequency-dependent polarizability is constructed from a discrete set of transition frequencies and oscillator strengths. This approximate representation is used in an analytical continuation for complex values of the frequency using a sequence of (N+J/N) Padé Approximants (with $J \geq -1$). Once the representation of the frequency-dependent polarizability in the upper half part of the complex plane is known, we can calculate its value along the real axis and consequently the photoionization cross section. The great advantage of the method resides on the fact that the use of a discrete representation for the dynamic polarizability explicitly avoids the use of continuum functions.

We have applied this method previously in the calculation of photoionization cross sections for the helium atom in its ground state and in the 2^1S and 2^3S metastable states. Calculations for the CO molecule are in progress.

Here we present calculations for the H^- atom. For this system we also computed the dynamic polarizability in the normal dispersion region. A study of the basis set dependence is also presented.

Part II

Self-consistent ab initio generalized valence bond (GVB) and configuration interaction (CI) calculations are presented for the ground states, valence and non-valence states, Rydberg states and π positive ion states of trans 1, 3-butadiene and all-trans 1, 3, 5-hexatriene molecules.

It is shown that the electronic spectra of these molecules can be rationalized in terms of a few valence excited states and a series of Rydberg states. The first singlet excited states of these molecules (1^1B_u) correspond to non-valence, non-vertical states.

It was found that to correctly describe the $1\,^1B_u$ and the $2\,^1A_g$ (valence) states of these molecules it is necessary to correlate not only the electrons of the π system but also the electrons of the $(C\text{-}C)_\sigma$ subspace.

It is also shown that the first two bands of the photoelectron spectrum (PE) of the butadiene molecule and the first three bands of the PE spectrum of hexatriene correspond to ionization out of the occupied π orbitals of these molecules.

Another important conclusion from our studies is that for this type of system, good quality GVB (n/PP) wavefunctions with the $2n\pi$ electrons correlated can be obtained by carrying out a Hartree-Fock calculation on the ground state followed by a GVB (n/PP) calculation on just the $2n\pi$ orbitals (keeping the σ HF space fixed). From this wavefunction accurate values for the transition energies of the valence states can be obtained. Work on all-trans 1, 3, 5, 7-octatetraene now in progress will provide a good test for this scheme.

TABLE OF CONTENTS

CHAPTER I

THEORETICAL STUDIES OF PHOTOIONIZATION

SECTION A

PRELIMINARIES

The basic idea of the approach is to explore the relation between the frequency dependent polarizability of a system and its photoionization cross section.

The frequency dependent polarizability is given by[1]

$$\alpha(\omega) = \sum_{n\neq 0} \frac{f_{on}}{\omega_{on}^2 - \omega^2} + \int_{\epsilon_I}^{\infty} \frac{g(\epsilon)\, d\epsilon}{\epsilon^2 - \omega^2} \tag{1}$$

where f_{on} and $g(\epsilon)$ are the oscillator strengths for the bound and continuum transitions, respectively, ω_{on} are the transition frequencies and ϵ_I the first ionization threshold. Extending (1) to complex frequencies,

$$\alpha(z) = \sum_{n\neq 0} \frac{f_{on}}{\omega_{on}^2 - z^2} + \int_{\epsilon_I}^{\infty} \frac{g(\epsilon)\, d\epsilon}{\epsilon^2 - z^2} \tag{2}$$

we see that the complex polarizability is analytical throughout the complex plane except for an infinite number of poles along the real axis (the ones in the positive part corresponding to the transition frequencies), and a branch cut in the photoionization interval $\epsilon_I \leq \mathrm{Re}(z) < \infty$.

To extract the real and imaginary parts of (2) we assume that $\alpha(z)$ is analytical also in the lower half plane for points very close to the real axis. Taking two points very close to the real axis, $z = \omega \pm i\eta$, $\eta \to 0$, the discontinuity across the branch cut is given by:

$$\mathrm{Re}\ \alpha(z) = \frac{\alpha(\omega + i\eta) + \alpha(\omega - i\eta)}{2} \tag{3a}$$

$$\mathrm{Im}\ \alpha(z) = \frac{\alpha(\omega + i\eta) - \alpha(\omega - i\eta)}{2i} \tag{3b}$$

Introducing the definition of $\alpha(\omega)$ in (3b) we obtain,

$$\text{Im } \alpha(z) = \frac{1}{2} \sum_{n\neq 0}^{\infty} \left[\frac{f_{on}}{\omega_{on}^2 - \omega^2 + i\eta} - \frac{f_{on}}{\omega_{on}^2 - \omega^2 - i\eta} \right] +$$

$$+ \frac{1}{2i} \int_{\epsilon_I}^{\infty} \frac{g(\epsilon)\, d\epsilon}{\epsilon + z} \left[\frac{1}{\epsilon - \omega - i\eta} - \frac{1}{\epsilon - \omega - i\eta} \right] \tag{4}$$

In the limit that $\eta \to 0$ ($z = \omega \pm i\eta \to \omega$) the discrete contributions cancel and recognizing that the expression in braces under the integral sign is just $2\pi i\, \delta(\epsilon - \omega)$ we finally obtain:

$$\lim_{\eta \to 0} \text{Im } \alpha(\omega \pm i\eta) = \frac{1}{2i} \frac{g(\omega)}{2\omega} 2\pi i = \frac{\pi g(\omega)}{2\omega} \tag{5}$$

Similarly, for the real part we have:

$$\text{Re } \alpha(z) = \frac{1}{2} \left[\sum_{n\neq 0} \left\{ \frac{f_{on}}{\omega_{on}^2 - \omega^2 + i\eta} + \frac{f_{on}}{\omega_{on}^2 - \omega^2 - i\eta} \right\} + \right.$$

$$\left. + \int_{\epsilon_I}^{\infty} \frac{g(\epsilon)\, d\epsilon}{\epsilon^2 - \omega^2 - i\eta} + \int_{\epsilon_I}^{\infty} \frac{g(\epsilon)\, d\epsilon}{\epsilon^2 - \omega^2 + i\eta} \right] \tag{6}$$

In the limit $\eta \to 0$ the first two terms become equal and because

$$\lim_{\eta \to 0} \int \frac{g(\epsilon)\, d\epsilon}{\epsilon^2 - \omega^2 \pm i\eta} = P \int \frac{g(\epsilon)}{\epsilon^2 - \omega^2} \mp \pi i g(\omega^2)$$

we obtain:

$$\operatorname*{Re}_{\lim \eta \to 0} \alpha(\omega + i\eta) = \sum_{n \neq 0}^{\infty} \frac{f_{on}}{\omega_{on}^2 - \omega^2} + P \int_{\epsilon_I}^{\infty} \frac{g(\epsilon)\, d\epsilon}{\epsilon^2 - \omega^2} \quad . \tag{7}$$

We can finally write that:

$$\lim_{\eta \to 0} \alpha(\omega + i\eta) = \sum_{n \neq 0}^{\infty} \frac{f_{on}}{\omega_{on}^2 - \omega^2} + P \int_{\epsilon_I}^{\infty} \frac{g(\epsilon)\, d\epsilon}{\epsilon^2 - \omega^2} + \frac{i\pi g(\omega)}{2\omega} \tag{8}$$

Since the photoabsorption cross section can be written as[2]

$$\sigma(\omega) = \frac{2\pi^2}{e}\, g(\omega) \quad ,$$

we obtain the relationship

$$\sigma(\omega) = \lim_{\eta \to 0} \frac{4\pi\omega}{e}\, \mathrm{Im}\left[\alpha(\omega + i\eta)\right] \tag{9}$$

between the total cross section and the imaginary part of the dynamic polarizability.

The advantage of using the dynamic polarizability to perform the analytical continuation resides on the fact that its analytical form is such that it can be written as a Stieltjes series. Once this is recognized, Padé Approximants provide an efficient way to perform the continuation. It is known from the theory of Pade Approximants that, for this type of series, any sequence of $[N + J/N]$ $J \geq -1$ of Padé Approximants will converge to the function $\alpha(z)$ in the cut, as N goes to infinity.[3] Of course we expect in practice to obtain convergence with small values of N.

For the sake of completeness let us show that the dynamic polarizability can indeed be written as a Stieltjes series. Baker[4] seems to be the first one to point out this relationship using an approach different from the one presented here.

It will be convenient to rewrite (1) in a more compact form,

$$\alpha(\omega) = \int_0^\infty \frac{(d_f/d\epsilon)}{\epsilon^2 - \omega^2} \, d\epsilon \tag{10}$$

where the generalized oscillator strength, $df/d\epsilon$, is defined as

$$\frac{df}{d\epsilon} = \left[\sum_{n=1}^{\infty} f_{on}\delta(\omega_{on} - \epsilon) + g(\epsilon) \right] d\epsilon \tag{11}$$

That (10) is equivalent to (1) can be shown by simple substitution of (11) on (10). The δ function will generate the summation over the discrete part of the spectrum and the second term of (11) will generate the integral over the continuum.

If we expand (10) in a Maclaurin series

$$\alpha(\omega) = \alpha(0) + \frac{\partial \alpha}{\partial \omega}\bigg|_0 \omega + \ldots + \frac{1}{n!} \frac{\partial^r \alpha}{\partial \omega^r}\bigg|_0 \omega^r \quad ,$$

the coefficients of ω can be written as

$$S_r = \int_0^\infty \frac{(df/d\epsilon)}{(\epsilon^2)^{r+1}} \, d\epsilon \tag{12}$$

Then the dynamical polarizability (10) can be written as a power series

$$\alpha(\omega) = \sum_{r=0}^{\infty} S_r \omega^{2r} \tag{13}$$

To prove that series (13) for $\alpha(\omega)$ is a Stieltjes series it suffices to show that the coefficients S_r can be written as

$$S_r = \int_0^{\infty} u^r d\gamma(u) \tag{14}$$

where $\gamma(u)$ is a bounded, nondecreasing function in the interval $0 \leq u < \infty$.[3]

Let us define the variable $u = 1/\epsilon^2$ and the following relations derived from this definition:

$$\epsilon = -u^{-1/2}, \quad d\epsilon = \frac{1}{2} u^{-3/2} du$$

Introducing these relations in equation (12) we obtain:

$$S_r = \int_0^{\infty} (df/d\epsilon) u^r \frac{1}{2} u^{-1/2} du$$

Introducing now the function $\gamma(u)$ defined as

$$\gamma(u) = \int_0^{u} (\tfrac{1}{2}) u^{-1/2} (df/d\epsilon) du \tag{15}$$

we establish the equivalence between equations (12) and (14). For excitations out of the ground state of a system is always true that

$$df/d\epsilon \geq 0$$

This last condition is sufficient to establish that the function $\gamma(u)$ is a nondecreasing, bounded function of variable u. Consequently, the dynamic polarizability can be written as a Stieltjes series.

In practice we cannot use definition (1) or any equivalent because they require the knowledge of all the bound and continuum states of the system. Instead we try to represent the dynamic polarizability by an "effective summation" over a discrete basis set

$$\alpha(\omega) = \sum_{n\neq 0} \frac{\tilde{f}_{on}}{\tilde{\omega}_{on}^2 - \omega^2} \tag{16}$$

Notice that equation (16) has the same analytical structure of equation (1) and can equally be represented by a Stieltjes series, that guarantees the convergence of the analytical continuation.

Our basic problem is then to obtain a set of "effective" oscillator strengths, $\tilde{f}_{on}$, and transition frequencies, $\tilde{\omega}_{on}$, that allow us to construct (using equation 16), a representation for the dynamic polarizability that exactly reproduces the true function at least in the range of energy pertinent to the process being studied.

References

1. See, for instance, P. W. Atkins, "Molecular Quantum Mechanics", Clarendon Press, London, 1970, pg. 409.
2. A. C. G. Mitchell and M. W. Zemansky, "Radiation and Excited Atoms", 2nd edition, Cambridge University Press, London, 1961.
3. G. A. Baker, "Essentials of Padé Approximant", Academic Press, New York, 1975.
4. G. A. Baker, Adv. Theoret. Phys., 1, 1 (1965).

SECTION B

THE PHOTODETACHMENT CROSS SECTION OF THE NEGATIVE HYDROGEN ION

I. INTRODUCTION

The photoionization cross section of the hydrogen negative ion has been subject of several calculations since Wildt[1] first suggested that it could be responsible for the visible and infrared opacity in the atmosphere of cooler late spectral type stars.

Chandrasekhar[2] and his co-workers pioneered these studies in a series of papers investigating the dependence of the cross section on the accuracy of the bound-state wave function. They also investigated the effect of the central field approximation for the free state.[3] The importance of taking into account exchange effects in the free wave function was first investigated by John[4] using the Hart-Herzberg twenty-parameter wave function for the ground state and the "1s" exchange approximation continuum function. A number of subsequent calculations have appeared. Geltman[5] employed the seventy-parameter bound-state wave function of Schwartz and variationally determined symmetrized continuum functions, containing terms corresponding to excited states of the hydrogen atom. This allowed him to treat both correlation and distortion of the residual hydrogen atom. Doughty et al.[6] employed a close-coupling approach for using a Hartree-Fock eigenfunction expansion for the continuum states which included up to 3d atomic orbitals of the hydrogen atom. Bell and Kingston[7] used the method of polarized orbitals to obtain a representation of the continuum. More recently Ajmera and Chung[8] used the variational method of Kohn-Feshbach to obtain free-state wave functions. A recent review of the photodetachment of H^- was given by Risley.[9]

While many of the above calculations have produced good results

for H^-, they are generally not easily extended to large systems, first because such highly accurate wave functions are not available for systems with more electrons and secondly because the generation of continuum functions by the methods used above becomes very cumbersome.[10]

Our interest is in developing a method which could be equally applied to larger systems. Thus we use highly accurate wave functions and methods practicable for polyatomic molecules, and we avoid the explicit use of continuum functions.[11] The method is based upon the relation between the cross section for photodetachment and the imaginary part of the frequency-dependent polarizability. As first suggested by Reinhardt and co-workers,[12d] we used a discrete basis set representation of the frequency-dependent polarizability which is used to make an analytical continuation in the complex plane. Details of the method and the calculations are presented in Secs. II and III. This method has been successfully applied to other small systems[12] but systematic studies of the basis set for the unbounded orbitals have not been reported. This is an important part of the problem since basis set expansions represent the most convenient approach to the treatment of large systems. Once we understand how to select small but adequate basis sets for the unbounded orbitals, the method is automatically extendable to larger systems, since the use of basis set expansions for the bound part of the system is well established.

II. METHOD

The basic difficulty with using a discrete or finite basis set for photoionization calculations is that we obtain only a finite number of transitions which are supposed to represent the continuum. That the discrete set does represent the continuum in some sense is indicated by the fact that the calculated sum over the discrete transitions (1) and its moments,

$$\sum_n f_{on} \tag{1}$$

(where f_{on} is the oscillator strength), is approximately equal to the integrated absorption for the continuum, (2), and its respective moments,

$$\int_{\epsilon_I}^{\infty} g(\epsilon)\, d\epsilon \tag{2}$$

(where ϵ_I is the ionization potential and $g(\epsilon)$ is the oscillator strength for the continuum). On the other hand it is clear that the oscillator strengths at every transition energy ω_{on} must be associated with a band of transitions near ω_{on}. The problem then is how to proceed from the theoretical results

$$\{f_{on}, \omega_{on}, n = 1, n_{max}\} \tag{3}$$

to a continuum function $g(\epsilon)$.

The approach we follow makes use of the relationship between $g(\omega)$ and the complex dynamic polarizability $\alpha(z)$.

The frequency-dependent polarizability is given by:

$$\alpha(\omega) = \sum_{n\neq 0} \frac{f_{on}}{\omega_{on}^2 - \omega^2} + \int_{\epsilon_I}^{\infty} \frac{g(\epsilon)\, d\epsilon}{\epsilon^2 - \omega^2} \quad , \tag{4}$$

where f_{on} and $g(\epsilon)$ are the oscillator strengths for the bound and continuum transitions respectively, ω_{on} the transition frequencies, and ϵ_I the first ionization threshold. Extending this definition to complex frequencies leads to

$$\alpha(z) = \sum_{n\neq 0} \frac{f_{on}}{\omega_{on}^2 - z^2} + \int_{\epsilon_I}^{\infty} \frac{g(\epsilon)\, d\epsilon}{\epsilon^2 - z^2} \quad . \tag{5}$$

The complex polarizability $\alpha(z)$ is analytical throughout the complex plane except for an infinite number of poles along the real axis (the ones in the positive region corresponding to the transition frequencies) and a branch cut in the photoionization interval $\epsilon_I \leq \mathrm{Re}(z) < \infty$.

Since the cross section can be written as[13]

$$\sigma(\omega) = \frac{2\pi^2}{c}\, g(\omega) \tag{6}$$

and since

$$\lim_{\eta \to 0} \alpha(\omega + i\eta) = \sum_{n\neq 0} \frac{f_{on}}{\omega_{on}^2 - \omega^2} + P \int_{\epsilon_I}^{\infty} \frac{g(\epsilon)\, d\epsilon}{\epsilon^2 - \omega^2} + i\, \frac{\pi\, g(\omega)}{2\omega} \quad , \tag{7}$$

we obtain the relationship

$$\sigma(\omega) = \lim_{\eta \to 0} \frac{4\pi\omega}{c} \operatorname{Im}[\alpha(\omega + i\eta)], \tag{8}$$

between the total cross section and the imaginary part of the dynamic polarizability on the real axis.

So far we converted the problem of obtaining $g(\omega)$ to that of obtaining the imaginary part of $\alpha(z)$. This latter task is accomplished by an analytical continuation procedure[14] as follows: (i) we construct an initial guess for $\alpha(z)$ from (3) as

$$\alpha(z) = \sum_{n \neq 0} \frac{\tilde{f}_{on}}{\tilde{\omega}_{on}^2 - z^2} \quad ; \tag{9}$$

this is approximate since each discrete $\tilde{f}_{on}$ represents a band of the continuum and thus should not be associated with a single $\tilde{\omega}_{on}$; (ii) using (9) we calculate $\alpha(z)$ at a number of points in the complex plane; (iii) these points are fitted by a Padé Approximant, providing a representation of $\alpha(z)$ in the complex plane; (iv) using this representation we calculate $\alpha(z)$ on the real axis where it is equal to $\alpha(\omega)$; and (v) the imaginary part of $\alpha(z)$ on the real axis thereby provides the cross section by Eq. (8). Having the representation for $\alpha(z)$ we can evaluate $\sigma(\omega)$ at a very large number of points with little effort.

The crucial point in this process is the fitting procedure. In this respect it is important to notice that the analytical form of the frequency-dependent polarizability is such that it can be written as a Stieltjes series.[15] Consequently, Padé Approximants[16] can be used as a very efficient way to perform the continuation. For this type of series, any sequence of [N+J/N] Padé Approximants (with $J \geq -1$)

will converge, as N goes to infinity, to the function $\alpha(z)$ in the cut. Of course, we hope to achieve convergence with small values of N.

There are two ways of using Padé Approximants to fit $\alpha(z)$. One is to use its analytical form and expand it in a Taylor series around some point z_0. The coefficients of the series can be used to construct the approximants by equating

$$f(z) = f(z_0) + a_1(z - z_0) + a_2(z - z_0)^2 + \ldots + a_n(z - z_0)^n = \frac{P_m}{Q_n}, \quad (10)$$

where P_m and Q_n are polynomials of degree m and n in $(z - z_0)$. Notice that for the particular case of $f(z) = \alpha(z)$ and z_0 chosen at the origin, the coefficients a_i are the sum rules. Although the approximants are determined by the information in f(z) at only one point, these unipoint-multipiece approximants have been successfully used to continue Taylor series expansions out of its range of convergence. In addition, inside the circle of convergence of the Taylor series, they usually converge faster than the series itself. Among several applications, this type of Padé has been used to calculate second-order optical properties of atoms and molecules.[17] However, there are some cases where this type of Padé Approximant presents numerical problems. For example, small errors in the coefficients can produce uncontrollable divergences far from the point of expansion. This implies that the use of higher-order Padé Approximants (to obtain better convergence) can be seriously affected by increasing error in the coefficients.[18]

This type of divergence can be circumvented by the use of multipoint-multipiece Padé Approximants. In these cases, instead of expanding the function around one single point, we expand it at several points, with a subsequent matching of the series. The extra points can be picked, for instance, in the regions where the Padé Approximant constructed from the previous series starts diverging. Multipoint-multipiece Padé Approximants have been the subject of recent theoretical investigations,[19] mainly in their relation to Stieltjes series, and many of the results for the normal Padé can be extended to the multipoint case. Several recent applications of two-point Padé Approximants have been reported in the literature.[20] In principle, this type of Padé should provide the best way of fitting the function since it contains several pieces of information about the function at each point. Increasing the number of points leads to additional algebra involved in the matching of the various series. Here, the approach is most useful if a small number of points is sufficient to assure convergence over the range of interest.

An alternative approach is to construct a Padé type-II Approximant.[21] This Padé is built not from the coefficients of a Taylor series expansion but from values of the function at different points. In the nomenclature used above, this is a multipoint-unipiece Padé Approximant, and is the type of Padé used in the present work. Here we do not have problems associated with uncertainties in the coefficients. Besides that, since we can, in principle, pick points covering most of our range of interest, it seems to be more efficient for the continuation than the usual unipoint-multipiece Padé Approximant.

III. WAVE FUNCTIONS AND BASIS SETS

A. Wave functions

The Hartree-Fock wave function of H^- is unbounded, i.e., above the energy of the H atom, and hence inappropriate to our studies. The simplest acceptable wave function is the five-term expansion:

$$\psi(^1S) = c_1 \phi^2_{1\bar{s}} + c_2 \phi^2_{2\bar{s}} + c_3\{\phi^2_{2\bar{p}x} + \phi^2_{2\bar{p}y} + \phi^2_{2\bar{p}z}\} . \qquad (11)$$

We solved for the orbitals and coefficients of this MC-SCF wave function using the GVBTWO program.[22] The resulting energy is -0.5251 h which is 0.0026 h (0.07 eV) above the exact energy but 0.0372 h (1.012 eV) below the Hartree-Fock energy.

As an approximation to the ^1P continuum states we solved for the wave functions

$$\psi(^1P) = (\phi_{1s}\phi_{npz} + \phi_{npz}\phi_{1s}) , \qquad (12)$$

where ϕ_{1s} is taken as the 1s orbital of the hydrogen atom and ϕ_{npz} are the variational solutions of (12) (given fixed ϕ_{1s}).

The final wave functions for the calculation were obtained from CI calculations using the above orbitals.[23] For the ^1S state we used the five orbitals from (11) plus the ϕ_{1s} orbital from (12) (orthogonalized), including all the allowed configurations (nine configurations). For the ^1P states we included the nine p_z orbitals from (11) and (12) plus the three s orbitals ($\phi_{1\bar{s}}$, $\phi_{2\bar{s}}$, ϕ_{1s}), allowing a full CI over these states (27 configurations).[33] These solutions were used to evaluate the oscillator strengths for the various $^1P \leftarrow {}^1S$ transitions. The basis set is discussed below.

B. Basis sets

All calculations were carried out using the Huzinaga [6s/3s] expansion for the 1s orbital ($\zeta = 1.0$) plus the inner two components of the (4p) expansion of the 2p orbital ($\zeta = 0.5$).[24] To this basis set we added diffuse s and p basis functions, as indicated below.

The uncertainty in choosing the basis set concerns what to include for the continuum wave functions. We cannot optimize the basis sets as we do for bound states. Instead we want an expansion leading to a good description of (at least) the region of the continuum most involved in the process. One criterion which we used to determine the quality of the basis sets is to require them to produce a distribution of oscillator strengths and transition frequencies which satisfy the sum rules (see Sec. IV-B for a discussion of the sum rule criterion).

It is important in this type of study to have a systematic way of changing both the number of basis functions and the range of exponents of the basis sets. We accomplished this by considering each member of the diffuse s and p basis sets to have orbital exponents as,

$$\zeta, \beta\zeta, \beta^2\zeta, \ldots,$$

that is, each orbital exponent is the geometrical factor β times the previous exponent. Various geometrical factors, β, were used with diffuse s and p functions lying in the range 0.04 to 0.00256. Explanatory calculations indicated that the diffuse s and p basis functions should have the same distribution of exponents and hence we took

$$\beta_s = \beta_p .$$

In Table I we show the spectra (f_{on} and ω_{on}) resulting from three different basis sets, all covering the same range (out to 0.00256) in exponents. From this table it is clear that the smoothest spectrum is tl one generated by the basis set [11s/11p; $\beta = 1/1.5$]. Of course smoothness is not a rigorous criterion for choosing a basis. A more fundament: criterion is the agreement with the sum rules arising from the spectra. We proceeded then by computing the sum rules for several basis sets using various sized basis sets with various geometrical factors. In some cases the s basis set was insufficient to describe the ground-state ^1S and the basis set was discarded.

Table II shows some typical results for several cases. For the three basis sets of Table I (which cover essentially the same range of exponents), we see that [7s/7p; $\beta = 1/2.5$] exceeds sum rules S_1, S_2 and S_3, while both [9s/9p; $\beta = 1/1.75$] and [11s/11p; $\beta = 1/2.5$] exceed the S_2 and S_3 sum rules. On the basis of this comparison, [7s/7p; $\beta = 1/2.5$] is clearly unsatisfactory.

We next considered variations in the number of s and p basis sets while keeping β fixed. From Table II it is clear that (a) for the geometrical factor $\beta = 1/2.5$ no improvement is obtained; (b) for $\beta = 1/1.75$, the addition and subtraction of basis functions to the basic [9s/9p] basis do not show any improvement; on the contrary, worse sum rules are obtained; (c) for $\beta = 1/1.5$ substantial improvement is obtained when the number of basis sets of the s-space is reduced.

On these considerations we selected $\beta = 1/1.5$ as the optimum geometrical factor. Figure 1 shows the resulting cross sections for some of the bases which violated the sum rule criterion.

Once the optimum geometrical factor was chosen, we turned our attention to the size, i.e., the number of basis functions in the basis set. Assuming that we have enough diffuse p functions in the basis set, the question to be answered is how many s diffuse functions are required? Table III shows the dependence of the H^- ground state energy on the size of the s basis, for $\beta = 1/1.5$, using the basis sets listed in Table IV. From Table III we see that only 7s basis functions are required. We selected this basis set [7s/11p, $\beta = 1/1.5$] as the optimum one. This basis set was the one used for the calculations of the cross sections and dynamic polarizability.

IV. RESULTS

The final spectra obtained are shown in Table V. These spectra were used to produce all the results described below.

A. Cross-section for photodetachment

Following the procedure outlined in Sec. II we performed the analytical continuation to obtain the cross sections. Figure 2 shows the results for two different analytical continuations, indicating the convergence of the calculation. The convergence is good for both velocity and length forms. Figure 3 shows our results in both forms compared with other theoretical results. The agreement among all calculations is good in general except in the region very near the threshold. Our best agreement over the entire range (Fig. 3), in both forms, is with Geltman[5] who used true continuum wave functions in his calculations. This suggests that we are representing the continuum well, at least for the region most involved in the process.

Comparing our results with the experiment in Fig. 4, we find good agreement. These experimental results are the relative measurements of Smith and Burch[25] normalized to the value of our cross section at 2.35 eV (5280 Å). These relative measurements have a maximum estimated uncertainty of ±3%. On the basis of the absolute integrated measurements of Branscomb and Smith,[26] Geltman put Smith and Burch results on an absolute basis, obtaining a value of 32.8 Mb at 2.35 eV (5280 Å), with an uncertainty of 20%. This value is in good agreement with our value of 30.56 Mb at 2.35 eV (5280 Å).

From Fig. 4 we also see that the agreement between the length and velocity forms of the cross sections is very good. Since for the exact wave functions $\Psi(^1S)$ and $\Psi(^1P)$ these two forms are equivalent, the agreement between them can be used as a test for the quality of the basis set. Of course close agreement between the two forms is only a necessary but not sufficient condition for an adequate basis set.

B. Sum rules

One way of estimating the quality of our results is to compute the sum rules associated with each distribution. Because the sum rules emphasize different regions of the spectra, they provide an estimate of the accuracy of the cross section at different values of energy. On the basis of the sum-rules criterion, Dalgarno and Kingston[27] were able to show that the cross sections calculated by Chandrasekhar should be in error. Geltman[5] analyzed his results in terms of his sum rules and concluded that his results should be low near the threshold. These sum rules can be expressed as

$$S_k = \sum_{n \neq 0} \frac{f_{on}}{\omega_{on}^k} \quad . \tag{13}$$

S_0 is the Thomas-Reich-Kuhn oscillator strength sum rule and S_2 is the static polarizability. The exact values of these sum rules contain contributions not only from transitions in which the hydrogen atom is left in its ground state but also from transitions in which the hydrogen atom is left in an excited state or even ionized. Thus the exact values can be used as upper bounds for the values computed when only the transitions leaving the hydrogen atom in its ground state are considered. Table VI shows our

sum rules compared with other calculations and with the upper bounds. Note that most results in Table VI are for the single channel in which the H atom is left in the 1s state, whereas the bound includes all processes. Thus theoretical values of S_i close to the bound need not indicate an accurate result.

Assuming Schwartz's bound for the static polarizability, Table VI shows that all the sum rules are satisfied. On the other hand, if Chung's[28] value is taken for the upper bound, we exceeded this value in both forms. This may indicate that the cross sections near threshold are somewhat large. Independent of which bound is used for the static polarizability, other calculations seem to indicate low values of the cross section near threshold. Consequently we expect the exact values near the threshold to lie somewhere between our results and the other calculations.

C. Dynamic polarizability

An alternative way of checking our distribution is to calculate the dynamic polarizability in the normal dispersion region below the threshold. Since there are no bound-bound transitions for H^-, it can be seen from (7) that both the real and imaginary parts of the dynamic polarizability are given directly by $g(\omega)$.

In general there are several alternate approaches to extracting the information contained in the frequency-dependent polarizability. First of all, if there is interest only in the absorptive properties of the system, we can neglect all the bound-bound transitions because the imaginary part of $\alpha(z)$ is given solely by the distribution $g(\omega)$ which only involves bound-free transitions. Indeed in the case of the hydrogen atom,[12d] a better description of the cross section was obtained when two bound-bound transitions were neglected. Another possibility is to construct the full representation for $\alpha(z)$ including all bound-bound transitions. In this case we can extract from $\alpha(z)$ both the dispersive and absorptive properties of the system. There is still another possibility which is to use the real part of $\alpha(z)$. Since it is directly related to the index of refraction by

$$n(\omega) - 1 = 2\pi N_0 \, \mathrm{Re}[\alpha(\omega)], \tag{14}$$

we could in principle use experimental index-of-refraction data and discrete oscillator strengths to perform the analytical continuation. Unfortunately these data are not accurate enough to produce good cross sections.[12d,29]

Figure 5 shows our results for the dynamic polarizability compared with a variational-perturbation calculation by Chung.[28] The curves parallel Chung's values up to 0.01 h and begin to deviate significantly above 0.023 h. Near the threshold (0.0275 h) the difference is very large. Although Chung's results are expected to be very accurate for lower energies (where they are converged values for a 140 Hylleraas-type wave function), they are not converged for $E > 0.023$ h (just the region where our values start deviating significantly from Chung's). While it is clear from Chung's results that inclusion of more terms in the expansion would not affect this region drastically, it is important to note that his wave function is contracted and cannot describe well the behavior of a diffuse system like H^- near the threshold. (This is clear from Chung's results for Li^+, a much tighter system, where a rapid increase in the region near the threshold is found and a faster convergence is obtained.) More recently, Adelman[31] developed an analytical expression for the dynamic polarizability of H^-, using Rotenberg and Stein's[32] wave function (a 33 Hylleraas term expansion plus a tail function) and an asymptotic approximation. His value for the static polarizability was 215.5 a.u., but if he uses Chung's value of 206 a.u., his results differ from Chung's results about 4.5 to 5.0% for $\omega \leq 0.025$ a.u. Very close to threshold this difference jumps to 6.6%, his value being larger than Chung's, but still much lower than our present results. We believe that this large discrepancy near threshold is due to the fact that Adelman's expression for $\alpha(\omega)$ is poleless, which could prevent it from increasing sufficiently in the region very close to threshold.

Thus while we expect Chung's value of the static polarizability to be more exact, we expect our dynamic polarizability to show a more correct behavior over the whole range.

Based on all the results presented above we conclude that the velocity form of the frequency-dependent polarizability gives the best results but that the agreement with the results from its length form is very good.

V. CONCLUSIONS

The results obtained permit us to conclude that a discrete basis set expansion can be effectively used to represent the continuum wave functions. This "discretization" of the continuum together with techniques of analytical continuation can be efficiently used to calculate cross sections for photoionization, once an adequate basis set is chosen. That makes the method potentially applicable to large systems.

For H^- there remains some uncertainty about the region near the threshold. This region remains unexplored experimentally. Although the uncertainty is not great enough to invalidate any conclusions about the importance of photoionization in H^-, it seems that the subject merits a new experimental investigation, using modern techniques such as tunable dye lasers and modern systems of detection.[30]

ACKNOWLEDGMENT

One of the authors (MACN) acknowledges Conselho Nacional de Pesquisas (BRASIL) for financial support and Universidade Federal do Rio de Janeiro for a leave of absence.

TABLE I. Dependence of the spectra upon basis set.[a] f_{on} = oscillator strength, ω_{on} = transition energy (eV).

[7s/7p ; β = 1/2.5]		[9s/9p ; β = 1/1.75]		[11s/11p ; β = 1/1.5]	
f_{on}	ω_{on}	f_{on}	ω_{on}	f_{on}	ω_{on}
0.043039	0.841215	0.025572	0.813537	0.017101	0.793612
0.215733	1.250041	0.114370	1.082266	0.076601	1.002800
0.454171	2.279275	0.246037	1.585558	0.168768	1.356880
0.437477	4.896766	0.294583	2.495641	0.212764	1.916556
0.418858	11.379151	0.322565	4.155460	0.250749	2.784818
0.051405	63.118341	0.282310	7.315295	0.228296	4.140133
		0.108864	14.017534	0.227801	6.289182
				0.211064	9.859149
				0.137689	16.633445

[a]The diffuse functions of these three basis sets cover the exponent range of 0.04 - 0.00256 for both s and p spaces. Since the geometrical factors are different, the first diffuse basis of each basis set are not exactly equal. They are 0.04000, 0.04202 and 0.04374 for β = 1/2.5, 1/1.75, 1/1.5, respectively.

TABLE II. Sum rules dependence on the basis sets.

Basis Sets	S_0	S_1	S_2	S_3
[7s/7p; $\beta = 1/2.5$]	1.625	15.06	228.1	4535.4
[7s/9p; $\beta = 1/2.5$]	1.574	14.95	227.9	4537.6
[9s/9p; $\beta = 1/2.5$]	1.574	14.96	227.9	4526.3
[7s/7p; $\beta = 1/1.75$]	2.048	15.61	228.9	4536.8
[9s/9p; $\beta = 1/1.75$]	1.394	14.54	226.5	4505.4
[11s/11p; $\beta = 1/1.75$]	1.849	15.44	228.3	4505.1
[11s/11p; $\beta = 1/1.5$]	1.531	14.81	227.2	4511.4
[9s/11p; $\beta = 1/1.5$]	1.829	14.84	210.7	3983.7
[7s/11p; $\beta = 1/1.5$]	1.51	14.2	208.3	3940
Bounds	2	15.0[a]	217 ± 7[b]	4000 ± 300[b]
			206.0[c]	

[a] C. L. Pekeris, Phys. Rev. 126, 1470 (1962).

[b] C. Schwartz, unpublished (cited in Ref. 5).

[c] Ref. 28.

Table III. Energy of the ground state ^1S of H^- for various basis sets ($\beta = 1/1.5$).

Basis sets	Energy (hartree)
(11s/11p)	-0.525099
(9s/11p)	-0.525098
(7s/11p)	-0.525097
(6s/11p)	-0.524980
(7s/11p) after CI	-0.525494
Hartree Fock[a]	-0.487930
Weiss S + P[b]	-0.526470
Exact[c]	-0.527750

[a]C. C. J. Roothaan, L. M. Sachs, and A. W. Weiss, Rev. Mod. Phys. 32, 186 (1960).

[b]A. W. Weiss, Phys. Rev. 122, 1826 (1961).

[c]C. L. Pekeris, Phys. Rev. 126, 1470 (1962).

Table IV. Largest basis set used (11s/11p) with the best geometrical factor $\beta = 1/1.5$. Exponents above the solid line are contracted together with relative coefficients as in the H atom basis functions. Exponents below the dotted lines are considered as diffuse functions (modified in various basis sets).

s Exponents	p Exponents
68.16	0.73
10.2465	0.17
2.34648	0.113
0.67332	0.04374
0.22466	0.02916
0.082217	0.01944
0.04374	0.01296
0.02916	0.00864
0.01944	0.00576
0.01296	0.00384
0.00864	0.00256
0.00576	
0.00384	
0.00256	

Table V. Spectrum obtained with the (7s/11p) basis set. Oscillator strengths, $\tilde{f}_{on}$ and transition frequencies, $\tilde{\omega}_{on}$.

$(\tilde{f}_{on})_{length}$	$(\tilde{f}_{on})_{velocity}$	$\tilde{\omega}_{on}$ (eV)
0.00888214	0.00869698	0.79335322
0.06835403	0.06603274	1.00254140
0.15545195	0.15523099	1.35662122
0.22477895	0.22949153	1.91629754
0.24558997	0.24070119	2.78455907
0.23131597	0.23283304	4.13987423
0.22792494	0.22992260	6.28895075
0.20792662	0.20578687	9.85880897
0.13857175	0.13693591	16.63336036

Table VI. Sum rules for H^- [see Eq.(13)]. Except as noted[h], all theoretical results are for the single channel in which the H atom is left in the 1s state. Thus the S_i should be less than the bound (which includes all processes).

	S_0		S_1		S_2		S_3	
	Length	Velocity	Length	Velocity	Length	Velocity	Length	Velocity
Geltman[a]		1.72	14.0[f]	14.2	198[g]	202.4	3570[g]	3742
Doughty et al.[b]			14.4	14.2	201	202	3630	3720
Bell and Kingston[c]			14.7	16.0	205	227	3700	4150
Langhoff et al.[h]	1.99		14.95		206.1			
Present Work	1.51	1.50	14.2	14.1	208.3	206.8	3940	3894
Bounds	2		15.0[f]		217 ± 7[d]		4000 ± 300[d]	
					206.0[e]			

[a] Reference 5.

[b] Reference 6.

[c] Reference 7.

[d] C. Schwartz, unpublished (cited in Ref. 5).

[e] Reference 28.

[f] C. L. Pekeris, Phys. Rev. 126, 1470 (1962).

[g] From Ref. 7.

[h] Reference 11d. These sum rules include the process where the residual hydrogen atom is left in the 2s excited state.

REFERENCES

[1]R. Wildt, Astrophys. J. 89, 295 (1939).

[2]S. Chandrasekhar, Astrophys. J. 128, 114 (1958) and references therein.

[3]S. Chandrasekhar and D. D. Elbert, Astrophys. J. 128, 633 (1958).

[4]T. L. John, Monthly Notices, Royal Astronomical Society 121, 41 (1960).

[5]S. Geltman, Astrophys. J. 136, 935 (1962).

[6]N. A. Doughty, P. A. Fraser, and R. P. McEachran, Monthly Notices, Royal Astronomical Society 132, 255 (1966).

[7]K. L. Bell and A. E. Kingston, Proc. Phys. Soc. (London) 90, 895 (1967).

[8]M. P. Ajmera and K. T. Chung, Phys. Rev. A 12, 475 (1975).

[9]J. S. Risley, in Atomic Physics IV, Proceedings of the Fourth International Conference on Atomic Physics, Heidelberg, Germany, 1974 (Plenum Press, New York, 1975).

[10]For a review of the methods used to calculate continuum wave functions see, for example, A. L. Stewart, Advances in Atomic and Molecular Physics 3, 1 (1967).

[11]See also: (a) P. W. Langhoff and C. T. Corcoran, J. Chem. Phys. 61, 146 (1974) where a discrete basis set is used in connection with a Stieltjes imaging procedure to obtain the cross section at discrete points; (b) P. W. Langhoff and C. T. Corcoran, Chem. Phys. Lett. 40, 367 (1976); (c) P. W. Langhoff, ibid. 22, 60 (1973); (d) P. W. Langhoff, J. Sims, and C. T. Corcoran, Phys. Rev. A 10, 829 (1974); (e) P. W. Langhoff, C. T. Corcoran, J. Sims, F. Weinhold, and R. M. Glover, ibid. 14, 1042 (1976); (f) H. Doyle, M. Oppenheimer, and A. Dalgarno, ibid. 11, 909 (1975), where a discrete set of Hylleraas-

type functions is used to expand the Green's function to obtain the scattering wave function.

[12](a) D. L. Yeager, M. A. C. Nascimento, and V. McKoy, Phys. Rev. A 11, 1168 (1975); (b) T. N. Rescigno, C. W. McCurdy, and V. McKoy, ibid., 9, 2409 (1974); (c) P. H. S. Martin, T. N. Rescigno, V. McKoy, and W. H. Henneker, Chem. Phys. Lett. 29, 469 (1974); (d) J. Broad and W. P. Reinhardt, J. Chem. Phys. 60, 2182 (1974).

[13]See, for instance, A. C. G. Mitchell and M. W. Zemansky, Radiation and Excited Atoms (Cambridge University Press, New York, 1971).

[14]For a review of this technique as applied to scattering problems see R. H. Haymaker and S. Schlessinger in: The Padé Approximant in Theoretical Physics, edited by G. A. Baker, Jr. and J. L. Gammel (Academic Press, New York, 1970).

[15]G. A. Baker, Jr., Adva. Theoret. Phys. 1, 1 (1965).

[16]Some recent reviews are: (a) Padé Approximants and their Applications, edited by P. R. Graves-Morris (Academic Press, New York, 1972); (b) J. L. Basdevant, Fort. Phys. 20, 283 (1972); (c) G. A. Baker, Jr., Essentials of Padé Approximants (Academic Press, New York, 1975). See also Refs. 14 and 15.

[17](a) P. W. Langhoff and M. Karplus, J. Opt. Soc. Am. 59, 863 (1969); J. Chem. Phys. 52, 1435 (1970); (b) P. W. Langhoff, J. Chem. Phys. 57, 2604 (1972).

[18]This type of problem was noticed by C. Schwartz, J. Comp. Phys. 1, 21 (1966) when trying to use Padé Approximants to extrapolate the Born series for scattering by strong potentials; by P. W. Langhoff and M. Karplus, Ref. 17b, in connection with summation of Cauchy series; by M. A. C. Nascimento and P. H. S. Martin, unpublished results, when trying to obtain the cross section for He (^{1}S) ground

state using the Padé to perform an analytical continuation.

[19](a) M. Barnsley, J. Math. Phys. 14, 299 (1973); (b) S. T. Epstein and M. Barnsley, ibid., 14, 314 (1973); (c) G. D. Allen, C. K. Chui, W. R. Madych, E. J. Narcowich, and P. W. Smith, J. Approximation Theory 14, 302 (1975).

[20]See for instance, G. A. Baker, Jr., G. S. Rushbrooke, and H. E. Gilbert, Phys. Rev. 135, 1272 (1964); A. Isihara and E. W. Montroll, Proc. Nat. Acad. Sci. U.S. 68, 3111 (1971); P. Sheng and J. D. Dow, Phys. Rev. B4, 1343 (1971).

[21]J. L. Basdevant, D. Bessis, and J. Zinn-Justin, Nuovo Cimento 60A 224 (1969); see also Ref. 16b.

[22]The GVB calculations were carried out with the Bobrowicz-Wadt-Goddard program GVBTWO. See F. W. Bobrowicz, Ph. D. Thesis, California Institute of Technology, 1974.

[23]The CI calculations were carried out with the Caltech spin-eigenfunction CI program. See Ref. 22.

[24]S. Huzinaga, J. Chem. Phys. 42, 1293 (1965).

[25]S. J. Smith and D. S. Burch, Phys. Rev. Lett. 2, 165 (1959); Phys. Rev. 116, 1125 (1959).

[26]L. M. Branscomb and S. J. Smith, Phys. Rev. 98, 1028 (1955).

[27]A. Dalgarno and A. E. Kingston, Proc. Phys. Soc. (London) 73, 455 (1959).

[28]K. T. Chung, Phys. Rev. A4, 7 (1971).

[29]K. Miller and G. A. Viano, J. Math, Phys. 14, 1037 (1973).

[30]See for instance, B. Steiner in: Case Studies in Atomic Collision Physics, edited by M. R. McDowell and E. W. McDaniel (North-Holland Publishing Co., Amsterdam, 1972), p. 485.

[31]S. A. Adelman, Phys. Rev. A 5, 508 (1972).

[32]M. Rotenberg and J. Stein, Phys. Rev. 182, 1 (1969).

[33]An attempt was made to use directly the solutions of Eq. (12) (improved virtual orbitals) for the ^1P states. The resulting cross sections showed the right shape but with spectrum shifted by ~ 1 eV, showing that CI effects are important.

FIGURE CAPTIONS

Fig. 1. The effect of different basis sets on the photoionization cross-section of H^-.

Fig. 2. The dependence of the calculated H^- photoionization cross section on different analytical continuations (dipole velocity form). The points in the complex plane used to calculate $\alpha(z)$ were chosen as previously (Refs. 12a,b,c) with $Re(z_i) = (\omega_{0i+1} - \omega_{0i})/2$ and $Im(z_i) = R(\omega_{0i+1} - \omega_{0i})$. The figure shows results for R = 0.75 (solid) and R = 1.00 (dashed). No appreciable changes are noticed as long as the points are near the real axis.

Fig. 3. Comparison among calculated photoionization cross sections for H^- using both (A) the length and (B) velocity forms for the transition matrix elements.

Fig. 4. Comparison of theoretical and experimental photoionization cross sections for H^-. Experimental points are relative measurements of Smith and Burch, Ref. 25, normalized to the value of our cross section at 2.35 eV (5280 Å). Solid line, dipole length form; dashed line, dipole velocity form.

Fig. 5. Theoretical dynamic polarizabilities.

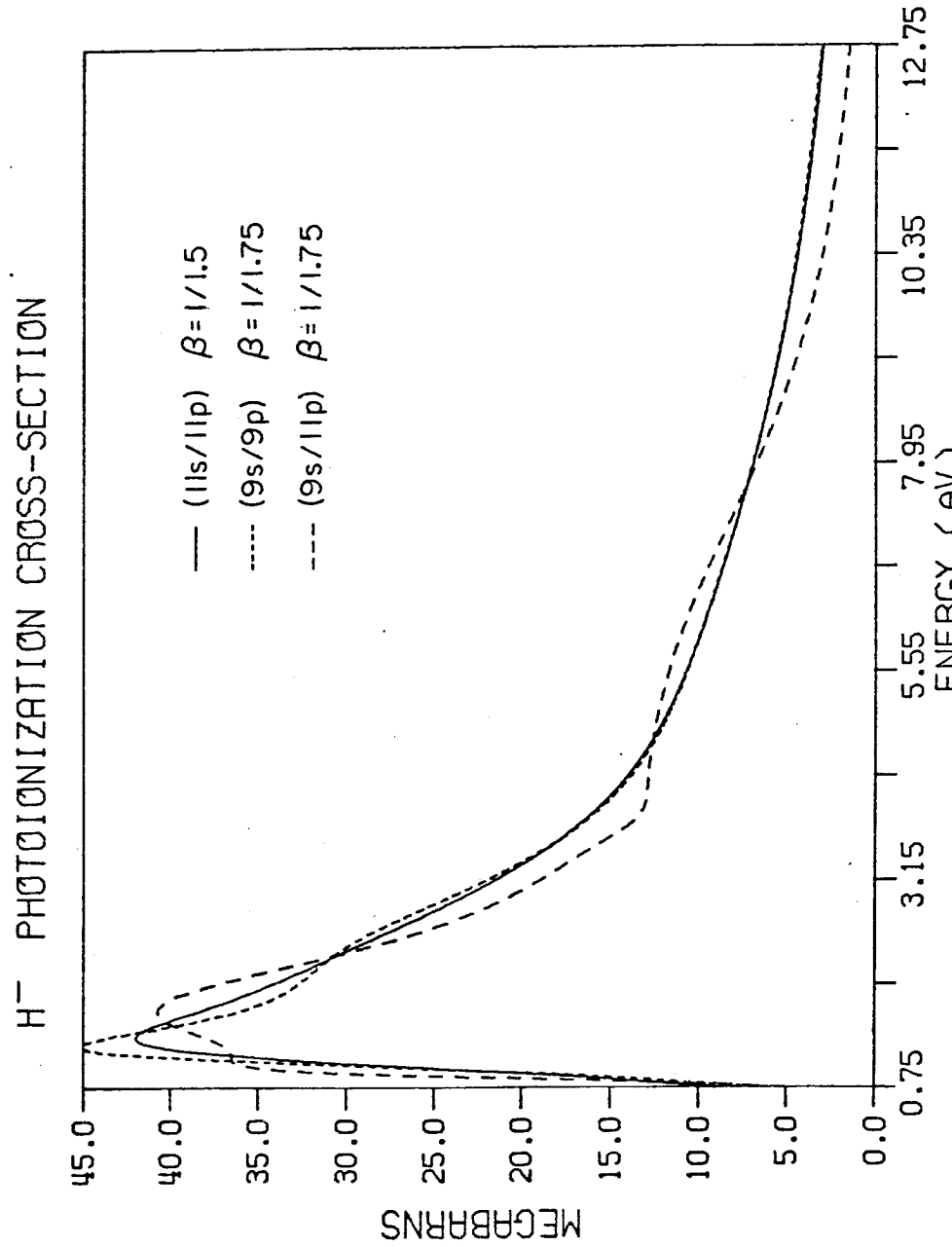
H⁻ PHOTOIONIZATION CROSS-SECTION
(11s/11p) β=1/1.5
(9s/9p) β=1/1.75
(9s/11p) β=1/1.75
MEGABARNS
45.0
40.0
35.0
30.0
25.0
20.0
15.0
10.0
5.0
0.0
0.75
3.15
5.55
7.95
10.35
12.75
ENERGY (eV)

Figure 1.

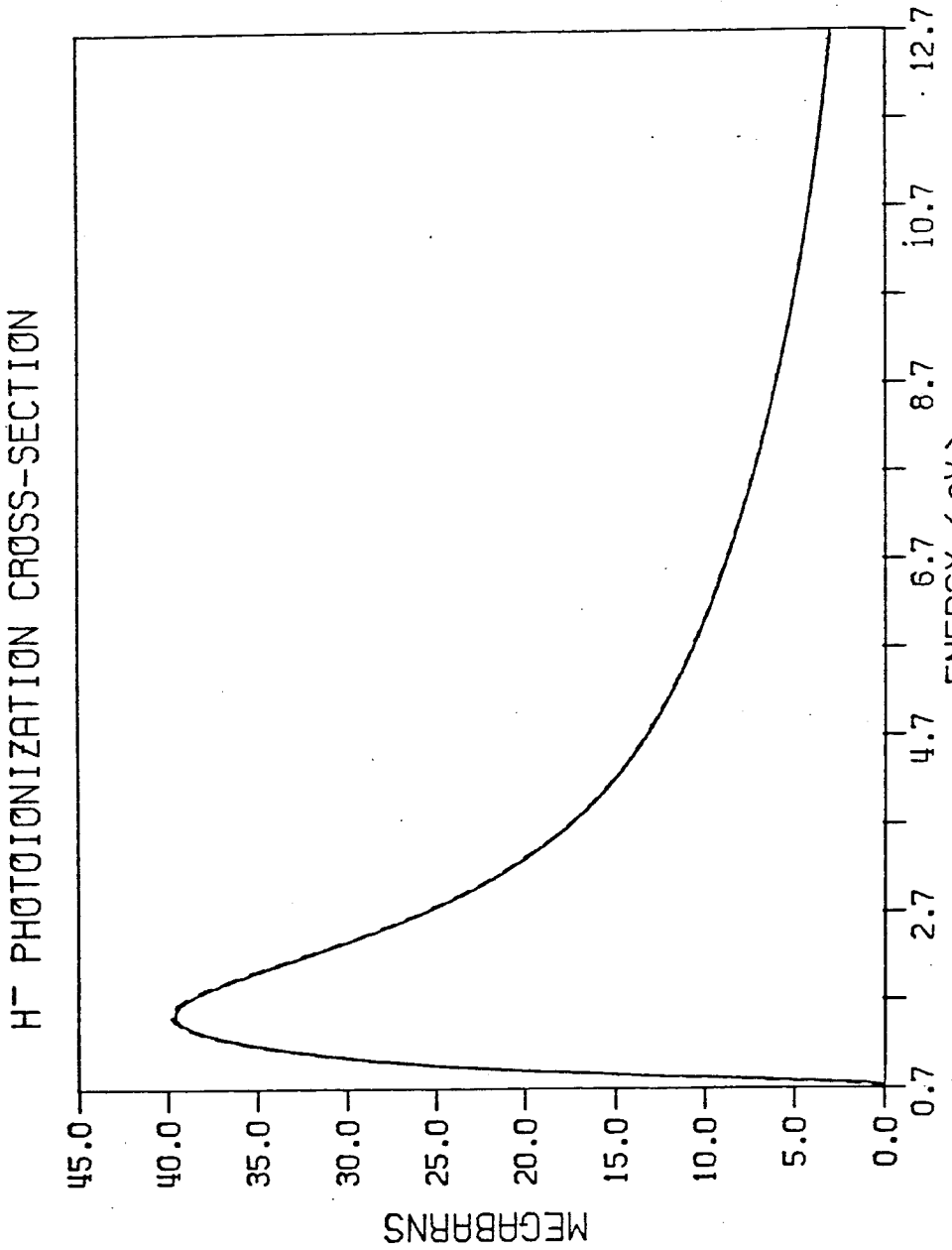
H⁻ PHOTOIONIZATION CROSS-SECTION
MEGABARNS
45.0
40.0
35.0
30.0
25.0
20.0
15.0
10.0
5.0
0.0
0.7
2.7
4.7
6.7
8.7
10.7
12.7
ENERGY (eV)

Figure 2.

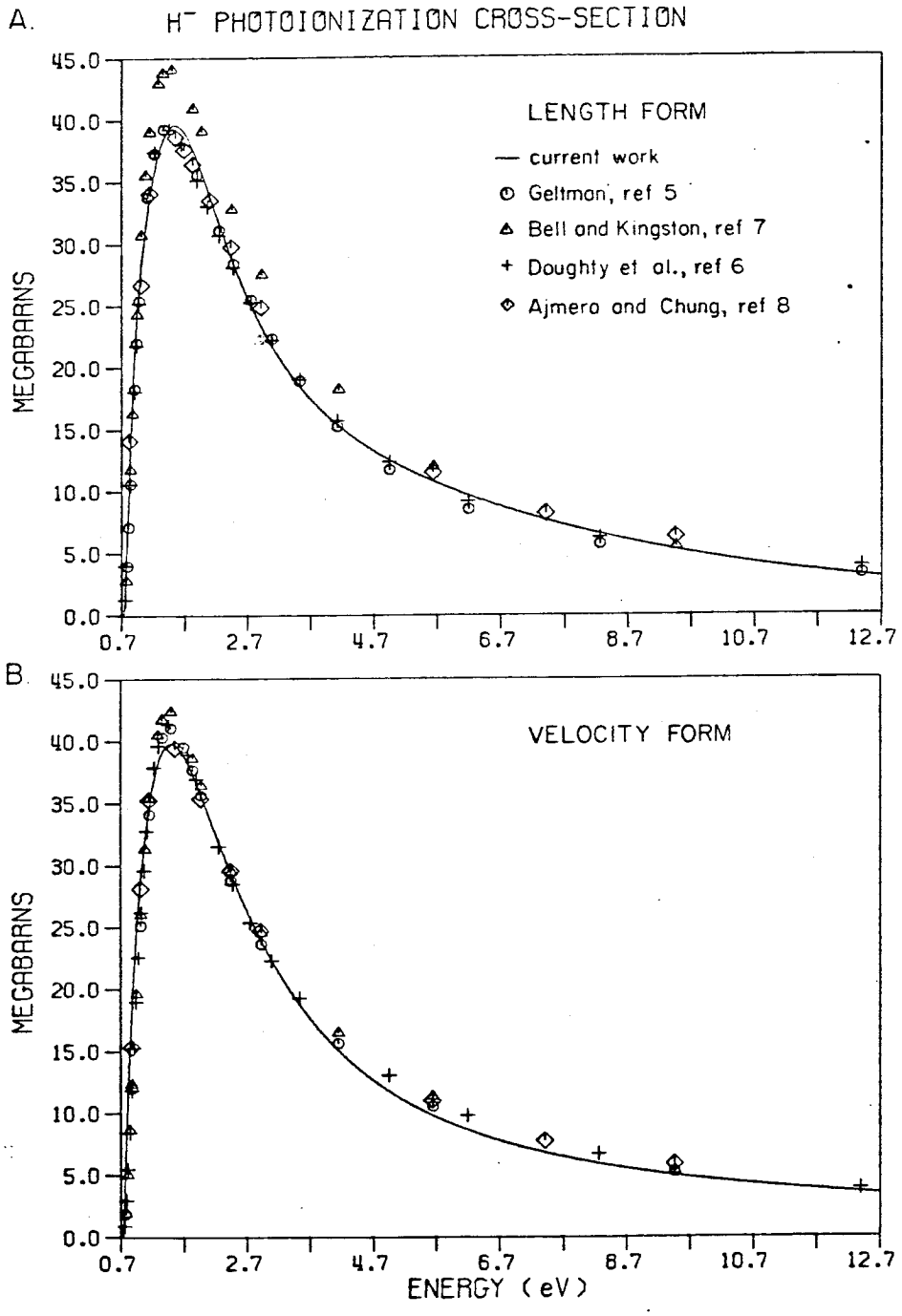
A.
H⁻ PHOTOIONIZATION CROSS-SECTION
LENGTH FORM
— current work
⊙ Geltman, ref 5
△ Bell and Kingston, ref 7
+ Doughty et al., ref 6
◇ Ajmera and Chung, ref 8
MEGABARNS
45.0
40.0
35.0
30.0
25.0
20.0
15.0
10.0
5.0
0.0
0.7
2.7
4.7
6.7
8.7
10.7
12.7
B.
VELOCITY FORM
MEGABARNS
ENERGY (eV)

Figure 3.

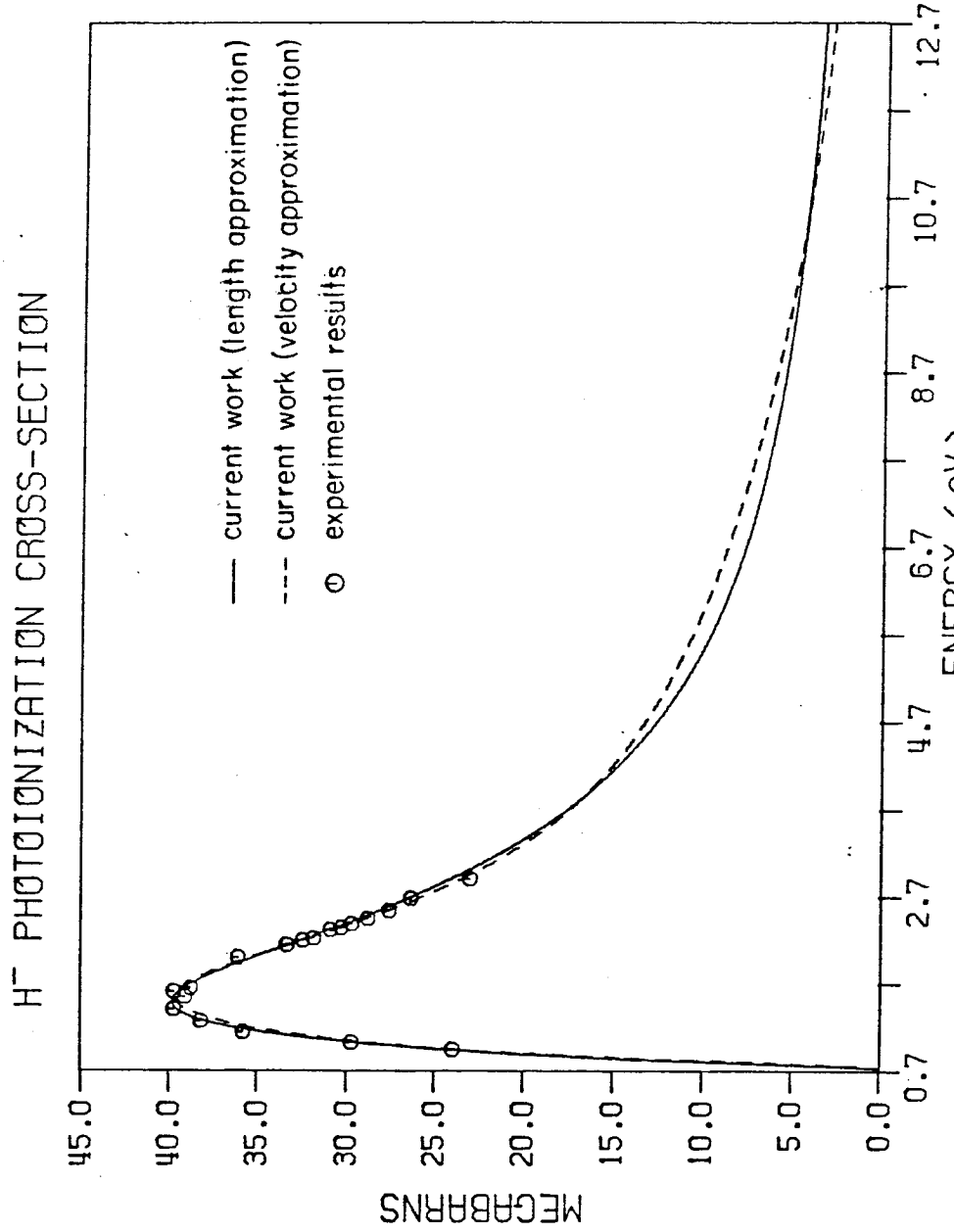
H⁻ PHOTOIONIZATION CROSS-SECTION
current work (length approximation)
current work (velocity approximation)
experimental results
MEGABARNS
45.0
40.0
35.0
30.0
25.0
20.0
15.0
10.0
5.0
0.0
0.7
2.7
4.7
6.7
8.7
10.7
12.7
ENERGY (eV)

Figure 4.

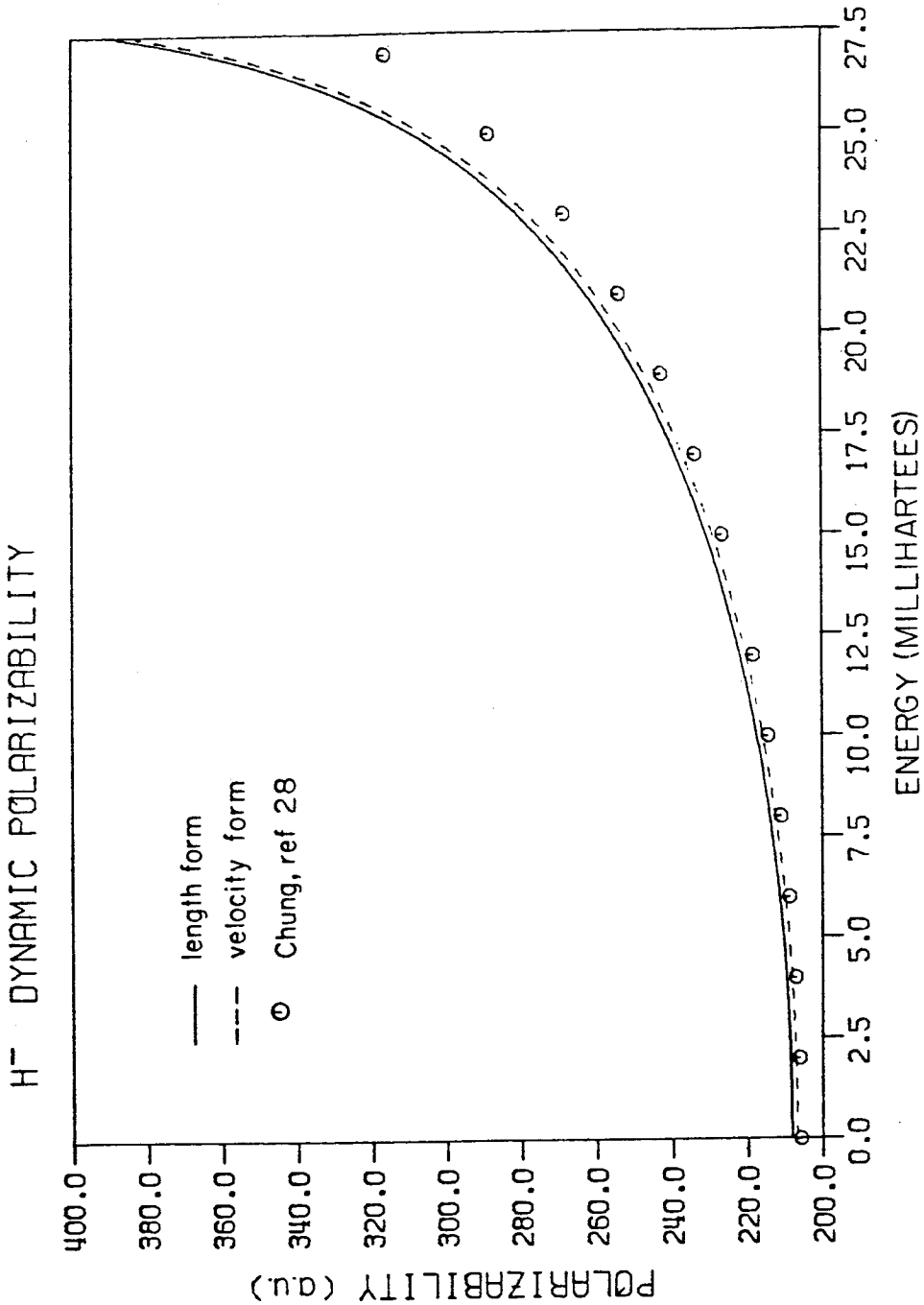
H⁻ DYNAMIC POLARIZABILITY
length form
velocity form
Chung, ref 28
POLARIZABILITY (a.u.)
400.0
380.0
360.0
340.0
320.0
300.0
280.0
260.0
240.0
220.0
200.0
0.0
2.5
5.0
7.5
10.0
12.5
15.0
17.5
20.0
22.5
25.0
27.5
ENERGY (MILLIHARTEES)

Figure 5.

CHAPTER II

THE ELECTRONIC STRUCTURE OF LINEAR POLYENES

SECTION A

THE VALENCE ELECTRONIC EXCITED STATES OF TRANS 1, 3-BUTADIENE AND TRANS-TRANS, 1, 3, 5-HEXATRIENE FROM GENERALIZED VALENCE BOND AND CONFIGURATION INTERACTION CALCULATIONS

1. Introduction

The electronic spectra of linear polyenes have been the subject of intensive experimental and theoretical studies since they were first prepared in the early 1930's. Most of the experimental results obtained in the period of 1930 to 1950 could be reasonably explained in terms of molecular orbital (MO) and valence bond (VB) arguments, despite the fact that these models predicted different (symmetry) ordering of the excited states [1]. More recently there has been a revival of interest in the subject mostly because of its relation to the chemistry of visual pigments [2]. Various polyenes have now been studied using such more sophisticated techniques as vacuum-ultraviolet [3,4] and electron-impact spectroscopy [5, 6, 7] as well as ion-impact [8] and multiphoton spectroscopy [9,10]. This has led to the discovery of new features and to corrections in old assignments, but there is still considerable uncertainty concerning the ordering and character of the excited states.

We report here the results of extensive ab initio generalized valence bond (GVB) and configuration interaction (CI) calculations on the valence excited states and on the positive ion states of trans-1, 3-butadiene (hereafter butadiene) and all trans-1, 3, 5-hexatriene (hereafter hexatriene). Similar studies on Rydberg-like excited states will be discussed in a separate publication.

2. Basis set and geometry

All the calculations reported in this paper were carried out using the Dunning [11] (3s/2p, 2s) contraction of the Huzinaga [12] double-zeta (DZ) (9s/5p, 4s) gaussian basis set. For the Rydberg and nonvalence states this basis set was augmented with diffuse 3s, 3p and 3d basis functions as will be described in a forthcoming publication. Inclusion of these diffuse basis functions does not change the description of the states described in this paper.

In all calculations we used the ground-state geometries as determined from electron diffraction by Traetteberg [13]. These geometries are summarized in fig. 1.

3. The GVB wavefunction

Before going into the details of the calculations, we will briefly review the form of the GVB wavefunctions and some of the terminology used in the succeeding sections [14].

For the ground-state of butadiene the Hartree-Fock (HF) wavefunction has the form of a Slater determinant,

$$\Psi_{HF} = \mathcal{A}[\phi_1 \phi_1 \phi_2 \phi_2 \cdots \phi_{15} \phi_{15} \alpha\beta \cdots \alpha\beta], \tag{1}$$

where each of the 15 orbitals is doubly-occupied and $\mathcal{A}$ is the antisymmetrizer or determinant operator. Two of the orbitals in (1) are π orbitals (i.e., antisymmetric with respect to the molecular plane) and the other 13 are σ orbitals. The GVB(2/PP) (PP stands for perfect pairing) wavefunction for this state has the form

$$\psi_{GVB(2/PP)} = \mathcal{A}[\Phi_\sigma(1,\ldots 26)\Phi_\pi(27\ldots 30)], \tag{2a}$$

where Φ_σ consists of 13 doubly-occupied σ orbitals,

$$\Phi_\sigma = \phi_1 \phi_1 \cdots \phi_{13} \phi_{13} \alpha\beta \cdots \alpha\beta, \tag{2b}$$

just as in the Hartree-Fock case and

$$\Phi_\pi = (\phi_a \phi_b + \phi_b \phi_a)(\phi_c \phi_d + \phi_d \phi_c)\alpha\beta\alpha\beta \tag{2c}$$

corresponding to a valence bond-like wavefunction for the two π bonds. In the GVB(2/PP) wavefunction all the 17 orbitals of (2) are calculated self-consistently with the restriction that the orbitals ϕ_a and ϕ_b are orthogonal to the orbitals ϕ_c and ϕ_d. No restrictions are made upon the shape and character of the orbitals in these wavefunctions. We

also considered wavefunctions in which σ orbitals were correlated just as in (2c). In general, GVB(n/PP) indicates that n electron pairs have been correlated.

4. Butadiene

In this section we describe the calculations performed on the various states of butadiene at the GVB and GVB-CI levels.

In order to understand the symmetries of the states, recall that in the simple MO description the four π MO's are in the order $1a_u$, $1b_g$, $2a_u$, and $2b_g$ (lowest energy first) with the first two doubly-occupied. Thus the positive ion states generated from ionizing an electron from a π orbital are ^2B_g (lowest) and ^2A_u states. The lowest triplet state corresponds to a $1b_g \rightarrow 2a_u$ orbital transition leading to a ^3B_u state and the next triplet state corresponds to a $1b_g \rightarrow 2b_g$ (or $1a_u \rightarrow 2a_u$) orbital transition leading to a ^3A_g state. Similarly, in the MO description the first singlet excited state would be ^1B_u.

In the valence bond model,the valence excited states of a conjugated system are obtained by placing one electron in each pπ orbital and then combining the spins so as to obtain states of proper spin and Pauli symmetry. For butadiene, four singly-occupied orbitals lead to two linearly independent singlet states as in $\hat{1}$ and $\hat{2}$.

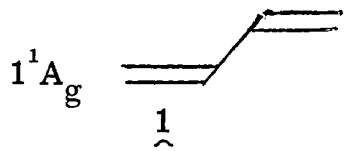

$\underset{\sim}{1}$

$\underset{\sim}{2}$

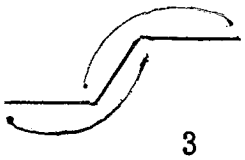

$\underset{\sim}{3}$

Structure $\underset{\sim}{3}$ can be written as $\underset{\sim}{3} = \underset{\sim}{1} - \underset{\sim}{2}$ and thus need not be considered. Orthogonalizing $\underset{\sim}{2}$ to $\underset{\sim}{1}$ leads to the structure

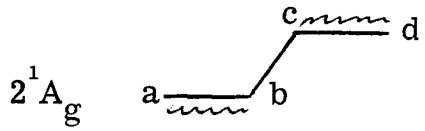

$\underset{\sim}{4}$

in which each of the π orbitals of a and b are coupled into a triplet state (indicated by wavy lines), the π orbitals of c and d are coupled into a triplet state but the four electrons are the coupled into a singlet state. Thus just as the ground state $\underset{\sim}{1}$ corresponds to combining a left ethylene singlet and a right ethylene singlet into an overall singlet, the wavefunction $\underset{\sim}{4}$ corresponds to coupling a left ethylene triplet and a right ethylene triplet into an overall singlet state. Both $\underset{\sim}{1}$ and $\underset{\sim}{4}$ have ^1A_g symmetry in the $\underset{\sim}{C_{2h}}$ symmetry group. Structure $\underset{\sim}{1}$ corresponds closely to the ground state of butadiene while $\underset{\sim}{4}$ corresponds to an excited state at ~ 7 eV. [Levin [28] carried out GVB calculations on the excited states of butadiene (but without the PP restriction) and showed that the GVB wavefunctions lead to the above description while the GVB energies are very close (0.2 eV) to those of a full π-CI.]

Combining four singly-occupied orbitals into triplet states leads to three linearly independent spin functions which can be written as

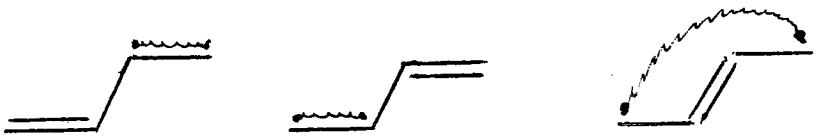

5 6 7

where the wavy lines indicate triplet pairing. Here 5 and 6 are orthogonal but correspond to coupling one triplet ethylene and one singlet ethylene to obtain an overall triplet state. Orthogonalizing 7 to 5 and 6 leads to

8

which corresponds to starting with two localized triplet ethylenes (as in 4) and combining their spins so as to obtain an overall (four-electron) triplet state. Structure 8 is of ^3B_u symmetry but 5 and 6 must be combined as

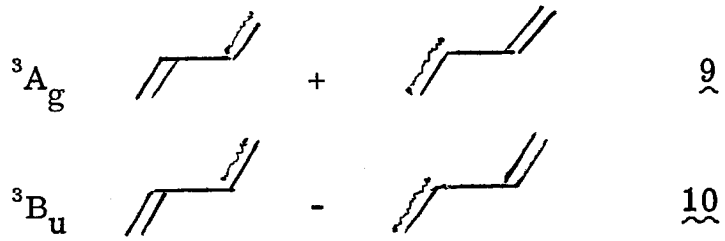

to obtain symmetry states of C_{2h}. Of these latter two triplet states, ^3B_u (10) is lower; the stabilization of 10 with respect to 5 is referred

to as the resonance energy. State ^3B_u (8) corresponds to exciting two ethylenes rather than one and hence is higher than either 9 or 10; ^3B_u (8) is related to $2\,^1A_g$ (4) but higher.

Summarizing, the VB model predicts a $1\,^1A_g$ (1) ground state; two triplet states, ^3B_u (10) and ^3A_g (9), at ~ 4 eV (a triplet excitation energy); and two states $2\,^1A_g$ (4) and $2\,^3B_u$ (8) at ~ 8 eV (twice the triplet excitation energy); in addition, there is a ^5A_g state slightly higher than these latter states.

Note that the VB description leads to two singlet states, both of ^1A_g symmetry. In order to obtain a ^1B_u state from four pπ orbitals, the VB description must utilize ionic configurations of the form

Self-consistent solutions (either HF or GVB) of the orbitals of the lowest ^1B_u state lead to one orbital that becomes quite diffuse (nearly Rydberg-like). As a result, we will postpone the discussion of the ^1B_u state to a subsequent paper dealing with Rydberg states. Here we will discuss only those states arising from non-ionic valence bond structures.

4.1 GVB calculations [15]

The ground state, $1\,^1A_g$, was studied using GVB(2/PP) with the two π bonds correlated and using GVB(5/PP) wavefunctions with the three CC σ bonds also correlated. For the lowest triplet (^3B_u) and the two lowest π positive ions (^2B_g and ^2A_u) we also carried out GVB(3/PP)

calculations with the three CC σ bonds correlated. In addition, for the lowest positive ion we also carried out a GVB(9/PP) calculation in which all nine σ bonds were correlated. The GVB orbitals from the ground state GVB(5/PP) calculations are shown in Fig. 2. In the GVB(9/PP) wavefunction for the ^2B_g state we found that the CC σ bond orbitals were essentially the same as in the 1 ^1A_g state (see Fig. 2); thus only the CH-like orbitals from this GVB(9/PP) calculation are shown in Fig. 3. All orbitals have qualitatively shapes of the form visualized in the simple valence bond description. It should be noted here that these orbitals are <u>not</u> forced to be localized; rather, this is the optimum form for maximizing electron correlation effects that emerge naturally from the GVB calculations.

4.2 GVB-CI calculations [16]

We considered three different basic types of CI calculations and various levels of excitation. In the simplest type, referred to as the π-CI, we considered only the π electrons of the various states. A second type of CI calculation was considered where the CC part of the σ structure was allowed to participate in the CI treatment. This type of CI was performed only for the ^1A_g singlet states and for the ^3A_g and ^3B_u triplet states. Finally, in the most complete set of calculations, referred to as all-valence CI, we included all the σ valence electrons.

In all the calculations and at all levels, we introduced <u>no</u> approximations for diagonalizing the CI matrix. The only restriction made in any calculation was on the level of excitation allowed.

4.2.1 π-CI calculations

In all of these calculations we allowed the four π electrons to readjust themselves among the eight π basis functions.

For these calculations we used the selfconsistent GVB π orbitals for each state with the exception of the ^3A_g state for which the ground-state GVB(5/PP) orbitals were used. The results of these calculations are shown in table 1 and compared with other calculations at the same level. It is important to notice the good agreement between the calculated and the experimental IP's for the ^2B_g and ^2A_u ions. This is an indication of the consistency of the calculations and allows us to use either the ground-state or ion state as the reference for calculating the transition energies.

4.2.2 π- CI's with partial inclusion of the σ structure

In these calculations we used as starting points the GVB(5/PP) wavefunction for the ground state and ^3A_g state and the GVB(3/PP) wavefunction for the ^3B_u state.

Our goal with these calculations is to get some insight into the importance of σ correlation for the various states as a preparative step for the all-valence CI calculations.

We considered up to double excitations in the σ GVB space but because of the larger size of the CI matrix (particularly for the triplets) we adopted intermediate levels of excitation in the π space. The strategy was first to consider all single excitations in the GVB σ space and for each configuration to include a full π-CI over the complete (eight MO's) π space; this is denoted as

$$[\text{full } \pi\text{-CI}] * [S(\sigma \rightarrow \sigma^*)]$$

or as CI-I. Following this we found an intermediate level of π-CI that would reproduce the results of CI-I to within 0.02 eV. Once this level was established, we then included double excitations in the GVB σ space.

For each state we will partition the eight π orbitals into two sets: four GVB orbitals from the GVB calculation and four remaining π orbitals referred to as the π virtual orbitals. From considerations of various restrictions on the π-CI portion of CI-I we found that the following CI (CI-II in table 2) leads to excitation energies within 0.02 eV (and to changes in the total energy by 0.08 eV) while reducing the size of the CI by a factor of 3. We carry out a full CI over the four GVB orbitals, and for each configuration we include all single excitations from each GVB orbital to each π virtual; this is denoted as

$$[\text{GVB}(\pi\text{-CI}) + \pi S] .$$

As an example of a more restricted CI, we report CI-III in table 2. This calculation included all single and double excitations within the GVB space plus, for each configuration, all single excitations from a GVB orbital to a virtual orbital. The result was errors of 0.17 to 0.54 eV in the excitation energies.

Next we included higher-order excitations in the σ space, CI-IV and CI-V; however, for a given level of π-CI, these σ excitations changed the excitation energies by only 0.02 eV.

The conclusions from these calculations are as follows:

a) σ correlation effects increase the $1\ ^1A_g$ - $2\ ^1A_g$ separation by 0.20 eV but have little effect (0.02 eV) on the lowest two triplet states.

b) An adequate level of CI is

$$[\text{GVB}(\pi\text{-CI}) + \pi\text{S}] * [\text{S}(\sigma \rightarrow \sigma^*)]$$

for the $2\ ^1A_g$ state and π-CI for the triplet states.

4.2.3 CI calculations including all valence orbitals

In this last step of our calculations we considered correlations involving all valence electrons (σ and π).

From the GVB(5/PP) and GVB(3/PP) calculations on the ground-state and on the ^3B_u state we obtained the corresponding pairs of natural orbitals for the (C–C) σ bonds. To obtain the natural orbitals corresponding to the (C–H) σ bonds one would solve for the GVB(11/PP) and GVB(9/PP) wavefunctions for the ground-state and triplet ^3B_u state, respectively. There are no computational difficulties in carrying out these calculations. However, because we also needed to carry out similar calculations for the nonvalence and Rydberg states, we used the following shortcut to generate these natural orbital pairs. We first solved for the GVB(9/PP) wavefunction of the ^2B_g positive ion state (the lowest ion state). Then we projected the first natural orbitals from the latter calculation onto the HF σ space of the ^1A_g and ^3B_u GVB wavefunctions, and the second natural orbitals onto the virtual (unoccupied) σ orbitals of the same wavefunctions. In this way we obtain a localized representation of the HF σ space nearly identical to that which would have been obtained from the first natural orbitals of a full GVB solution on the ^1A_g and ^3B_u states. In addition, we obtain a good approximation of the correlating (second natural) orbitals that would have been obtained from the full GVB calculations.

The results of the last section show that double excitations in the (C-C) σ space are not important to describe the valence excitation energies of the π system. Similarly, we would expect double excitations in the (C-H) σ space to be even less important. However, it is still possible that double excitations in the full σ space could be important. At this level of calculation, we have 22 electrons (18 σ + 4 π) distributed over 26 MO's (18 σ + 8 π). Consequently, we will examine ways of reducing the level of excitation.

We started with the study of the effect of single excitations in the σ GVB space. This set of CI calculations was performed based on the following strategy. From the full π-CI configuration list for each state, we selected all configurations contributing an energy lowering* of 0.001 h or more. From these selected configurations we allowed single excitations in the full π space times single excitations in the full σ space. To this list of configurations we added the complete configuration list for the full π-CI. The results of these calculations (CI-VI) are shown in table 3. The results do not differ appreciably from the ones obtained in the last section, that is, the transition energies are practically the same and nearly all configurations involving σ excitations come from excitations within the (CC) σ GVB space. Configurations involving excitations within the (CH) σ space contribute an energy lowering of the order of 0.0001 h and lower.

---

*The energy lowering of a configuration is defined as the difference in energy of the state when the given configuration is deleted from the full configuration list without reoptimizing the coefficients of the remaining configurations.

To investigate the effect of double excitations in the σ space, we recombined the localized pairs of natural orbitals to obtain a set of symmetry orbitals (reducing the number of configurations by a factor of two). We started again from the selected configurations of a full π -CI (now with symmetry orbitals) which contribute an energy lowering of 0.001 h and from those we allowed all single and double excitations (SD) in the σ space times all single excitations in the π space. We also added the full list of configurations relevant to the respective full π-CI's. The results of these calculations (CI-VIII) are also shown in table 3. Using the symmetry orbitals we repeated the first set of CI calculations (involving only single σ excitations) including now the configurations with an energy lowering of 0.0001 h in the selected list. The results of these calculations (CI-VII) reproduce those obtained in the last section, indicating that the effect of σ correlation can be well established using only the (C-C) σ subspace.

5. Hexatriene

We now proceed to describe the calculations carried out for the hexatriene molecule. Calculations were performed at the HF, GVB, HF-CI, and GVB-CI levels.

For the hexatriene molecule in the MO description the π electronic configuration is $(1a_u)^2\ (1b_g)^2\ (2a_u)^2$ with $E(1a_u) < E(1b_g) < E(2a_u)$, and the lowest unoccupied (valence) orbitals are $2b_g$ and $3a_u$ with $E(2b_g) < E(3a_u)$. The positive ion states generated from this configuration are, in order of increasing energy, 1^2A_u, ^2B_g and 2^2A_u. The lowest triplet state corresponds to the transitions $2a_u \rightarrow 2b_g$ and $2a_u \rightarrow 3a_u$ (or $1b_g \rightarrow 2b_g$) which lead to ^3B_u (lowest) and ^3A_g states. As discussed in section 4, the ^1B_u state requires diffuse basis functions and will not be discussed here.

The VB description of the π system of hexatriene leads to the five singlet states and nine triplet states of which we will discuss only the lower ones. The two lowest singlet structures are

1^1A_g 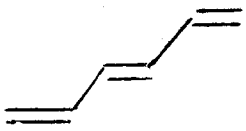 and 2^1A_g 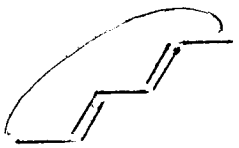

11 12

both of which correspond to ^1A_g states. Here 11 is the ground state and 12 is an excited ^1A_g state analogous to 2 for butadiene.

For the triplet state the lowest configurations are

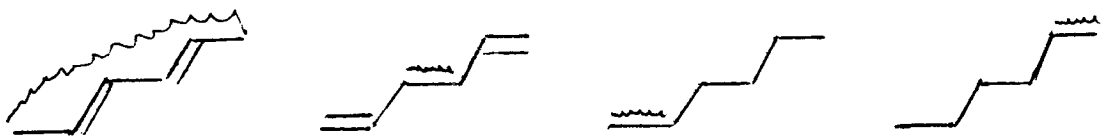

13 14 15 16

of which 13 and 14 lead to ^3B_u symmetry while 15 and 16 combine into one ^3B_u and one ^3A_g state.

5.1 HF and GVB calculations [15]

For a molecule of this size, GVB calculations of the same quality as those described for butadiene becomes costly. However, it is still possible to obtain good quality π natural orbitals for a CI calculation.

The ground state, $X\ ^1A_g$, was first solved self-consistently at the HF level. After that, the HF σ core was frozen and we calculated the GVB(3/PP) wavefunction for the π space. Following that, to allow for σ core relaxation, the π natural orbitals were frozen and we again solved self-consistently for the σ core. No significant changes were found, indicating that we can safely use the natural π orbitals from the GVB(3/PP) calculation with this frozen HF σ core.

Using the frozen HF σ core for the ground-state, we solved for a GVB(2/PP) wavefunction for the ^3A_g state. We solved for the three most stable VB structures, 13, 14, and 15. The transition energies calculated from these wavefunctions are 4.27 eV, 4.01 eV and 4.28 eV for structures 13, 14 and 15, respectively.

We also solved self-consistently at the HF level for the triplet ^3B_u state, for the π ions (^2A_u, ^2B_g) and for a valence singlet ^1B_u state. The transition energies computed at this level are shown in table 4.

Since there have been suggestions [4,17] that $\sigma \rightarrow \pi^*$ states could be responsible for transitions observed at 6.57-7.25 eV and 7.40 eV, we investigated these states. To do this we solved self-consistently for both ^1B_g and ^1A_u states using the ground-state orbitals and allowing the excitation from the highest occupied σ orbital to the π space. The result for these states are also shown in table 4.

5.2 HF-CI calculations [16]

These HF-CI calculations were carried out using the HF orbitals described above. All calculations were performed with the respective σ cores frozen, so we refer to them as π-CI calculations. Our DZ basis set furnishes 12 π MO's to describe the π space. Starting from the HF configurations for each state, we allowed up to quadruple excitations among the 12 π MO's. This level of excitation includes most of the correlation effects and yet leads to quite manageable calculations. The results of these calculations are shown in table 5. Again it is important to notice the excellent agreement between theoretical and experimental values of the ionization potentials (errors -0.12, 0.10, and 0.05 eV), indicating the consistency of the calculations.

As in the case of butadiene, the second $2\,^1A_g$ state (calculated at 5.62 eV) is significantly above the dipole allowed $1\,^1B_u$ state (experimental origin at 4.95 eV).

For the $\sigma \rightarrow \pi^*$ states the CI calculations were performed (now with seven electrons in the π space) allowing up to quadruple excitations. The results of these calculations are also given in table 5. These states are calculated to be at 9.18 eV and 11.51 eV. Thus, even considering that these are results of a partial CI treatment, it is quite improbable that refinements could lower their energy (by 2 to 4 eV) down to ~ 7 eV. Our conclusion is that these $\sigma \rightarrow \pi^*$ states cannot be responsible for the observed transitions. Rydberg and nonvalence states are more likely to occur in those regions, as will be shown in a forthcoming publication.

The results for the triplet states are in good agreement with experiment but a better description can be obtained from the GVB wavefunctions as will be discussed below.

5.3 GVB-CI calculations [16]

To perform these calculations we used the orbitals obtained from the GVB calculations described in section 5.1.

As discussed in section 3, we know that GVB wavefunctions already have some correlation effects built in, and that other effects not originally present can easily be incorporated in a CI treatment. Thus we expect (at least for the lower excited states) that a good description can be obtained from CI calculations using the GVB space.

In general we try to represent the excited states with a partial or full CI in the GVB space plus single excitations to the virtual space to allow for orbital readjustments.

In the first set of calculations we performed a full π-CI in the GVB space allowing single excitations to the virtual space, denoted as [GVB(π-CI)] * [πS]. The results of these calculations are shown in table 6. It is important to emphasize that the size of the CI matrix for these GVB-type CI's is considerably smaller (for example, for the ^1A_g states: 3800 spin eigenfunctions for HF-CI and 1435 spin eigenfunctions for GVB-CI) than the ones generated at the HF-CI level. One can see from table 6 that these calculations exactly reproduce the results of HF-CI calculations. For the sake of comparison we also performed this type of CI calculation for the butadiene molecule, and the results are also shown in table 6.

Our final goal with these GVB-CI-type calculations was to establish an intermediate level of excitation in the GVB space such as to reproduce the results of full π-CI calculations. Even more ambitious would be to find a level of description where the valence states (and possibly the ions) could be described in terms of the ground-state wavefunction within certain well-established limits. The existence of such a level would allow us to treat even larger polyene molecules at moderate costs. Table 7 shows the results of such a calculation for the butadiene and hexatriene molecules [based on the GVB(5/PP) wavefunction for butadiene and the GVB(3/PP) wavefunction for hexatriene]. Thus a CI calculation with up to triple excitations in the GVB

space and allowing single excitations into the virtual space furnishes results of the same quality as a full π-CI calculation (except for the butadiene ions and for the first hexatriene ion).

6. Discussion

From the results presented above we conclude that the valence states of these polyene molecules can be correctly described at a π-CI level with the exception of the 2^1A_g states (where the π-CI excitation energies are ~ 0.25 eV too low).

Figure 4 summarizes our best estimates of the transition energies for the valence states and ion states of butadiene and hexatriene.

The triplet states for both butadiene and hexatriene molecules are in good agreement with experiment. For the hexatriene molecule the $\tilde{c}\ ^3B_u$ and the $\tilde{d}\ ^3A_g$ states have not been identified experimentally. Our calculations (fig. 4) predict them to occur at 5.1-5.2 eV and 6.92 eV, respectively. The $\tilde{c}\ ^3B_u$ state is probably masked by the strong $X^1A_g \rightarrow 1^1B_u$ transition which occurs in the same region [7]. The second $\tilde{d}\ ^3A_g$ state occurs in a region exhibiting several features [7] (usually attributed to singlet transitions). It is possible that a careful examination of each feature by means of a variable angle electron impact experiment could reveal this state.

About the $\sigma \rightarrow \pi^*$ transitions in hexatriene, they are far too high to explain the features observed at 6.57-7.25 eV and 7.40 eV. These transitions are more probably due to non-valence and Rydberg states, as will be discussed in a forthcoming publication.

A special comment has to be made about the second singlet $2\,^1A_g$ states concerning their nature and location. There have been suggestions that this state would occur below the strong dipole-allowed state ($1\,^1B_u$), based on interpretation of experimental results in larger polyenes [18, 19]. Results of semi-empirical π-type calculations were used to support this hypothesis despite the fact that the ordering of the excited states depended on the level of excitation considered [20, 21]. For butadiene ab initio calculations [22] as well as recent multiphoton [9] and electron-impact studies [5, 7] do not show evidence for the existence of such a state below the ^1B_u state. Table 8 shows our results for different levels of π-CI for the singlet ^1A_g states and for the non-valence ^1B_u state for butadiene. At no level of excitation does the second ^1A_g state occur below the ^1B_u state. This is also true for the hexatriene molecule. This clearly shows the inadequacy of the approximate π-type theories to describe these states. Our conclusion from the theoretical and experimental studies is that (for the ground state geometry) there is <u>no</u> singlet state occurring below the origin for the $1\,^1B_u$ state of butadiene and hexatriene. Another look at table 8 shows an interesting results. While the excitation energies for the $2\,^1A_g$ state do not differ appreciably in going from a full π-CI to SD-πCI, it is considerably larger at the single excitation level. This is consistent with the fact that this state is mainly a doubly-excited state. Dunning [22a] has discussed the possibility of representing the excited states of butadiene in terms of excitonic structures. He showed that the $2\,^1A_g$ state could be described in terms of two ethylenic T (triplet) structures, a description that was confirmed by Levin [28] with full GVB calculations. This is exactly the picture that

results from our CI calculations at every level (with the obvious exception to the S π-CI level) when using the orbitals from the GVB(5/PP) wavefunction. It could be argued that this result is somehow biased because of the localized nature of the GVB(5/PP) wavefunction. However, even using delocalized π orbitals, the $2\,^1A_g$ state is dominated by doubly-excited configurations (but with increased contributions from singly-excited configurations). The same results are obtained for hexatriene. These results lead us to the conclusion that the $2\,^1A_g$ state is a doubly-excited TT-like state. (In valence bond language, such a state corresponds to an orthogonal spin coupling, i.e., a different bonding structure.) The results for butadiene show that the $2\,^1A_g$ state may be shifted 0.2 to 0.3 eV by σ readjustments. We did not perform comparable calculations on the hexatriene molecule but a similar effect is expected; assuming effects of the same magnitude as in butadiene, the $2\,^1A_g$ state should occur at approximately 5.87 eV for the hexatriene molecule.

A simple estimate can be made of how long the linear polyene has to be before the 2^1A_g state occurs below the 1^1B_u state. The experimental values of the 1^1B_u transition energies for butadiene, hexatriene and octatetraene were used in an exponential fit against chain length together with the fact that the value of this transition should converge asymptotically to $\sim 18,000\ cm^{-1}$ (2.23 eV) as the chain length increases indefinitely [1]. The calculated 2^1A_g transition energies were fitted to another exponential. From these curves we find that the $2\,^1A_g$ state should occur below the $1\,^1B_u$ state for the case of 1,3,5,7,9,11-dodecahexane (12 carbon atoms and six double bonds).

There exists some experimental evidence that a g state does lie below the ^1B_u in diphenyl octatetraene (DPO) and diphenyl hexatriene (DPH) [10]. If these assignments are correct, a possible explanation is that the $2\,^1A_g$-like states are strongly stabilized by conjugation with the ring. The fact that they are more affected than the corresponding ^1B_u states might be attributed to the non-valence character of these latter states.

The calculations for the ion states help resolve some assignments on the photoelectron spectra of these molecules.

For the butadiene molecule there has been some controversy about whether the second band at 11.4 eV in the photoelectron spectra should be assigned as ionization out of the lowest π orbital ($1a_u$) or out of the highest (a_g) σ orbital [23]. Semi-empirical calculations [24] have suggested that the highest occupied σ orbital should lead to a lower IP than the 1π (a_u) orbital. Our calculations clearly assign the 11.4 eV band to the ^2A_u π ion, resulting from the removal of one electron out of the π (a_u) orbital. This result is in agreement with recent experiments using variable angle photoelectron spectroscopy [25].

For hexatriene, a similar situation exists in the literature. Semi-empirical calculations [26] predict the highest σ (a_g) occupied orbital to occur above the lowest π orbital ($1a_u$). In this case the photoelectron spectrum [27] is not sufficiently resolved in the region of the band, at 11.60 eV, to allow a more detailed analysis. Our calculations are in excellent agreement with the first two experimental IP's and places the third π ion at 11.55 eV. This leads us to conclude that the third band in the photoelectron spectrum is due to the third π ion state, 2^2A_u.

7. Summary

The main conclusions of our calculations are:

a) the valence states of these polyene molecules can be accurately described at a π-CI level. The largest error is for the $2\ ^1A_g$ states where excitation energies are $\frac{1}{4}$ eV too low;

b) to correctly describe the $2\ ^1A_g$ states, it is necessary to include σ correlation effects. These states are mainly doubly-excited states and they occur significantly above the origin for the $1\ ^1B_u$ state;

c) the effects of σ correlation on the valence states can be well established using only the subspace of (C-C) σ orbitals;

d) for alternate polyenes a good approximation to the GVB(n/PP) wavefunction with the $2n\ \pi$ electrons correlated can be obtained by carrying out an HF calculation on the ground state followed by a GVB(n/PP) calculation on just the $2n\ \pi$ orbitals (keeping the σ HF space fixed). From this wavefunction accurate values for the transition energies of the valence states can be obtained. This is an important conclusion since it establishes the possibility of extending this type of calculation to larger polyene molecules at moderate costs;

e) the first two ions of butadiene and the first three ions of hexatriene correspond to removal of one electron out of the π orbitals of these molecules. This result is of importance in assigning the photoelectron bands of these molecules.

Acknowledgments

One of the authors (MACN) acknowledges the Conselho Nacional de Pesquisas (Brasil) for financial support and the Universidade Federal do Rio de Janeiro for a leave of absence. This work was supported by grants from the National Science Foundation (CHE73-05132) and the NIH (GM-23971) National Institute of General Medical Sciences. Computing assistance was obtained from the Health Sciences Computing Facility of the University of California, Los Angeles, supported by the National Institutes of Health, Research Resources Grant RR-3.

Table 1

Results of full π-CI calculation for the valence states of butadiene[a]

State	Experimental	Present Results	Dunning et al.[b]	Shih et al.[c]
$X\,^1A_g$		-154.92796	-154.94105	-154.9181
$2\,^1A_g$		6.83	6.77	6.67
$\tilde{b}\,^3A_g$	4.93[d]	5.10	5.04	4.95
$\tilde{a}\,^3B_u$	3.22[d], 3.20[e]	3.35	3.45	3.24
^2B_g	9.00[f]	8.87		
^2A_u	11.50[f]	11.32		

a) Ground state energies in hartrees, transition energies in eV.

b) Ref. [22a].

c) Ref. [22c].

d) Ref. [5a].

e) Ref. [8].

f) Ref. [25].

Table 2

Effect of CC σ correlations on the valence states of butadiene

CI-type and ground state energy (hartrees)	Transition energies (eV) $2\,^1A_g$	$1\,^3B_u$	$1\,^3A_g$
0: [Full π-CI] only (-154.92796)	6.83	3.35	5.10
I: [Full π-CI] $*$[S($\sigma \rightarrow \sigma^*$)] (-154.97613)	7.01	3.37 (3.58)[a]	5.29[a]
II: [GVB(π-CI)] $*$[πS] $*$[S($\sigma \rightarrow \sigma^*$)] (-154.97301)	7.03	3.35 (3.55)[a]	5.29[a]
III: [GVB(SDπ-CI)] $*$[πS] $*$[S($\sigma \rightarrow \sigma^*$)] (154.96893)	7.18	3.54 (3.90)[a]	5.83[a]
IV: [GVB(π-CI)] $*$[πS] $*$[SD($\sigma \rightarrow \sigma^*$)] (-155.00416)	7.05		
V: [GVB(Sdπ-CI)] $*$[πS] $*$[SD($\sigma \rightarrow \sigma^*$)] (-155.00022)	7.18	3.57 (3.90)[a]	5.83[a]

a) These numbers were based on a CI using the orbitals of the ground state GVB(5/PP) wavefunction rather than the self-consistent excited state orbitals. The resulting error in the excitation energy is about 0.20 eV for CI-I and CI-II and about 0.35 eV for CI-III and CI-V.

Table 3

Effect of CH and CC σ correlations for the valence states of butadiene.[a] [See Sec. 4.2.3 for details on the configuration selection procedure.]

CI Calculation	Transitions Energies (eV)				
	$2\,^1A_g$	$a\,^3B_u$	$b\,^3A_g$	$1\,^2B_g$	$1\,^2A_u$
II: [GVB(π-CI)]*[πS]*[S_{CC}(σ→σ*)][a]	7.03	3.35	5.29		
VI: [SELπ-CI]*[S(σ→σ*)][b]	7.04	3.35	5.30	8.93	11.37
VII: [SELπ-CI]*[S(σ→σ*)][c]	7.06	3.34	5.33		
VIII: [SELπ-CI]*[SD(σ→σ*)][d]	7.08	3.36	5.31	8.95	11.40
Experimental Results		3.22[e]	4.93[e]	9.00[g]	11.50[g]
		3.20[f]			

a) Only CC sigma excitations.
b) Transition energies relative to the ground state, $X\,^1A_g$, at -155.00866 hartrees.
c) Transition energies relative to the ground state, $X\,^1A_g$, at -155.00783 hartrees.
d) Transition energies relative to the ground state, $X\,^1A_g$, at -155.01537 hartrees.
e) Ref. [5a].
f) Ref. [8].
g) Ref. [25].

Table 4

Hartree-Fock transition energies for the valence states of 1,3,5-hexatriene

State	Transition Energy (eV)
$X\,^1A_g$ (-231.72322 hartree)	0
^1B_u (valence, $2a_u \rightarrow 2b_g$)	6.02
^3B_u ($2a_u \rightarrow 2b_g$)	2.71
^2B_g (ionize $1b_g$)	10.33
^2A_u (ionize $2a_u$)	7.23
^1B_g ($\sigma \rightarrow \pi^*$)	9.56
^1A_u ($\sigma \rightarrow \pi^*$)	11.99

Table 5

HF-π-CI results for the valence states of 1,3,5-hexatriene

State	ΔE(eV)	
$X\,^1A_g$ (-231.81913 h)		
$2\,^1A_g$	5.62	
$1\,^1B_u$ (valence)	6.56	
$1\,^1A_u$ ($\sigma - \pi^*$)	11.51	
$1\,^1B_g$ ($\sigma - \pi^*$)	9.18	
$\tilde{a}\,^3B_u$ ($2a_u \rightarrow 2b_g$)	2.73	2.61(1.9-3.5)[a], 2.57[b], 2.58[c]
$\tilde{b}\,^3A_g$ [f]	4.37	$\approx$4.2[d], 4.11[a] (3.6-4.6)
$\tilde{c}\,^3B_u$ [g]	5.28	
$1\,^2A_u$ (ionize $2a_u$)	8.33	8.45[e]
$2\,^2A_u$ (ionize $1a_u$)	11.55	11.60[e]
$1\,^2B_g$ (ionize $1b_g$)	10.53	10.43[e]

a) Ref. [7].

b) N. G. Minnaard and E. Havinga, Rec. Trav. Chim. 92 (1973) 1179.

c) D. F. Evans, J. Chem. Soc. (1960) 1735.

d) F. W. E. Knoop and L. J. Oosterhoff, Chem. Phys. Lett. 22 (1973) 247.

e) Ref. [27b].

f) Mainly a mixture of ($2a_u \rightarrow 4a_u$) (54%) and ($1b_g \rightarrow 3b_g$) (46%) configurations.

g) Equal mixture of ($1a_u \rightarrow 2b_g$) and ($2a_u \rightarrow 4b_g$) configurations.

Table 6

GVB-CI calculations for the valence states of butadiene and 1,3,5-hexatriene[a]

	[GVB(π-CI)]*[πS]	Full π-CI[b]	Exp. Results[c]
Butadiene			
$X\,^1A_g$[d]	-154.92506	-154.92796	
$2\,^1A_g$	6.84	6.83	
$a\,^3B_u$[e]	3.34	3.35	3.32,3.30,3.20
$b\,^3A_g$	5.10	5.10	4.80,4.93
Hexatriene			
$X\,^1A_g$[d]	-231.81497	-231.81913	
$2\,^1A_g$	5.62	5.62	
$1\,^1B_u$ (valence)	6.56	6.56	
$\tilde{a}\,^3B_u$	2.71	2.73	2.61
$\tilde{e}\,^3B_u$	5.20	5.28	
$\tilde{b}\,^3A_g$	4.32	4.37	4.2,4.11

a) As discussed in the text we used in these calculations the GVB(5/PP) wavefunction and the GVB(3/PP) wavefunction for the ground state and ^3B_u state of butadiene, respectively. For hexatriene we used the GVB(3/PP) wavefunction for the ^1A_g states and for the valence ^1B_u, and the GVB(2/PP) wavefunction for the triplet states.

b) For the case of the hexatriene molecule the results of this column correspond to HF π-CI's up to four excitations.

c) See tables 1 and 5 for references.

d) Ground state energies in hartrees.

e) For this particular state we really do not have a GVB π space. The full π-CI was restricted to the four more important orbitals in the full π-CI description, allowing single excitations to the remaining four orbitals.

Table 7

GVB-CI calculations for the valence states of butadiene and 1,3,5-hexatriene, using the respective ground state wavefunctions.

	[GVB(π-CI)]*[πS]	Full π-CI[a]
Butadiene		
$X\,^1A_g$[b]		-154.92796
$2\,^1A_g$	6.78	6.83
$\tilde{a}\,^3B_u$	3.43	3.35
$\tilde{b}\,^3A_g$	5.04	5.10
^2B_g	9.24	8.87
^2A_u	11.81	11.32
Hexatriene		
$X\,^1A_g$[b]	-231.80820	-231.81913
$2\,^1A_g$	5.70	5.62
^1B_u (valence)	6.78	6.56
$\tilde{a}\,^3B_u$	2.62	2.74
$\tilde{b}\,^3A_g$	4.20	4.37
$\tilde{c}\,^3B_u$	5.12	5.28
$1\,^2A_u$	8.25	8.45
$2\,^2A_u$	11.70	11.60
^2B_g	10.37	10.43

a) For the case of hexatriene the results of this column correspond to an HF-CI up to quadruple excitations.

b) Ground state energies in hartrees.

Table 8

Dependence of the transition energies to the $2\,^1A_g$ and ^1B_u of butadiene on the degree of excitation[a]

Calculation	$X\,^1A_g$ (hartrees)	$2\,^1A_g$ (hartrees)	$\Delta E(X\,^1A_g - 2\,^1A_g)$ eV	$\Delta E(X\,^1A_g - 1\,^1B_u)$ eV	$\Delta E(X\,^1A_g - 1\,^1B_u)$ eV non-vertical
S	-154.86460	-154.58811	7.52		5.44
SD	0.92532	0.67096	6.92	6.74	6.44
SDT	0.92565	0.67630	6.78	6.72	6.41
Full π-CI	0.92796	0.67665	6.83	6.79	6.47

a) This geometry corresponds to all C-C bonds equal to 1.40 Å (with the double bond between the middle carbon atoms) and a symmetric 0.8° degrees CC bending. The CI results were obtained using a GVB(4/PP) wavefunction.

References

[1] For a recent review see B. Hudson and B. Kohler, Ann. Rev. Phys. Chem. 25 (1974) 437.

[2] B. Honig and T. Ebrey, Ann. Rev. Biophys. Bioeng. 3 (1974) 151.

[3] R. McDiarmid, J. Chem. Phys. 64 (1976) 514.

[4] R. M. Gavin Jr. and S. A. Rice, J. Chem. Phys. 60 (1974) 3231.

[5] O. A. Mosher, W. M. Flicker and A. Kuppermann, J. Chem. Phys. 59 (1973) 6502; W. M. Flicker, O. A. Mosher and A. Kuppermann, Chem. Phys., in press.

[6] D. E. Post Jr., W. M. Hetherington III and B. Hudson, Chem. Phys. Lett. 35 (1975) 259.

[7] W. A. Flicker, O. A. Mosher and A. Kuppermann, Chem. Phys. Lett. 45 (1977) 492.

[8] J. H. Moore Jr., J. Phys. Chem. 76 (1972) 1130.

[9] P. M. Johnson, J. Chem. Phys. 64 (1976) 4638.

[10] G. R. Holton and W. M. McClain, Chem. Phys. Lett. 44 (1976) 436.

[11] T. H. Dunning, J. Chem. Phys. 53 (1970) 2823.

[12] S. Huzinaga, J. Chem. Phys. 42 (1965) 1293.

[13] W. Haugen and M. Traetteberg in "Selected Topics in Structure Chemistry", P. Andersen, O. Bastiansen and S. Furberg, editors, Universitetsforlaget, Oslo, 1967, p. 113; M. Traetteberg, Acta Chem. Scand. 22 (1968) 628.

[14] For a more detailed discussion see for instance, W. A. Goddard III, T. H. Dunning Jr., W. J. Hunt and P. J. Hay, Acc. Chem. Res. 6 (1973) 368.

[15] The GVB calculations were carried out with the GVBTWO program (Bobrowicz-Wadt-Goddard). See F. W. Bobrowicz, Ph. D. Thesis, California Institute of Technology (1974).

[16] The CI calculations were carried out with the Caltech spin-eigenfunction CI program. See ref. [15].

[17] M. Karplus, R. M. Gavin Jr. and S. A. Rice, J. Chem. Phys. 63 (1975) 5507.

[18] B. S. Hudson and B. E. Kohler, Chem. Phys. Lett. 14 (1972) 299.

[19] R. L. Swofford and W. H. McClain, J. Chem. Phys. 59 (1973) 5740.

[20] K. Schulten and M. Karplus, Chem. Phys. Lett. 14 (1972) 305.

[21] J. Koutecký, J. Chem. Phys. 47 (1967) 1501.

[22] (a) R. P. Hosteny, T. H. Dunning, Jr., R. R. Gilman, A. Pipano and I. Shavitt, J. Chem. Phys. 62 (1975) 4764;
(b) R. J. Buenker, S. Shih and S. D. Peyerimhoff, Chem. Phys. Lett. 44 (1976) 385;
(c) S. Shih, R. J. Buenker and S. D. Peyerimhoff, ibid. 16 (1972) 244.

[23] D. W. Turner, C. Baker, A. D. Baker and C. R. Brundle, "Molecular Photoelectron Spectroscopy", Wiley-Interscience, London, 1970, p. 168.

[24] N. C. Baird and M. J. S. Dewar, Theoret. Chim. Acta, 9 (1967) 1.

[25] R. M. White, T. A. Carlson and D. P. Spears, J. Electron Spectrosc. 3 (1974) 59.

[26] C. Fridh, L. Asbrink and E. Lindholm, Chem. Phys. Lett. 15 (1972) 282.

[27] M. Beez, G. Bieri, H. Bock and E. Heilbronner, Helv. Chem. Acta 56 (1973); E. E. Astrup, H. Bock, K. Wittel and P. Heimbach, Acta Chem. Scand. A29 (1975) 827.

[28] G. Levin, Ph.D. Thesis, California Institute of Technology, 1974.

Figure Captions

Figure 1. experimental geometries of 1,3-butadiene and 1,3,5-hexatriene (angles in degrees, interatomic distances in Å). Both molecules are in the yz plane, with the z axis along the central CC bond and the origin at the central bond mid-point.

Figure 2. GVB pair orbitals for the ground state of butadiene. Long dashes indicate zero amplitude, solid lines and short dashes indicate positive and negative amplitudes, with a spacing of 0.05 atomic units between various contours.

Figure 3. GVB CH pair orbitals for the ^2B_g positive ion of butadiene. Same convention as fig. 2 is used for the amplitudes.

Figure 4. Best results for the transition energies (eV) of the valence states and ion states of butadiene and hexatriene.

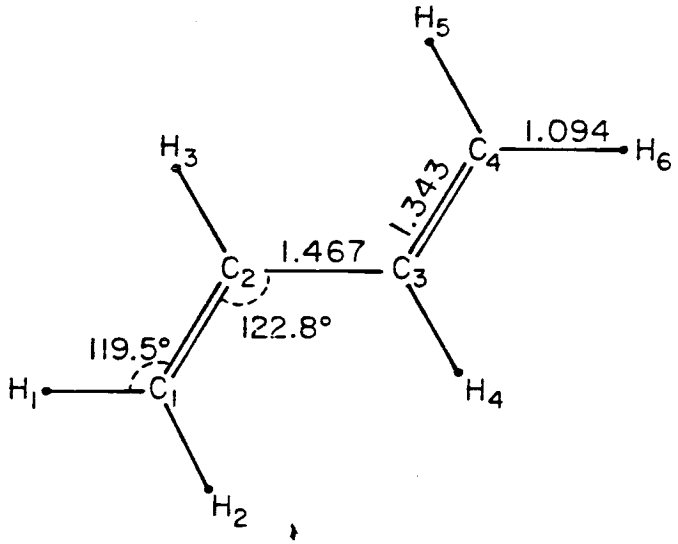

(a) 1,3-trans-butadiene

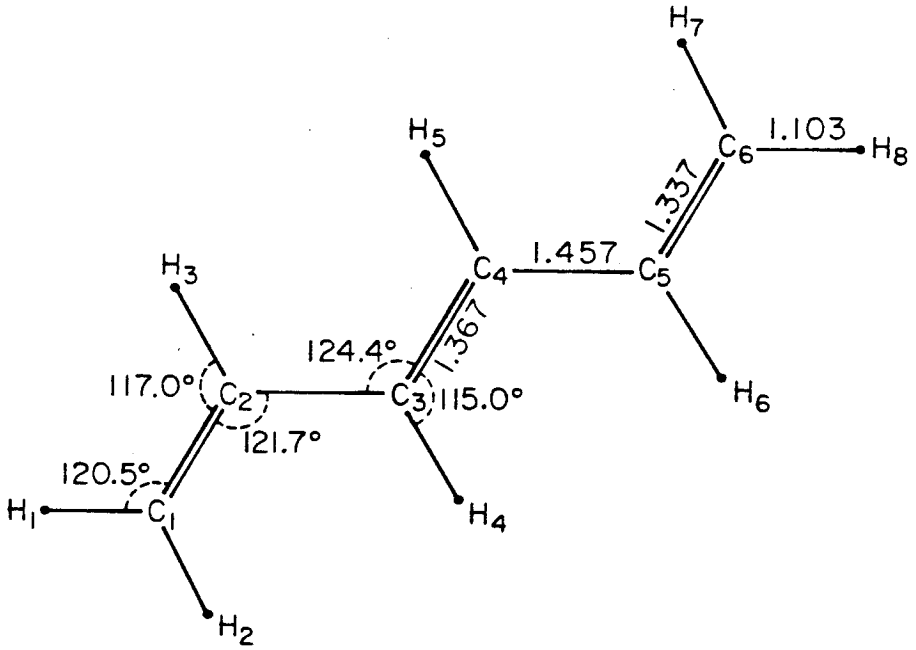

(b) 1,3,5-trans-hexatriene

Figure 1

GVB ORBITALS BUTADIENE ($X\ ^1A_g$)

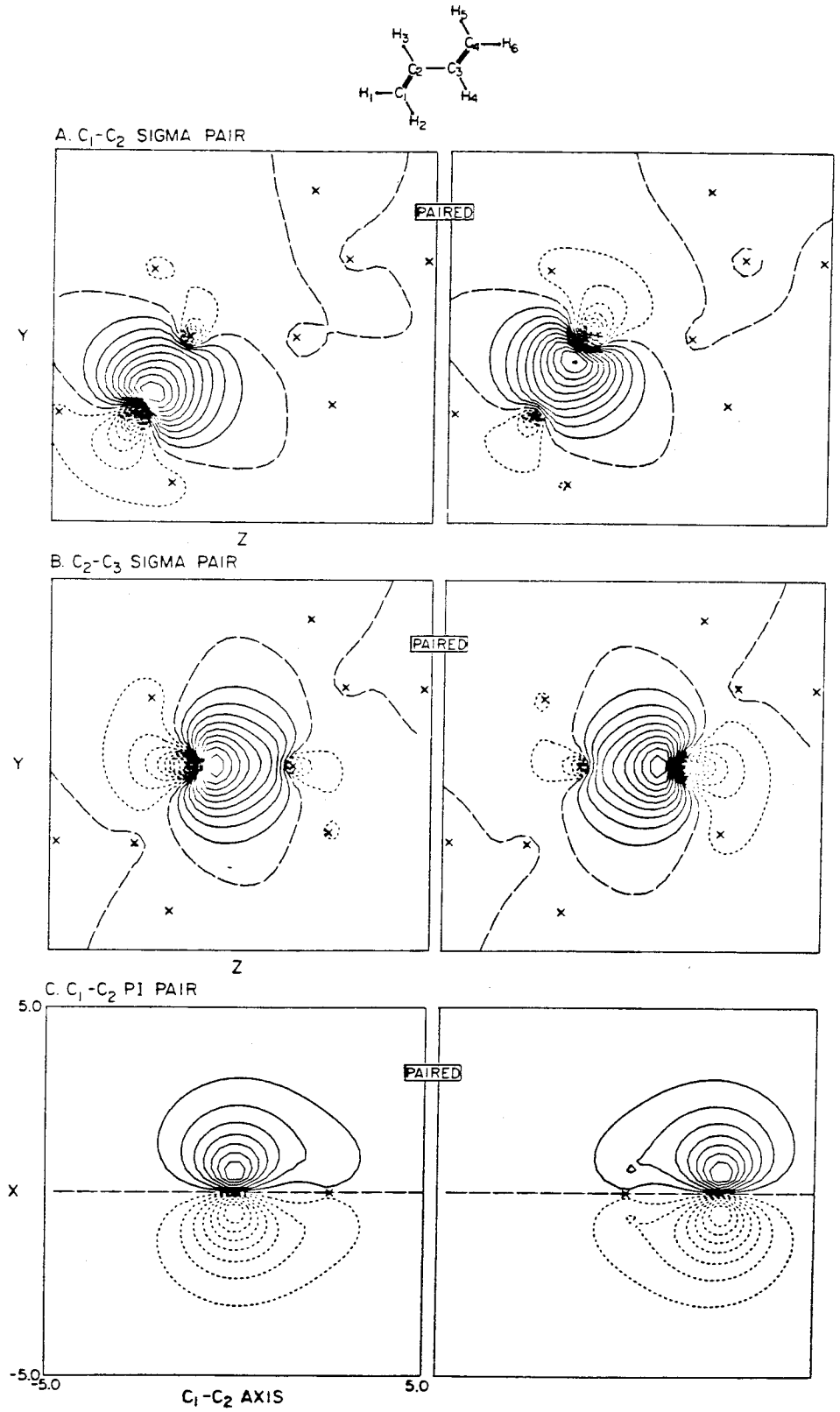

Figure 2

GVB ORBITALS BUTADIENE (^2B_g)

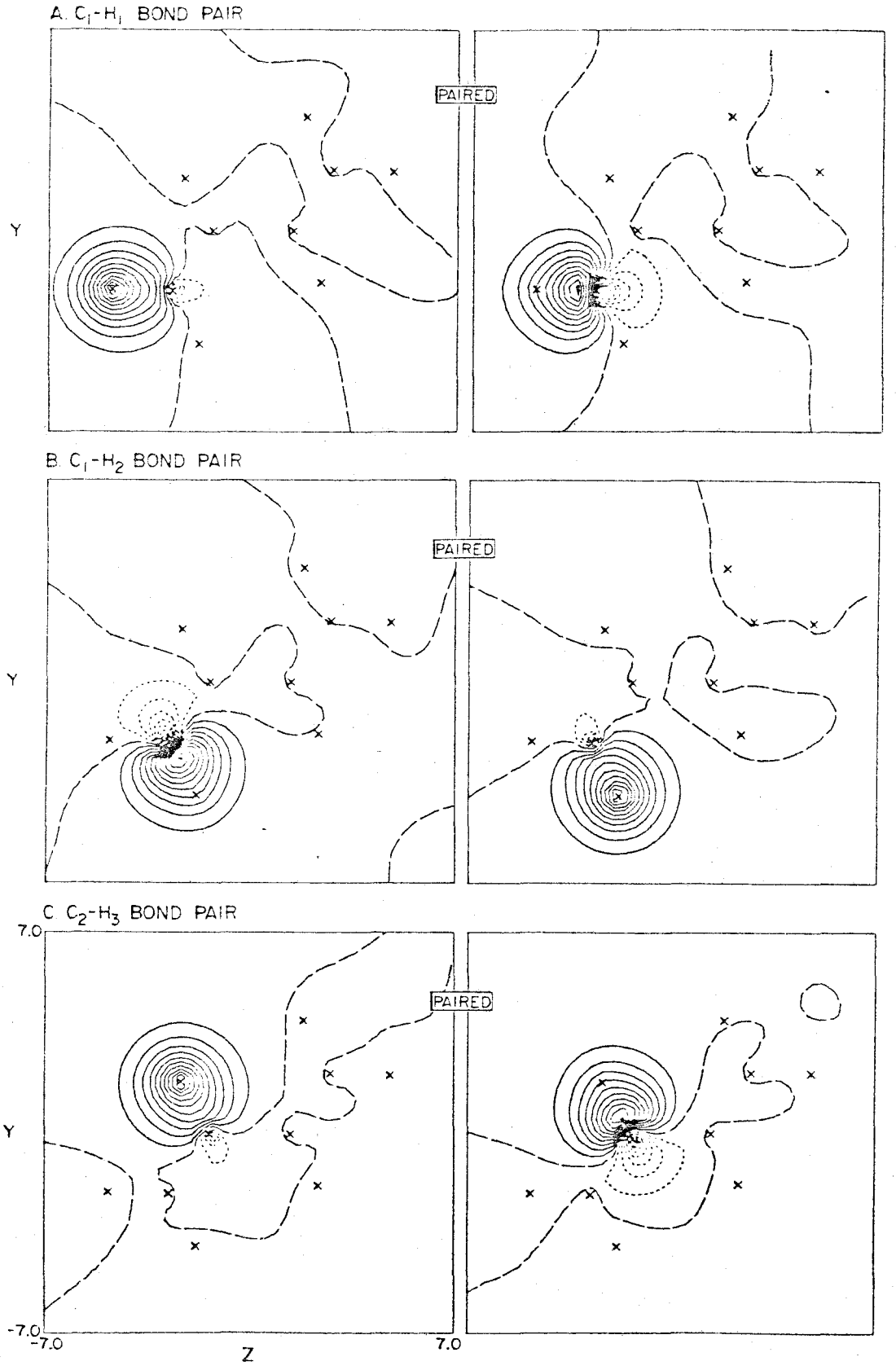

Figure 3

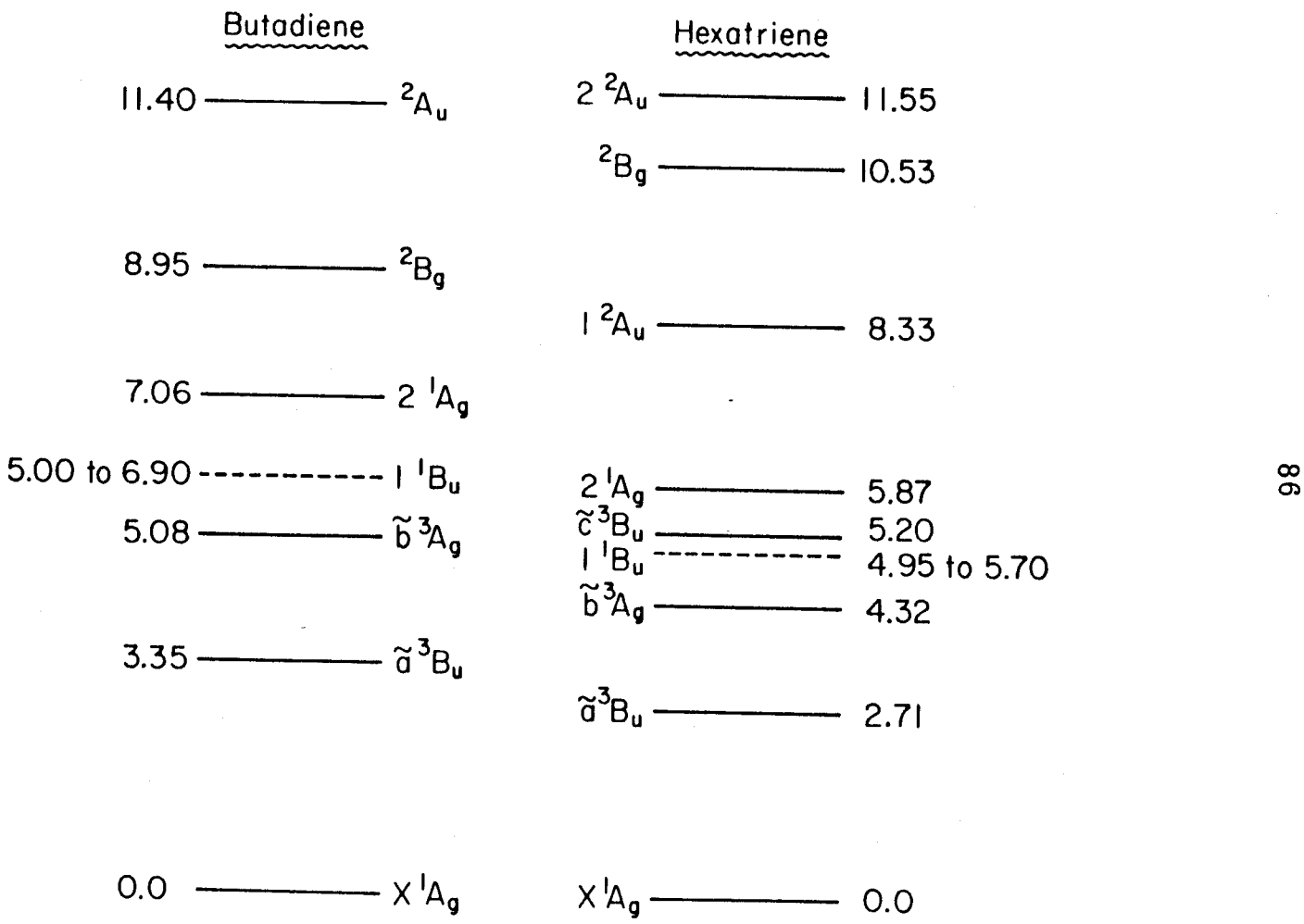
Butadiene
Hexatriene
11.40
^2A_u
$2\ ^2A_u$
11.55
^2B_g
10.53
8.95
^2B_g
$1\ ^2A_u$
8.33
7.06
$2\ ^1A_g$
5.00 to 6.90
$1\ ^1B_u$
$2\ ^1A_g$
5.87
5.08
$\tilde{b}\ ^3A_g$
$\tilde{c}\ ^3B_u$
5.20
$1\ ^1B_u$
4.95 to 5.70
$\tilde{b}\ ^3A_g$
4.32
3.35
$\tilde{a}\ ^3B_u$
$\tilde{a}\ ^3B_u$
2.71
0.0
$X\ ^1A_g$
$X\ ^1A_g$
0.0

Figure 4

SECTION B

A GENERALIZED VALENCE BOND DESCRIPTION OF THE NON-VALENCE AND RYDBERG STATES OF TRANS 1, 3-BUTADIENE AND TRANS-TRANS 1, 3, 5-HEXATRIENE MOLECULES

I. Introduction

Because of the role of particular polyenes in the photochemistry of vision there have recently been numerous experimental studies of the excited states of various polyenes.[1-16] However, there is still considerable uncertainty in both the nature and the assignment of even the smaller polyenes such as 1,3-trans-butadiene and 1,3,5-trans-hexatriene (hereafter referred to as butadiene and hexatriene, respectively).

In a previous publication (hereafter referred to as Part I),[17] we presented results of extensive ab initio generalized valence bond (GVB) and configuration interaction (CI) studies for the valence states of butadiene and hexatriene molecules. In this paper we complete the previous calculations with results for the non-valence and Rydberg states of these molecules.

For hexatriene we have considered only vertical transitions (same geometry as the ground state). For butadiene some exploration of the potential surface for the excited ^1B_u state (lowest $\pi \rightarrow \pi^*$) was carried out. These studies are used to assign the observed one- and two-photon spectra of butadiene and hexatriene.

II. Geometry and Basis Set

As in Part I, we used the ground state geometries as determined experimentally by electron diffraction techniques.[18] In the description of the valence states in Part I, we used the Dunning[19] (3s/2p, 2s) contraction of Huzinaga's[20] double-zeta (DZ) (9s/5p, 4s) gaussian basis set. This basis set was augmented with diffuse basis functions of 3s, $3p_{\sigma}$, $3p_{\pi}$, and $3d_{\pi}$ character in order to provide an adequate description of the Rydberg excited states.

III. Butadiene Rydberg States

In this section we describe the calculations performed for the Rydberg states of the butadiene molecule. The ^1B_u ($\pi \rightarrow \pi^*$) states will be discussed in the following section.

To understand the symmetry of the states that can be generated, we recall that (a) a simple molecular orbital (MO) description of butadiene leads to four π MO's, $1a_u$, $1b_g$, $2a_u$, and $2b_g$, in order of increasing energy. Thus the ground state corresponds to the electronic configuration $(1a_u)^2(1b_g)^2$; and (b) the molecular designation of the atomic orbitals in butadiene is ns = a_g; np = a_u, b_u; n_d = a_g, b_g; and nf = a_u, b_u.

The Rydberg state will have overall symmetries B_g ($1b_g \rightarrow ns, nd\sigma$), A_u ($1b_g \rightarrow np_\sigma, nf_\sigma$), A_g ($1b_g \rightarrow nd_\pi$), and B_u ($1b_g \rightarrow np_\pi, nf_\pi$). Transitions to the ^1A_u and ^1B_u states will be optically allowed while transitions to the ^1A_g and ^1B_g states will be forbidden.

A. Basis Sets. In order to describe the σ Rydberg excited states, we augmented the valence basis set with 12 diffuse basis functions of 3s, $3p_x$, and $3p_y$ characters ($\xi_{3s} = 0.023$, $\xi_{3p} = 0.021$) centered at each carbon atom. An IVO calculation[21] with this basis (referred to as basis A) provides an adequate description of the 3s, $3p_\sigma$, $3p_{\sigma'}$, $3d_\sigma$, $3d_{\sigma'}$, and $3d_{\sigma''}$ Rydberg orbitals.

In solving self-consistently (and also at the CI level) for the Rydberg states of butadiene it is desirable to
reduce the size of the basis set without sacrificing the accuracy of the results. To this purpose we performed several calculations at the IVO level, and these results are summarized in Table I.

From Table I we see that excluding the 3p basis functions (basis B) reduces the number of diffuse basis functions to four but at the sacrifice of serious errors in even the $3p_\sigma$ orbitals. On the other hand, from the plots of the 3s, $3p_\sigma$, and $3p_{\sigma'}$ orbitals in Fig. 1 (a, c, e) it appears that four off-centered 3s-like basis functions might adequately describe these states. Choosing appropriate coordinates (see Table I) for the 3s-like basis functions (basis C) leads to adequate results for the first four Rydberg states. Figure 1 (b, d, f) shows the first three Rydberg states obtained from the calculation with basis C (compare with Fig. 1a, c, d).

An alternative approach is to use both 3s and $3p_\sigma$ basis functions but to center them at the C_1-C_2 and C_3-C_4 bond midpoints. This basis (D) has half the diffuse basis from basis A but leads to an excellent description of the first five Rydberg orbitals. This approach was used for the calculations on the hexatriene molecule, and we recommend this approach for similar calculations on larger polyenes.

For the π Rydberg states we considered a basis augmented by one $3p_\pi$ basis on each carbon atom (basis E) and a basis with two $3p_\pi$ basis functions at each carbon atom plus a set of $3d_\pi$ basis functions at the C_1-C_2 and C_3-C_4 bond midpoints. From Table I we see that basis E is quite accurate for the $3p_\pi$ Rydberg orbital but that the second $3d_\pi$ ($3d_{xz}$) orbital is off by 0.25 eV (compare with basis F).

B. Character of the Rydberg Orbitals. Although these orbitals have the overall characteristics expected from the designated names (3s, 3p, 3d, etc.), there are clear effects due to the influence of the molecule.

In Fig. 1 (a, c, e) we show the first three σ Rydberg orbitals (using basis A). These orbitals can be easily associated with the 3s(a) and the two $3p_\sigma$ (c, e) atomic orbitals. The molecule affects the 3s orbital in such a way that instead of its spherical symmetry, its shape (in the molecular plane) resembles more one of an ellipse with its major axis along the line joining the C_1C_4 carbon atoms. The two $3p_\sigma$ orbitals are less distorted but still rotated relative to the molecular coordinate system. If one uses the coordinate system shown in Fig. 1, the three orbitals in Fig. 1 (a, c, e) can be classified as 3s, $3p_{\bar{y}}$, and $3p_{\bar{z}}$.

In Fig. 2 (a, c, e) we show the three $3d_\sigma$ orbitals (using basis A). They also show clear distortion effects due to the molecule, but it is still possible to classify them in the ($\bar{x}$, $\bar{y}$, $\bar{z}$) coordinate system. Figure 2 (b, d, f) shows the same three orbitals in the $\overline{xz}$ plane. Comparison of their amplitude plots in both planes allows us to classify them as $3d_{\bar{z}^2}$ $3d_{\overline{yz}}$, and $3d_{\bar{x}^2-\bar{y}^2}$. Notice that while orbitals 2a and 2e seem to overlap, this is not the case because they are IVO orbitals of the same calculation and consequently orthogonal. This is more clearly seen in Figs. 2b and 2f. Also from Fig. 2c (or 2e) one would be tempted to classify the orbital as $3d_{\bar{y}^2-\bar{z}^2}$, but it really has to be associated with the $3d_{x^2-y^2}$ atomic orbital. It seems that the planarity of the molecule restricts most of its amplitude to the yz plane.

Figure 3 shows the 3p and $3d_\pi$ orbitals (using basis E). Interestingly enough, they are not rotated relative to the molecular coordinate system. Amplitude plots of the two $3d_\pi$ orbitals in both the yz and xz planes allow us to classify them as $3d_{xy}$ (a, b) and $3d_{xz}$ (c, d).

Figure 4 shows the two 4f orbitals (using basis E) in both xz and $\overline{xz}$ planes.

From Figs. 1, 2, 3, and 4 we see that even for a large molecule such as butadiene the shape of the Rydberg orbitals resembles very much the corresponding atomic orbitals. While the σ atomic orbitals leading to the Rydberg molecular orbitals seem to couple strongly (causing shape distortions and rotations), there appears to be much less coupling between the π atomic orbitals.

Table II shows transition moments computed using these orbitals and their spatial extension (given in terms of second moments).

C. Hartree-Fock and GVB Calculations. In this section we will describe the calculations performed on the Rydberg states at the Hartree-Fock (HF) and GVB levels.

1. ^1B_g and ^1A_u States. The ^1B_g and ^1A_u Rydberg states correspond to excitations out of the $1b_g$ (π) orbital to the 3s and $3p_{\bar{y}}$, $3p_{\bar{z}}$ orbitals. These transitions add one more electron to the σ space. We have not correlated the σ valence orbitals in the SCF calculations in order to avoid any additional constraints that might affect the various Rydberg states differently.

Using the IVO's obtained with basis set C [Table I(a)] as starting guesses for the excited orbitals, we solved self-consistently, at the HF level, for the ^1B_g [$1b_g(\pi) \rightarrow 3s$] and ^1A_u [$1b_g(\pi) \rightarrow 3p_\sigma$] Rydberg states.

2. ^1B_u and ^1A_g States. The ^1A_g and ^1B_u Rydberg states correspond to excitations out of the $1b_g(\pi)$ orbital to the $3d_\pi$ and $3p_\pi$ orbitals, respectively. Since they are both π states, we do not expect that correlating the σ valence orbitals will cause any constraints to the description of these states.

Using the IVO's obtained with basis set E (Table I) as starting guesses for the excited orbitals ($3p_\pi$ and $3d_\pi$), we constructed GVB(3/PP)[22] wavefunction for both the ^1A_g and ^1B_u states. These wavefunctions correspond to correlating the three $(C\text{-}C)_\sigma$ bonds.

Because the $^1A_g\,[1b_g(\pi) \rightarrow 3d_\pi]$ Rydberg state is not the lowest state of this particular symmetry, the GVB(3/PP) wavefunction will not represent the "pure" Rydberg state. Nevertheless, the self-consistent orbitals generated will be adequate to describe a diffuse open-shell state. The final description of this Rydberg state is obtained as a higher root of a CI calculation. It is very easy to distinguish, in the CI calculations, the Rydberg ^1A_g state from the valence X ^1A_g and 2 ^1A_g states, as will be discussed in the next sections.

The $^1B_u\,[1b_g(\pi) \rightarrow 3p_\pi)$ Rydberg state has the same symmetry as the strong dipole-allowed ^1B_u state observed experimentally (peak) at 5.95 eV. So, if this latter transition corresponds to a vertical transition (same geometry as the ground state), our GVB(3/PP) description should correspond to the ^1B_u state and not to the $3p_\pi$ Rydberg state. From now on we consider the vertical transition to correspond to the $3p_\pi$ Rydberg state and defer the discussion of the ^1B_u $(\pi \rightarrow \pi^*)$ state to the next section. It is interesting to note that there are indications, even at the IVO level, that the vertical transition should most probably correspond to a $3p_\pi$ Rydberg state. From Table I we can see that the Rydberg states with the same $\underline{\ell}$ quantum number occur close to each other. Of course, in a perfect "central field" they would be degenerate. Since the transitions to the $3p_\sigma$ states can be unambiguously assigned and since the π IVO state always occurs in the same region of the two

$3p_\sigma$ states, it is reasonable to suppose that this π state should correspond to the $3p_\pi$ Rydberg transition. As will be seen below, after these states are solved for self-consistently and the CI calculations are performed, the final states also occur in the same region of the spectrum.

D. Full π-CI Calculations. The first set of CI calculations[23] was performed using the respective HF or GVB wavefunctions obtained in the previous section.

For the singlet ^1B_g Rydberg states the π space was formed by the eight HF π MO's. To the diffuse self-consistent 3s orbitals we added three more σ orbitals, obtained from the IVO calculations, properly reorthogonalized to the occupied σ orbitals. Using these 12 orbitals ($8\pi + 4\sigma$) we performed a full π-CI while simultaneously allowing the σ electrons to readjust in the full σ space. The first CI root of this calculation corresponds to the 3s Rydberg state and the second one to the first $3d_\sigma$ Rydberg state. Table III shows the results of this calculations and compares them with other results obtained at the same level.

The ^1A_u ($3p_\sigma$) states were obtained by a similar calculation using the appropriate orbitals. The results are also shown in Table III.

For the ^1A_g ($3d_\pi$) Rydberg states we started from the GVB(3/PP) wavefunction described above. From our augmented basis set we obtain 12 π MO's. To these orbitals we added six π IVO's properly reorthogonalized to the occupied π MO's. Using this space (18 π MO's) we performed a full π-CI calculation. Four CI roots were obtained from this calculation in order to project out the ground state and the first valence excited ^1A_g states. These can be clearly distinguished from the Rydberg states. The first root is dominantly a closed-shell valence state, while

the second one is dominantly a double excited valence state. The next two roots correspond to dominantly single excited diffuse configurations and represent the Rydberg states. The results obtained for these Rydberg states are also shown in Table III.

For the ^1B_u states we proceeded in an analogous way. Starting from the 12 π MO's from the GVB(3/PP) calculation on the ^1B_u state, we added six π IVO's properly orthogonalized to the occupied π MO's and performed a full π-CI among the 18 π MO's. The results of this calculation are shown in Table III.

E. All-Valence CI Calculations. In this second set of CI calculations we allowed all but the C_{1S}-like orbitals to participate in the CI treatment.

In these calculations the CI matrices are considerably larger than the ones generated in the previous calculations. Because of this we have to limit ourselves to lower levels of CI excitations. In so doing, we follow exactly the same strategy used in Part I, where we examined σ effects on the valence states. Here we also used both localized and delocalized descriptions of these states.

The localized description calculation was designed to detect any flux of charge along the bonds in the σ space resulting from the redistribution of charge in the π space. To obtain the localized description of these states, one should have to solve, in principle, for at least a GVB(9/PP) wavefunction for each one of the states. There are no computational difficulties in carrying out these calculations, but they are too costly. It would be interesting to devise a simplified but physically meaningful way of obtaining the σ natural pairs. Since Rydberg states

correspond to excitation of an electron to an orbital that is in general much larger than the dimensions of the molecule, one can look at these states as being composed of one electron plus a residual positive core. Since all the Rydberg states with which we are dealing result from excitations out of the same π ($1b_g$) orbital, the remaining positive core will look quite alike for all these states. This positive core corresponds basically to the ^2B_g ion. Following this argument, we solved for a GVB(9/PP) wavefunction for the ^2B_g ion state. The first natural orbitals from this latter calculation were then projected onto the occupied HF σ core of each one of the Rydberg states. The second natural orbitals were projected onto the virtuals (unoccupied) HF space of each one of the Rydberg states. In this way we obtained a localized presentation of the HF σ space nearly identical to the one that we would have obtained from the first natural orbitals of a full GVB solution. In addition, we obtained a good approximation to the correlating (second natural) orbitals that would have been obtained from the full GVB calculations.

Once the localized description was obtained, we proceeded in exactly the same way as in Part I. We started from the full π-CI configuration lists of each one of the states and selected all the configurations contributing an energy lowering of 0.001 h or more. From these we allowed all single excitations in the π space times all single excitations in the full σ space. To these new lists we added the respective configuration lists corresponding to the full π-CI's described in the previous section. With these final lists we performed the CI calculations. The results of these calculations are shown in Table IV. We

did not find any special σ-π mixed effect, but again, as in the case of the valence states (Part I), all the important configurations involving σ excitations came from excitations within the (CC) σ subspace. If one compares the results in Table III and IV, one notices that the results of the full π-CI calculations do not differ appreciably from the present results, mainly for the first roots of each symmetry.

To study the effect of higher excitation levels, we recombined the natural orbitals to obtain a set of symmetry orbitals. In so doing we reduced considerably the number of configurations and that allowed us to increase the level of excitation.

With the delocalized description we first considered the same type of CI described above but now including all the configurations from the respective full π-CI lists that contributed an energy lowering of 0.0001 h or more. No appreciable changes were found relative to the previous CI. Next we started again from the selected lists including the configurations contributing an energy lowering of 0.001 h or more. From these configurations we allowed single excitations in the π space times (S + D) excitations in the σ space. To these lists we added the respective lists corresponding to the full π-CI's of the previous section. Again, no appreciable changes occurred and practically all the configurations including double excitations in the σ space involved the (C-C) σ subspace.

From these calculations one can conclude that the Rydberg states of butadiene can be very well represented at a full π-CI level. While not shown in Table III, it is also true that the first states of each symmetry can be well represented at intermediate levels of excitation

in the π space. Another conclusion that results from these calculations is that the σ effects can be well established using only the (CC) σ subspace.

As one can see, most of the electron spectra of trans-butadiene can be explained in terms of Rydberg transitions.

IV. The ^1B_u ($\pi \rightarrow \pi^*$) Transition

Most of our attention was directed to this particular state since it has bravely resisted all the theoretical descriptions so far. The initial motivation for our study of the electronic spectra of polyenes was basically to obtain the correct descriptions of these states. The initial idea[24] that finally proved to be not completely wrong came from a simple analysis of the VB description of these states. As discussed in Part I, while the ^1A_g states can be described mostly by covalent structures, the ^1B_u states need polar structures for their description. Such a large redistribution of charge in the π space should correspond to a complete readjustment of the σ structure. Because all the calculations (ab initio and semi-empirical) only considered π-CI's, the σ readjustments could not be properly accounted for. So we proposed[24] to investigate the effects of σ correlation in the ordering of the energy levels of polyenes.

In what follows we describe our attempts to correctly describe this state. We feel that it is more convenient to separate at this point the work performed on the vertical transition and on the non-vertical transition.

A. The Vertical Transition. This transition has been previously discussed in connection with the Rydberg states. At that point we assigned it to a Rydberg $3p_\pi$ state. It seems more appropriate to discuss it fully here since it was the failure to correlate this state with the ^1B_u ($\pi \rightarrow \pi^*$) state that led us to investigate the non-vertical transition.

The first set of calculations for this transition has been described before in Secs. III.D and III.E. We only want to add that besides the GVB(3/PP) calculation, we also performed a GVB(4/PP) calculation[22]

where we also correlated the (C_2-C_3) π bond. The GVB(4/PP) wavefunction gives a slightly better description of the state but when both wavefunctions are used to perform a full π-CI calculation, the results are practically the same. From Sec. III.A we know that at the full π-CI level the energy for this vertical transition is 6.79 eV, which is $\sim$ 0.8 eV higher than the experimental value for the ^1B_u ($\pi \rightarrow \pi^*$) transition.

We next decided to investigate the possibility of any stabilizations by resonance effects. For that we considered localized excitations and tried to describe the system as a ground state (N) ethylenic unit coupled with an excited (V) ethylenic unit. We cannot solve self-consistently for a localized ^1B_u state because it collapses into the X ^1A_g ground state (the C_{2h}, A_g, and B_u irreducible representations both correlate with the A′ representation of the C_s group). The alternative was to generate localized IVO's. To do that we started from the localized description of the ground state and calculated IVO's considering excitations from both localized C-C π orbitals. These IVO's, properly reorthogonalized to the occupied π orbitals of the GVB wavefunction for the vertical state, were used in a full π-CI calculation. No dramatic changes were observed and the localized excitation model was temporarily abandoned.

We next turned our attention to the original idea of including σ correlation effects.[24] While similar calculations have already been described for the Rydberg states, they were initially designed for the study of σ effects on the ^1B_u ($\pi \rightarrow \pi^*$) state.

Here we performed a more detailed calculation that the one previously described in Sec. III.E, starting with the inclusion of the (C-C)

σ subspace only. We started from the GVB(4/PP) wavefunction and chose the lowest level of π excitation that exactly reproduces the full π-CI description of the state. While the higher roots (n ^1B_u) have to be described at the full π-CI level, the first ^1B_u can be very well described by a π-CI up to double excitations. The three (C-C) σ natural orbitals were recombined to obtain symmetry orbitals. To the 12 π MO's used in the full π-CI calculation we added the six (C-C) σ orbitals. Using these 18 orbitals (12 π + 6 σ) we performed a CI calculation allowing up to double excitations in the π space times single excitations in the (C-C) σ subspace. At this level of calculation we obtained a transition energy of 6.68 eV.

In the next step of our calculation we included the full σ valence space. The natural orbitals for the (C-H)σ space were obtained from the corresponding natural orbitals of the GVB(9/PP) wavefunction for the ^2B_g ion. The procedure to obtain these orbitals has been described before (see Sec. III.E). Once the localized σ structure was obtained, we proceeded to perform the CI calculations in exactly the same way as described for the Rydberg states in Sec. III.E. The results obtained from this calculation followed the general trends observed before, i.e., that most of the σ effects can be described within the (C-C)σ subspace. One exception was observed, however, in which excitations from the (C-H) σ space to the (C-C) σ space were found to contribute an energy lowering much larger (0.001-0.004 h) than was previously observed in connection with the valence and Rydberg states. These configurations describe the mechanism

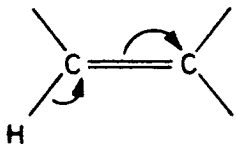

in which the net positive charge is left on the hydrogen atom instead of in the carbon atom. That this mechanism should provide some stabilization can be understood in terms of the relative electronegativities of carbon and hydrogen.

For the next CI calculation we recombined the natural orbitals to obtain a set of symmetry orbitals. Using this new set of orbitals we performed a similar CI calculation but now including in the selected list all the configurations from the full π-CI that contributed an energy lowering of 0.0001 h or more.

The results of the two last calculations are basically the same and the final value for the transition energy is 6.67 eV.

At this point in our calculations we are still $\sim$ 0.7 eV higher than the experimental value for the ^1B_u ($\pi \rightarrow \pi^*$) state.

Before looking at the possibility of a non-vertical transitions, we decided to investigate the influence of adding extra p_π and d_π basis functions to our basis set. It seems to be true that d functions play an important role in stabilizing the V(π-π^*) state of ethylene. So we decided to investigate its role in the stabilization of the vertical ^1B_u state of butadiene. The augmented basis set for this study corresponds to basis set E of Table I. The effect of the extra basis functions can be conveniently studied at the IVO level. From our experience we know that the transition energies from IVO's should not differ more than $\sim$ 0.4 eV (mainly for the first state of a particular symmetry) from the final value obtained after SCF optimization of the state and CI calculation. So, any drastic effects caused by the extra basis functions should be detected at the IVO level. If we look at Table I (basis set E)

we see that the inclusion of the extra basis functions did not affect at all the transition energy for the $3p_\pi$ state. On the other hand, the $3d_\pi$ Rydberg states showed an appreciable stabilization, which is quite reasonable. Besides that, the MO coefficients for the d functions are much smaller than the ones corresponding to the p basis functions, and our experience tells us that no drastic changes should be expected after the SCF calculation is performed. From these results we can conclude that the failure to describe correctly the ^1B_u ($\pi \rightarrow \pi^*$) state is not due to a basis set problem. We do not expect d functions to play any important role, at least for the description of the vertical transition.

Finally, we have computed the oscillator strength for the transition $X\ ^1A_g \rightarrow\ ^1B_u$ (vertical) using the full π-CI wavefunctions. This is not the best description of these states, and the oscillator strength (0.341) should not be taken absolutely but compared with the oscillator strength for the non-vertical state calculated at the same level of description. As we will see in the next section, the oscillator strength for the "non-vertical transition" is much larger.

It seems to us that from the results presented above, one can assign the vertical $X\ ^1A_g \rightarrow\ ^1B_u$ transition to a ^1B_u $3p_\pi$ Rydberg state. The only possibility left now for the ^1B_u ($\pi \rightarrow \pi^*$) is of a non-vertical transition.

B. Non-vertical Transitions. In this section we will describe our various attempts to describe the ^1B_u ($\pi \rightarrow \pi^*$) transition using optimized geometries for the excited state (referred to here as non-vertical transitions). We considered symmetric stretched and bent structures, asymmetric stretched structures, and twisted geometries. It will be

more convenient to describe each one of the changes in geometry separately.

Most of our study of these structures was performed at the GVB(1/PP) level corresponding to correlating the π bond between the middle carbon atoms. When, at this level, a reasonable change in energy relative to the vertical state was observed, the calculation was carried further on. For these particular structures a GVB(4/PP) wavefunction was constructed and used to perform full π-CI and π-CI with inclusion of the (C-C) σ subspace.

In all these calculations we used the same augmented basis set used to describe the vertical transition (basis E, Table I).

1. Symmetric Stretched Structures. Initially we considered only symmetric stretched structures.

In the first structure studied we simply inverted the double and single bonds relative to the ground state geometry. So, this structure corresponds to $(C_1\text{-}C_2) = (C_3\text{-}C_4) = 1.46$ Å and $(C_2 = C_3) = 1.34$ Å. At the GVB(1/PP) level, this structure is less stable than the vertical state but at the GVB(4/PP) level it is slightly more stable (0.0021 h).

Next we considered a set of structures where the $C_2\text{-}C_3$ double bond was kept fixed (1.34 Å) and the terminal bonds varied. Figure 5a shows the dependence of the GVB(1/PP) wavefunction energy on the terminal (C-C) bond distance. It is interesting to notice that the only structure that is more stable than the vertical state is the one corresponding to all (C-C) bonds equal to 1.34 Å. For this last structure we solved for a GVB(4/PP) wavefunction. No real improvement relative to the GVB(4/PP) description of the vertical transition was found.

Following that we decided to increase the middle (C-C) double bond and, keeping it fixed at 1.38 Å, we again varied the terminal (C-C) bond lengths. Here all the structures considered showed a reasonable stabilization ($\sim$ 0.27 eV) relative to the vertical transition. Figure 5b shows the dependence of the GVB(1/PP) wavefunction energy on the terminal (C-C) bond length. Interestingly enough, we again found that the most stable structure corresponded to all (C-C) bonds equal to 1.38 Å.

After that, we decided to increase further the (C_2-C_3) bond distance to 1.40 Å. Because of the previous results we first solve for the equal bond lengths structure, at the GVB(1/PP) level. After that we considered one structure with terminal bond lengths equal to 1.43 Å. This last structure was found less stable than the previous one (1.40 Å), and that was enough to establish that, again, the structure corresponding to equal bonds will be the more stable of this set of structures.

Relative to the previous sets of structures [with (C-C) = 1.38 and 1.34 Å], both structures of this set (1.40 Å) are more stable.

Following that, we further increased the double bond length to 1.43 Å and performed a GVB(1/PP) calculation for the case of all equal (C-C) bonds but we found the structure less stable than the ones with shorter bonds.

At this point we decided that the best structures should correspond to the all-equal (C-C) bond lengths and among these the one with (C_2-C_3) = 1.40 Å was the best. Figure 6 shows the dependence of GVB(1/PP) wavefunction energy on the (C-C) bond length for the equal bond structures.

For three of these structures [with $(C_2\text{-}C_3)$ = 1.34, 1.40, and 1.43 Å] we solved for a GVB(4/PP) wavefunction. Again, at this level the structure with $(C_2\text{-}C_3)$ = 1.40 Å was found to be the most stable. At this level of calculation, this last wavefunction corresponds to a stabilization of ~0.43 eV relative to the GVB(4/PP) wavefunction for the vertical transition.

Using this best structure, we performed a full π-CI calculation. We found at this level a transition energy equal to 6.47 eV. To include σ effects we first looked for the lowest possible level of excitation in the π space that would reproduce the results of a full π-CI calculation. We found that the state could be very well described considering up to double excitations in the π space. We then recombined the (C-C) σ bonds from the GVB(4/PP) calculation to obtain symmetry orbitals. Using these 18 orbitals (6 σ + 12 π) we performed a CI calculation allowing up to double excitations in the π space times all single excitations in the σ space. At this level of calculation we found a transition energy of 6.15 eV, which, when compared with the vertical transition energy (6.67 eV) gives us a good indication that the ^1B_u ($\pi \rightarrow \pi^*$) should correspond to a non-vertical transition. It is important to notice that while σ correlation stabilizes the vertical transition by 0.12 eV, for the non-vertical transition the same effect is of 0.32 eV, approximately three times larger!

2. Simultaneous Symmetric Stretch and Bend. The results of the last section were very stimulating and we decided to investigate if further stabilization could be accounted for in terms of bending modes. Since the difference between the observed state (at 5.95 eV) and the

state found in the last section is small, it is possible that low energy bending modes can provide further stabilization.

Starting from our most stable structure [with all (C-C) bonds equal to 1.40 Å] we investigated the effects of $-CH_2$ rocking and (C-C) bending. We followed here the same strategy used before. We looked at different geometries at the GVB(1/PP) level and, if any noticeable difference was found, we proceeded further on with GVB(4/PP) calculations.

We considered first the terminal $-CH_2$ rockings. Figure 7b shows the dependence of the GVB(1/PP) wavefunction energy on the angle of rocking. It is clear from the figure that this mode does not provide any stabilization.

Next we considered symmetric (C_1-C_2) and (C_3-C_4) bendings. Figure 7a shows the behavior of the GVB(1/PP) wavefunction energy with the angle of bending. We found a minimum at 0.8° corresponding to a stabilization of 0.0021 h relative to the unbent structure. Using this last structure, we calculated a GVB(4/PP) wavefunction that showed a stabilization of $\sim$ 0.0013 h relative to the GVB(4/PP) wavefunction of the unbent structure. Using this geometry, we performed a CI calculation including the (C-C) σ subspace analogous to the one described for the unbent structure. At this level of calculation we found a transition energy of 6.12 eV.

Using the full π-CI wavefunctions, we calculated the oscillator strength for the transition $X\ ^1A_g \rightarrow\ ^1B_u$, where the ^1B_u corresponds to the most stable bent structure above. We found a value of 0.636 which is to be compared with the oscillator strength for the vertical transition (0.341).

At this point it would be interesting to reinvestigate the importance of extra p and d basis functions in the description of the non-vertical state. To do this we included in our augmented basis the same set of p and d functions we used in our study of the vertical transition (see Sec. IV.A). Here we made use of IVO's again in the following way. We know that after solving self-consistently for the ^1B_u state $[\sigma(1a_u)^2 (1g_g)(1a_u)]$ if any IVO calculation is done using $\sigma(1a_u)^2(1b_g)^2$ as core, we obtain exactly the $2a_u$ orbital of the self-consistent calculation. So we expect that if the extra basis functions will cause any improvement in the $(2a_u)$ orbital, this should be apparent from the IVO calculation. The result of this calculation is that after including the extra basis functions the energy of the $2a_u$ orbital is practically the same (~ 0.01 eV lower). We also used the ground state core but no improvement was noticed. So, again it seems that the extra stabilization needed will not result from improvements in the basis set.

3. Asymmetric Stretch. Before we can conclude that any of the previously studied structures is the most favorable one for the ^1B_u $(\pi \rightarrow \pi^*)$ state, we have to examine further possible structures. With this intention, we performed a few calculations on asymmetric stretched and polar structures.

The use of asymmetric stretched structures naturally forces us to introduce polar form because it would be unreasonable to assume one terminal bond (in principle, completely equivalent to the other one) is larger than the other unless some charge transfer to one of the terminal carbon atoms is allowed.

Here the computational effort will be considerably larger since we have only one element of symmetry left, namely, the plane of the

molecule. This implies that the ^1A_g and ^1B_u states will now belong to the same irreducible representation (A′) of the C_s point group and that ^1B_u states can only be obtained at the CI level, after the ^1A_g states are projected out.

We initially solved for asymmetric structures of the type

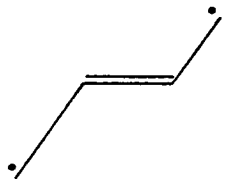

starting from the symmetrically stretched [all (C-C) = 1.40 Å] and varying one of the terminal bond lengths. We considered at the GVB (1/PP) level, structures with one of the terminal bonds equal to 1.54 Å (S1) and 1.64 Å (S2). The former structure (S1) was found to be the most stable. One cannot compare the energies of these structures with the symmetric stretched ones because at this level what we obtain is a bad description of the ground state (X ^1A_g) and not of a ^1B_u state.

Using structure S1 we performed a full π-CI calculation. The root corresponding to the ^1B_u state gives a transition energy of 7.16 eV. We did not perform similar CI calculations with the structure S2. The reason for that was not because that structure was found less stable than S1 structure at the GVB(1/PP) level (since that only tells us that a worse representation of the ground state is being obtained but does not say anything about the CI root corresponding to the ^1B_u state) but because we do not believe that a stabilization by $\sim$1.16 eV can be achieved only by increasing the terminal bond length by 0.1 Å.

4. Polar Forms. We next considered polar forms of the type

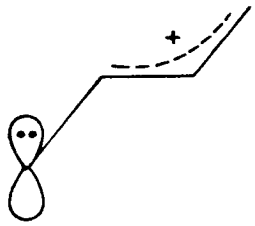

which can be viewed as formed by an allyl system attached to a $-CH_2$ group. The bond distances in the allyl group were kept equal to 1.40 Å (which, by the way, happens to be equal to the optimized bond distance for the allyl group) and we solved for different values of the terminal bond.

We considered two different values of the terminal bond length (1.54 and 1.64 Å) and solved for a GVB(2/PP) wavefunction for each one of these structures. To force the system to retain its polar structure we put in different "classes" the basis functions corresponding to the atoms of the allyl group and the ones corresponding to the terminal $-CH_2$ group. That forces the hamiltonian matrix to be block-diagonalized in such a way that these two classes do not mix. The GVB(2/PP) wavefunctions correspond to correlating the π bond in the allyl group and the electron pair in the p orbital at the terminal carbon atom. To properly describe in-out correlations in the terminal atom we added to the augmented basis set an extra p_π basis function on each carbon atom. This extra basis function was scaled in such a way that its exponent (ζ = 0.05) is in geometric progression with the outer p exponent of the double-zeta basis set and with the diffuse p (ζ = 0.021) basis function previously added.

At the GVB(2/PP) level the structure with a terminal bond equal to 1.54 Å is slightly more stable, but at the full π-CI level they give practically the same description of the root corresponding to the ^1B_u state. This state is found at $\sim$7.0 eV. The second root of these CI calculations is a doubly-excited valence state (at $\sim$6.6 eV) which corresponds to the $2\,^1A_g$ state. The interesting thing is that in both CI calculations the dominant configuration for this state ($2\,^1A_g$) contains an excitation of one of the electrons of the terminal carbon atom back to the allyl system. This is in accordance with the fact that covalent structures are more important than polar structures in describing the ^1A_g states.

We did not try to include σ effects in any of the calculations described in this section because we do not believe that these effects could be responsible for the necessary stabilization ($\sim$1 eV). Besides that, the size of the CI matrices become very large because of the reduced symmetry and the necessity of solving for at least three roots makes the calculations impractical.

5. Twisted Geometries. We finally looked at the effect of twisting the terminal $-CH_2$ group. Experimental results suggest and theoretical calculations seem to confirm that the V state of ethylene is stabilized by twisting the $-CH_2$ group out of the plane of the molecule. So, our last chance of finding any similarities between these two systems is to show that this effect can equally stabilize the ^1B_u state of butadiene.

We did not attempt to construct a potential surface for this motion but looked only at the 90° twisted configuration that in the case

of the ethylene molecule represents the most stable configuration. So we expect that any drastic changes caused by twisting the $-CH_2$ group should be apparent from our study of the fully twisted configuration.

We chose a geometry that again resembles an allyl system attached to a $-CH_2$ group, the difference being that now the $-CH_2$ group is 90° twisted relative to the plane of the allyl group

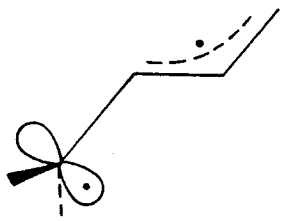

The carbon-carbon bond lengths in the allyl group were taken as equal to 1.40 Å and the terminal bond length equal to 1.54 Å. At the Hartree-Fock level we obtained an energy of -154.2270 h for this structure. This energy is so high that it is very improbably that CI effects can lower it to a value compatible with the state observed experimentally. So, we decided not to proceed further with this calculation.

Instead, we decided to look at the polar form

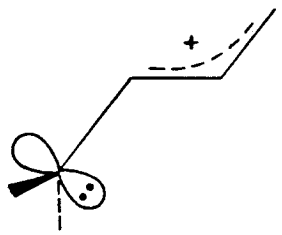

using the same geometry as above. At the Hartree-Fock level this structure is much more stable (E = -154.6742 h) than the nonpolar one. Using this Hartree-Fock π space we performed a full π-CI calculation

and solved for three CI roots. The transition energies obtained are excessively large (11.73 and 12.98 eV) to have any connection with the kind of state that we are trying to represent. The interesting thing about this calculation is that after twisting, the calculated states acquire a pure valence character. The diffuse MO's do not give any contribution at all to the states we solved for. Because of that, the identification of these states with the original ^1A_g and ^1B_u states is more difficult to be made. It is important to mention that after twisting the $-CH_2$ group the σ electronic distribution is significantly changed. So, any correct treatment of this structure must include some description of σ correlation. We did not attempt to do so because we do not believe that a stabilization of ~ 6 eV could be obtained on the basis of this effect.

Before closing this section we should mention that in an earlier calculation, Shih et al.[25] also looked at twisted geometries of the butadiene molecule. In their calculation they considered simultaneously twisting of both $-CH_2$ terminal groups. These groups were rotated by the same amount and in the opposite sense so as to keep C_2 symmetry. The advantage of performing the motion in this way is that under C_2 symmetry the ^1A_g and ^1B_u states will correlate with different irreducible representations. They[25] found that at a 30° twisting angle the ^1B_u state was stabilized by an amount of ~ 0.2 eV, but they conclude that this stabilization should represent an overestimation because of the excessive valence character ascribed to this state (they did not include diffuse functions in the calculation). On the basis of our present results, we would expect the states corresponding to twisting both

-CH_2 groups to be valence-like. This implies that the absence of diffuse functions does not represent any drawback in the calculation by Shih et al.[25] However, an important factor that can modify the results of their study is the lack of treatment of σ correlation, since the changes on the σ system are even larger in this case.

V. Hexatriene

We proceed now to describe the calculations performed for the hexatriene molecule.

In this case we have two more electrons in the π space and a simple MO description gives a ground state corresponding to the electronic configuration $(1a_u)^2 (1b_g)^2 (2a_u)^2$ plus three unoccupied orbitals $2b_g$, $3a_u$, $3b_g$ in order of increasing energy. This molecule has the same symmetry as butadiene and the atomic orbitals will have symmetries $\underset{\frown}{ns} = a_g$; $\underset{\frown}{np} = a_u$; $\underset{\frown}{nd} = a_g, b_g$; $\underset{\frown}{nf} = a_u, b_u$.

The first dipole allowed state will correspond to the $2a_u \rightarrow 2b_g$ transition which gives rise to a ^1B_u state. Again, as in butadiene, this is not a valence state, the $\pi^*(2b_g)$ orbital having some diffuse character.

The Rydberg states for this molecule will have overall symmetries $B_g(2a_u \rightarrow np_\sigma, nf_\sigma)$, $A_u(2a_u \rightarrow ns, nd_\sigma)$, $A_g(2a_u \rightarrow np_\pi, nf_\pi)$ and $B_u(2a_u \rightarrow nd_\pi)$. Transitions to the ^1A_u and ^1B_u states will be optically allowed while transitions to the ^1A_g and ^1B_g states will be forbidden.

A. Basis Set. In order to describe the σ Rydberg states we initially augmented the valence basis set with diffuse basis functions of 3s, $3p_y$ and $3p_z$ character ($\zeta_{3s} = 0.023$, $\zeta_{3p} = 0.021$) centered on each carbon atom. An IVO calculation with this basis set (basis A, Table V) gives an adequate description of the 3s, $3p_\sigma$, $3p_{\sigma'}$, $3d_\sigma$, $3d_{\sigma'}$, and $3d_{\sigma''}$ Rydberg orbitals. This same basis (A) also generates $4p_\sigma$, $4f_\sigma$, and $5g_\sigma$ Rydberg orbitals. Figure 8 shows the first three σ Rydberg orbitals generated with this basis.

As we did in the butadiene case, we again reduced the size of the basis set (without loss of accuracy) in order to perform the SCF and CI calculations. To this purpose we augmented the valence basis set with one set of 3s, $3p_y$ and $3p_z$ basis functions centered at the C_1-C_2, C_3-C_4 and C_5-C_6 bond midpoints. As we can see from Table V (basis B) and Figure 8 (b, d, f), this basis set gives a very good description of the σ Rydberg states.

B. Character of the Rydberg Orbitals. As for butadiene, the Rydberg orbitals for hexatriene very much resemble the corresponding atomic orbitals.

The σ Rydberg orbitals again show clear distortions and are rotated relative to the molecular coordinate system, but the π Rydberg orbitals seem to be oriented along the molecular coordinate system.

Figure 8 (a, c, e) shows the first three σ Rydberg orbitals (using basis A) which can be classified relative to the $(\bar{x}, \bar{y}, \bar{z})$ system (Figure 8) as 3s(a), $3p_{\bar{y}}$ (c) and $3p_{\bar{z}}$ (e). Similarly, the $3d_\sigma$ orbitals on Figure 9 can be classified as $3d_{\bar{z}^2}$ (a, b), $3d_{\bar{y}\bar{z}}$ (c, d) and $3d_{\bar{x}^2-\bar{y}^2}$ (e, f). This latter orbital shows much more amplitude in the molecular plane than the equivalent one in butadiene.

Figure 10 shows the first three π Rydberg orbitals, obtained from basis set C (Table V). Amplitude plots in both xy and $\bar{x}\bar{z}$ planes allow us to classify them as $3d_{xy}$ (a, b) and $3d_{\bar{x}\bar{z}}$ (c, d). Figure 11 shows the two 4f orbitals ($4f_{xz^2}$ and $4f_{xy^2}$) in both $\bar{x}\bar{z}$ and xy planes.

Table VI shows the transition moments and spatial extension (second moments) computed using these Rydberg orbitals.

C. Hartree-Fock Calculations. For the σ Rydberg states we used the IVO's obtained with basis set B (Table V) as starting guesses for the excited Rydberg orbitals.

Using the first IVO of of $a_g(3s)$ symmetry and $b_u(3p_\sigma)$ symmetry we solved self-consistently for the $^1A_u(3s)$ and $^1B_g(3p_\sigma)$ Rydberg states.

For the π Rydberg states we used the IVO's obtained with basis set C (Table V) as starting guesses for the excited Rydberg orbitals.

Similar to the case of butadiene, the Hartree-Fock solution for the $^1A_g(3p_\pi)$ Rydberg state will not correspond to a "pure" state. But because this latter state is very different in character from the valence ^1A_g states it will be easily identified at the CI level, as discussed in the next section.

The ^1B_u states in the case of hexatriene correspond to the nd_π Rydberg states. Using the first IVO of $b_g(3d_\pi)$ symmetry obtained from basis set C (Table V) we solved self-consistently for the $^1B_u(3d_\pi)$ state.

We did not try to search for a $^1B_u(\pi \rightarrow \pi^*)$ corresponding to a non-vertical transition, because the optimization of this state is much more complex. The problem will be certainly simplified after a correct description is found for the butadiene case.

The Hartree-Fock results for the Rydberg states are shown in Table VII.

D. CI Calculations. The set of CI calculations to be described below were performed using the orbitals generated by each one of the SCF calculations respectively, plus some IVO's properly reorthogonalized to the HF occupied orbitals.

Because the CI matrices generated are very large, we limited ourselves to the first two Rydberg states of each symmetry with exception of the ^1A_g states. In that case, the need to project out the ground state and the 2^1A_g valence state forces us to solve for four roots to obtain the first two ^1A_g Rydberg states. This makes the calculation very impractical.

1. The ^1A_u states (ns, nd_σ). The CI calculation for these states was performed in the following way. The π space was formed by the orbitals generated in the SCF calculation. The σ space was formed using the 3s orbital solved self-consistently plus 5σ IVO's $(2a_g + 3b_u)$ obtained from basis set B (Table V), reorthogonalized to the HF σ core. Using these spaces we allowed up to triple excitations among the 12π MO's while simultaneously allowing the σ electron to readjust a mong the 6σ MO's. The first root of this CI calculation corresponds to the 3s Rydberg state and the second to the $3d_\sigma$ Rydberg state. Both states are optically allowed and should be observed in both uv and electro n-impact experiments. The results of this calculation puts the 3s state at 5.97 eV and the first $3d_\sigma$ $(3d_{z^2})$ state at 6.72 eV.

One attempt was made to estimate the transition energy of the second $3d_\sigma$ Rydberg state using the IVO results corrected for CI effects. This correction was based on the CI effects observed for lower Rydberg states of butadiene and hexatriene. Following this procedure we found the second $3d_\sigma$ Rydberg state at 6.80 eV. This state could be correlated to the transition observed experimentally at ~6.9 eV.[2a] However, from the experimental point of view the bands observed at ~6.75 eV, 6.90 eV and 7.08 eV appear to be vibronic peaks of a single electronic

transition.[26] Again experimentally this transition has been tentatively assigned to a $2\,^1B_u(\pi \rightarrow \pi^*)$ state[2a] and also to a $\sigma \rightarrow \pi^*$ state.[27] As previously discussed in Part I, the $\sigma \rightarrow \pi^*$ states are at much higher energies and that leaves the $2\,^1B_u(\pi \rightarrow \pi^*)$ as a sole candidate for this assignment. If one looks at Tables I and V, one can see that at the IVO level the $3d_\sigma$ Rydberg states of both butadiene and hexatriene are $\sim 0.1 - 0.2$ eV apart. From this observation another interpretation of the three-band system (6.75 eV, 6.90 eV and 7.08 eV) can be made, namely that they could correspond to the three $3d_\sigma$ Rydberg states ($3d_{\bar{z}^2}$, $3d_{\bar{y}\bar{z}}$ and $3d_{\bar{x}^2-\bar{y}^2}$, respectively).

2. The ^1B_g states (np_σ). The CI calculations for these states were performed in an analogous way to the one described for the ^1A_u states.

The π space was formed from the orbitals generated by the SCF calculation. The σ space was formed by the $3p_\sigma$ self-consistently optimized orbital plus 5σ IVO's ($3a_g + 2b_u$) properly reorthogonalized to the HF σ orbitals.

Using these space, the CI calculation was performed allowing up to triple excitations among the 12π MO's and simultaneously allowing the σ electron to readjust among the 6σ MO's. The two CI roots obtained correspond to the two $3p_\sigma$ Rydberg states. We found those states at 6.00 eV ($3p_{\bar{y}}$) and 6.20 eV ($3p_{\bar{z}}$).

These ^1B_g states occur in the same region of optically allowed transitions and could well be masked by these transitions. Also in the electron impact spectrum at 0° angle these transitions should exhibit small cross-sections.

Recently a two-photon absorption experiment in the region of 6.23 eV indicated the presence of a parity-forbidden state.[8] A more recent study of its intensity dependence on the laser beam polarization indicated a state of A_g symmetry.[28] As will be discussed below, we also calculate a ^1A_g Rydberg state at 6.26 eV. But the same experiment[8] does not show the presence of a ^1B_g state at 6.2 eV. To try to explain why this transition was not observed we calculated two-photon transition rates for both ^1A_g and ^1B_g Rydberg states. To do that we derived expressions for the two-photon transition rate from a single beam of elliptically polarized light for each one of the transitions. From these expressions the rates for linearly and circularly polarized light can be easily obtained. The derivations can be found elsewhere.[29] We used IVO states to perform the summation over the intermediate states. At this level of calculation we found the ratio between the transition rates for the ^1A_g and ^1B_g states equal to ~ 4 for linearly polarized light and ~ 10 for circularly polarized light. We have computed two-photon transition rates for the butadiene molecule (for other purposes) using full π-CI wavefunctions. To have an idea of how the CI results differ from the ones using IVO states, we recalculated the rates for the butadiene case using IVO states. A factor of ~ 5 was found between the ratios $(\omega^1A_g/\omega^1B_g)$ for the two calculations. If one uses this as an estimate for the CI effects in hexatriene, one can say that the ^1A_g transition might be ~ 20-50 times more intense than the ^1B_g transitions. While these numbers represent only estimates, we can safely say that the ^1A_g transition is more intense than the ^1B_g transition.

3. The ^1A_g states (np_x). For those states the π space was composed of the HF π orbitals for this state plus π IVO's ($3a_u + 3b_g$) obtained with basis set C (Table IV). Using this space we performed the CI calculation considering up to quadruple excitations.

As discussed above, because we have first to project out the valence ^1A_g states we only obtained the first ^1A_g Rydberg state which corresponds to the $3p_x$ state. This state is easily identified with the third root of the CI calculation. The first root is a valence closed-shell state and corresponds to the $X\,^1A_g$ ground state of the system. The second root is also a valence state and shows a doubly-excited dominant configuration characteristic of the $2\,^1A_g(\pi \rightarrow \pi^*)$ valence state. Finally, the third root corresponds to the diffuse open-shell configuration of the Hartree-Fock calculation and is identified with the $^1A_g(3p_x)$ Rydberg state. We found this state at 6.26 eV in excellent agreement with the state at 6.23 eV observed in the two-photon absorption experiment.[8]

An estimate for the higher ^1A_g Rydberg states was made following the same procedure used for the $3d_\sigma$ Rydberg states. In this way we found the $4f_{\overline{xz}}{}^2$ state at 7.19 eV and the $4f_{\overline{xy}}{}^2$ state at 7.81 eV. The $4f_{\overline{xz}}{}^2$ state can be tentatively correlated with the observed transition at 7.25 eV[2,5] and the $4f_{\overline{xy}}{}^2$ state with the one observed at 7.77 eV.[2,5] Experimentally the first transition (7.25 eV) has been assigned to a vibronic component of the $2\,^1B_u(\pi \rightarrow \pi^*)$ state[2a] and the second one (7.77 eV) was assigned to a $4f_{\overline{xy}}{}^2$ Rydberg state.[2a] If we assume that the three-band system (discussed in connection with the $3d_\sigma\ ^1A_u$ Rydberg

states) at 6.75 eV, 6.90 eV and 7.08 eV correspond to the $3d_\sigma$ states that leaves the 7.25 eV transition unassigned. On the basis of our present results a plausible assignment of this band is its identification with the $4f_{\overline{xz}}{}^2$ Rydberg state.

4. The ^1B_u states ($3d_\pi$). The CI calculations for these states were carried out in exactly the same way as described for the ^1A_g states. The π space was formed using the HF π orbitals for the ^1B_u state plus 6π IVO's ($3a_u + 3b_g$) reorthogonalized to the HF π orbitals. Using this space we solved for two CI roots allowing up to quadruple excitations. These two roots correspond to the two $3d_\pi$ orbitals. We found these states at 6.27 eV and 6.68 eV.

We also tried to estimate the transition energy for the $4d\pi$ Rydberg state following the same procedure used for the $3d_\sigma$ (^1A_u) states. In this way we obtained a transition energy of 7.41 eV for the $4d_{\overline{xz}}$ state which correlates well with the transitions observed experimentally at 7.46-7.48 eV.[2,5] These transitions have been tentatively assigned to the $3\ ^1B_u$ ($\pi \rightarrow \pi^*$) state[2a] or to a $\sigma \rightarrow \pi^*$ state.[27] Again, from Part I we know that this transition does not correspond to a $\sigma \rightarrow \pi^*$ transition. As for the $2\ ^1B_u$ ($\pi \rightarrow \pi^*$) state, nothing can be said at the moment about the nature and location of the $3\ ^1B_u$ ($\pi \rightarrow \pi^*$) state.

VI. Discussion

We now proceed to discuss the results of both calculations comparing our results with the experimental spectra and other theoretical calculations. As will be apparent from the discussion, most of the spectra of these molecules can be explained in terms of a few valence states plus a series of Rydberg transitions.

It will be more convenient to discuss each molecule separately.

A. Butadiene Molecule. Except for the $1\,^1B_u$ state experimentally observed at 5.95 eV (peak)[4] our present calculation can provide assignments for most of the observed transitions. Table X shows our results (including the valence states) and compare them with experimental results. Except for a few transitions our assignments agree with the results of a recent ab initio calculation.[30]

The transitions observed experimentally at ~3.2 eV and ~4.9 eV can be unambiguously assigned to the two lower triplets ^3B_u and ^3A_g states, corresponding to the $\tilde{a}$ and $\tilde{b}$ bands.

The next transition, observed experimentally at ~5.95 eV[4,31] and assigned to the $1\,^1B_u$ state ($\tilde{A}$ band system), constitute the most serious challenge to the theoretical description of the electronic states of polyenes. We think that our calculations provided enough evidence that this transition is non-vertical. Our best estimate locates this transition at 6.12 eV and that corresponds to a "state" with all C–C bond distances equal to 1.40 Å and with the (C–C) terminal bonds symmetrically bent 0.8° degrees relative to the ground-state geometry (see Section IV.A.2). We believe that a more detailed investigation of

the symmetric stretched geometries will provide the final answer to the problem. If one looks at Figure 6 for example we see that the differences of energies among the structures with shorter (C-C) bonds (1.40 Å and less) are relatively small. We decided to proceed further with the calculations of the structure, with all (C-C) bond distances equal to 1.40 Å, because, at the GVB(1/PP) level, this structure was the most stable one. From the ($\pi + \sigma$) CI calculations we learned that the effects of σ correlation for this structure were approximately three times larger than the corresponding effects for the vertical transition. This effect could be even larger for shorter (C-C) bond lengths. That means that while at the GVB(1/PP) level the differences of energy were small, it is possible that at higher levels of calculation structures with shorter (C-C) bond lengths (i.e., shorter than 1.40 Å) could become more stable. It is also possible that the σ effects can be large enough to provide the extra (0.12 eV) stabilization for this transition. The small differences of energy among these stretched structures could provide an explanation for the broadness of the band observed experimentally as being a result of (C-C) stretching progressions. We plan further studies in this direction.

We assigned the system band $\tilde{B}$ [32] observed at ~ 6.27 eV to the ^1B_g (3s) Rydberg state. This transition has been recently observed in a two-photon absorption experiment. While no polarization studies were performed, on the basis of the present calculation this transition can be unambiguously assigned to the $1\,^1B_g$ (3s) Rydberg state, since no other parity-forbidden states were predicted in this region. This assignment also agrees with the results of Buenker et al. [30]

In the region between 6.0 eV and 7.0 eV two more transitions have been observed experimentally, one at 6.64 - 6.66 eV[3,4] and another at 6.80 - 6.81 eV.[3,4] In this same region our calculations predicted three states, namely, the $1\,^1A_u(3p_{\bar{y}})$ at 6.61 eV, the $^1B_u(3p_{\bar{x}})$ state at 6.67 eV and the $2\,^1A_u(3p_{\bar{z}})$ state at 6.78 eV. The transition at 6.80 - 6.81 eV can be assigned to the $2\,^1A_u(3p_{\bar{z}})$ Rydberg state but the transition at 6.64 - 6.66 eV could be equally assigned to the $1\,^1A_u(3p_{\bar{y}})$ state or the $^1B_u(3p_{\bar{x}})$ state. At this point the assignment has to be decided in terms of the relative intensities of the transitions. For this purpose we calculated oscillator strengths for all three transitions at the full π-CI level. We found f values of 0.0026 for the ^1A_u state, 0.1096 for the $2\,^1A_u$ state and 0.3410 for the $^1B_u(3p_{\bar{x}})$ state. From these results it is quite reasonable to assume that the $1\,^1A_u(3p_{\bar{y}})$ may not be observed. So we assigned the transition observed at 6.64 - 6.66 eV ($\tilde{C}$ band)[32] to the $^1B_u(3p_\pi)$ Rydberg state. The transition at 6.80 eV - 6.81 eV ($\tilde{D}$ band)[32] we assign to the $2\,^1A_u(3p_{\bar{z}})$ Rydberg state. Our assignments in this region differ from the ones by Buenker et al. since they do not assign any transition corresponding to the $\tilde{D}$ band.

Several transitions are observed experimentally in the region between 7.0 eV and 8.0 eV.[3,4] These were designated as $\tilde{E}$, $\tilde{F}$, and $\tilde{G}$ band systems by Herzberg.[32]

The first of these bands ($\tilde{F}$) is observed at 7.07-7.08 eV.[3] McDiarmid[3] assigns this transition to the first member (n=3) of a p-allowed Rydberg series (series 2). More recently, Wiberg et al.,[12] from a comparative study of the vibrational structures of the uv and

photoelectron spectra (PE) also assigned this transition as the origin of a Rydberg series. We do not find any Rydberg transitions in this region. On the contrary, we find the $2\,^1A_g$ ($\pi \rightarrow \pi^*$) valence state at 7.06 eV and another recent ab initio calculation also finds this state in the same region (7.02 eV).[30] From the McDiarmid[3] analysis one sees that this transition fits her Rydberg series 2 but with the largest deviation between calculated and observed values. Besides, the fact that the spectrum of solid butadiene shows a presence of a weak absorption in this region supports the identification of this transition with a valence state. We assign this transition to the $2\,^1A_g$ ($\pi \rightarrow \pi^*$) valence state.

The uv absorption in the 7.27-7.86 eV region was originally assigned to a $X \rightarrow \tilde{E}$ band system[32] and is by far the most complicated structure of the spectrum. From the McDiarmid[3] analysis of the uv spectrum and from the electron-impact (EI) results of Flicker et al.,[4] it is quite clear that this $\tilde{E}$ band has several components. Transitions are observed at 7.27, 7.47, 7.63, 7.79, and 7.85 eV in the uv spectrum[3] and at 7.28, 7.48, 7.60, and 7.80 eV in the EI spectrum.[4] We find several Rydberg transitions in this region. In Table IX we list the components of the $\tilde{E}$ band system as predicted by our calculations. The first three observed transitions (7.33, 7.47, and 7.65 eV) are assigned to parity-forbidden transitions that can be made vibronically allowed. The last two transitions (7.79 and 7.85 eV) correspond to higher members of the dipole-allowed Rydberg series np_x and np_z. These assignments are consistent with the fact that the first three transitions are very weak, while the last two are relatively more

intense. The $3\,^1B_g$ ($3d_{\bar{y}z}$) Rydberg state at 7.40 eV does not result from the CI calculations. From Table I we can see that our basis set (basis C) cannot represent well the second $3d_\sigma$ orbital. But we can still make a good estimate of the transition energy in the following way. From Table I we have an estimate of the transition energies for both $3d_\sigma$ Rydberg orbitals, and from Table IV we have the CI correction for the $3d_{\bar{z}}{}^2$ Rydbert state. Assuming the same CI corrections for both states, we obtain the $3d_{\bar{y}\bar{z}}$ state at 7.40 eV. The observed transition at 7.63-7.64 eV[3] can be correlated with either the $4\,^1B_g$ (4s) state or the $3\,^1A_g$ ($3d_{xy}$) state. We expect the transition to correspond most probably to the $3d_{xy}$ state since the first member of the ns series is very weak. Our assignments of the components of the $\tilde{E}$ system band differ appreciably from the ones by Buenker et al.[30] Recently, Wiberg et al.[12] proposed that all the transitions in this region are vibrational components of a single Rydberg transition with the origin at 7.06 eV.

The next two observed transitions correspond to bands $\tilde{G}$ and $\tilde{H}$ at 8.0 eV and 8.18 eV, respectively.[3,4] We assign these transitions to the ^1B_u ($4f_{x^3}$) and ^1B_u ($5p_x$) π-Rydberg states.

In order to understand the many transitions converging to the first IP, we examined the various Rydberg series for which our calculations provided the first members. First of all, we have to conclude that our ^1B_u ($4f_{xz^2}$) state calculated at 8.91 eV is in error (see Table IV). If this assignment is correct, it would imply that all the other transitions between 8.2 and 8.9 eV should correspond to the fourth and fifth members of the different Rydberg series. From Table I (basis E) it is also clear that our basis set cannot represent well the $4f_{xz^2}$

orbital found at ~1 eV higher than the $4f_{x^3}$ orbital when we expect them to be nearly degenerate.

Table X shows the results of our studies on five different Rydberg series. The other possible series were discarded because their first members showed very low intensity or because their first members cannot be well represented by our basis set. One example of the former is the $np_{\bar{y}}$ (n^1A_u) series whose first member ($3p_{\bar{y}}$) is very weak (f = 0.0026). An example of the latter is the nf_{xz^2} series.

Typical quantum defects (δ) for molecular spectra are[33] $\delta_s \sim 1.0$, $\delta_p \sim 0.6$, $\delta_d \sim 0.1$, and $\delta_f \sim 0.0$ with deviations of ± 0.2 units.

From Table X we can see that

a) the quantum defects obtained are in the range expected for each type of series. The fact that the δf_{x^3} is larger than expected can be attributed to a possible strong coupling between those states and the np_x states since they both have the same symmetry;

b) for $n \geq 9$ all the series are practically degenerate;

c) the optically allowed np_x (^1B_u), $np_{\bar{z}}$ (^1A_u) and nf_{x^3} (^1B_u) Rydberg series can account for all the transitions observed in this region.

The disagreement between our calculated transitions and the ones observed for larger n's is certainly because our series converges to a lower ionization potential.

This region of the butadiene spectrum has been recently analyzed by McDiarmid[3] and Ellison[15] using uv absorption spectroscopy and by Johnson[7] using three-photon absorption spectroscopy. In Ellison's analysis[15] he finds a single Rydberg series with the first member (n = 3) at 7.06 eV. McDiarmid[3] analyzes this region in terms of four

Rydberg series. She assigns two of the series to p-allowed series and the other two to d or f series. Johnson[7] proposes the existence of three Rydberg series in the molecule with two of them almost degenerate. He proposes an n(p, f) ^1B_u series with a very strong f component, an n(p, f) ^1A_u series, and another n(p, f) ^1A_u series with strong p character.

From our analysis we conclude that the transitions in this region can be explained in terms of an np_x ^1B_u series, an nf_{x^3} ^1B_u series, and an np_z ^1A_u series. We also expect an nf_σ ^1A_u series to be present in this region. Because our basis set cannot describe adequately f_σ states, we do not present any results for this series. But we expect, as in the case of the np_x and np_z, that both f series will be nearly degenerate even for small $\hat{n}$.

Finally, the transitions observed at 9.53 eV and 11.04 eV in the electron-impact spectrum[4] may correspond to $\sigma \rightarrow \pi^*$ transitions. In trans-hexatriene we found $\sigma \rightarrow \pi^*$ transitions in these regions of the spectrum. It also could correspond to excitations out of the inner π ($1a_u$) orbital.

B. Hexatriene Molecule. The electronic spectrum of this molecule is much less understood than the spectrum of butadiene. Experimentally only the two lowest triplet states ($1\,^3B_u$ and $1\,^3A_g$), the strong $1\,^1B_u$ state and more recently a parity forbidden ^1A_g state can be unambiguously assigned. Our calculations can contribute to a quantitative assignment of most of the observed transitions. Table XI shows the complete results of our calculations and compares them with the available experimental results. Unfortunately, this molecule is com-

putationally more complex than the butadiene molecule and we have to restrict ourselves to a few states of each symmetry.

The two lowest observed transitions at ~2.6 eV and ~4.2 eV have been assigned to the first two triplet states.[5,34,35] Our calculation confirms the assignments. We find the $1\,^3B_u$ state at 2.71 eV and the $1\,^3A_g$ state at 4.23 eV.

The next experimentally observed transition corresponds to the strong dipole allowed $1\,^1B_u$ state.[2b,5,34] Similar to the butadiene case this is a very broad band covering the range from ~4.95 eV to ~5.70 eV.[1] We did not try to search for a description of this state but from what we learned from the butadiene calculation this is most probably a non-vertical transition. Once the structure of this state in butadiene is known, it would provide the guidelines to the description of the corresponding state in hexatriene. We plan a more detailed investigation on the butadiene state and once its structure is determined we will extend the calculation to the hextriene molecule.

The next transition observed in the uv spectrum corresponds to a series of weak bands covering the range from ~5.70 eV to 6.44 eV. These transitions correlate with the bands at 6.06 eV, 6.25 eV and 6.42 eV observed in the electron impact experiment.[5] From the analysis of the uv spectrum[2] it was found that only a few of these bands could be fitted in the progressions found for the $X\,^1A_g \rightarrow 1\,^1B_u$ transition, even if rather large anharmonicities are assumed for the vibrations. From that observation it was concluded that the majority of the observed bands in this region could well be associated with electronic states other than the $1\,^1B_u$ state. These transitions have been assigned

to the parity-forbidden $2\,^1A_g$ and $3\,^1A_g$ states[2] and more recently to an optically allowed $2\,^1B_u$ state.[27]

The first state predicted by our calculations to occur in this region is the valence $2\,^1A_g$ state at 5.87 eV. Earlier semi-empirical calculations[36] predicted this state to occur below the $1\,^1B_u$ state. The analysis of both uv[2] and electron-impact[5] spectra do not show any evidence for such a state below the $1\,^1B_u$ state. This $2\,^1A_g$ state could well be associated with the weak bands in the region between 5.70 eV and 5.89 eV of the uv spectrum. The electron-impact spectrum at 70° shows a weak feature at ~5.9 eV which is not present in the spectrum at 0° angle.[5] Since optically forbidden transitions are in general more prominent at larger scattering angles, that feature could be an indication of a parity forbidden transition. However, this observation is far from being conclusive. Besides the fact that the resolution of the two spectra is different, several factors could contribute to simulate such a weak feature. A more convenient way of veryfying the presence of this state would be by means of a two-photon absorption experiment. To have an idea of how strong this transition would be, we calculated the two-photon transition rate for the $X\,^1A_g \rightarrow 2\,^1A_g$ transition using our best CI description of these states. We found transition rates equal to 7.1×10^{-51} F^2 sec^{-1} for the case of linearly polarized light and 1.2×10^{-50} F^2 sec^{-1} for the case of circularly polarized light (F is the photon flux in photons/cm^2 sec). Since fluxes of the order of 10^{25}-10^{26} are currently available (from nitrogen-pumped dye lasers for instance) the transition should be observable.

In this same region (5.70 eV - 6.44 eV) our calculations predict two optically allowed Rydberg states and three parity forbidden Rydberg states. The first transition, at 5.97 eV, corresponds to the $1\,^1A_u$ 3s Rydberg state. This state could well be associated with the bands in the region of 5.94 eV - 6.09 eV in the uv[2] spectrum and with the 6.06 eV feature of the electron-impact spectrum.[5] The next three transitions calculated in this region correspond to parity forbidden Rydberg states at 6.00 eV ($1\,^1B_g$, $3p_{\bar{y}}$), at 6.20 eV ($2\,^1B_g$, $3p_{\bar{z}}$) and at 6.26 eV ($3\,^1A_g$, $3p_x$). From these, the first two transitions are very weak and may not be observed even in a two-photon absorption experiment (see Section V.B.2). It is interesting to notice that these same transitions in butadiene (in which case they are optically allowed) are also weak and one of them is almost certainly not observed. The transition at 6.26 eV corresponding to the $3\,^1A_g$ ($3p_x$) Rydberg state has been recently observed in a two-photon absorption experiment.[8] Finally, the last transition in this region predicted by our calculations occurs at 6.27 eV and corresponds to the ^1B_u ($3d_{\overline{xz}}$) Rydberg state. This transition can be correlated with the bands at 6.28 eV in the uv[2] spectrum and at 6.25 eV in the electron-impact spectrum.[5] We found no other transitions at higher energies in this region that could be correlated to the bands observed at 6.38 - 6.44 eV in the uv[2] spectrum and with the peak at 6.42 eV in the electron-impact spectrum.[5]

In a reinterpretation of the uv spectrum this whole system of bands (5.70 eV - 6.44 eV) was assigned to a $2\,^1B_u$ state.[27] From our calculations it is clear that more than a single transition are present in this region.

The next band system observed in the uv spectrum corresponds to a series of medium intensity bands covering the range between 6.53 eV and 7.30 eV.[2] This band system was initially assigned to a $2\,^1B_u$ state[2] and more recently to a $\sigma \rightarrow \pi^*\ ^1A_u$ state.[27] The corresponding peaks in the electron-impact spectrum are observed at 6.57 eV, 6.75 eV, 6.93 eV, 7.08 eV and 7.25 eV.[5] In this region (6.53-7.30 eV) we found several transitions which we proceeded to analyze.

First of all, from Part I we know that the $\sigma \rightarrow \pi^*$ states occur at much larger energies and should not be associated with any transition in this region.

The only transition predicted by our calculation to occur around 6.5 eV corresponds to a ^1B_u valence state at 6.56 eV. If we assume that the last few bands of the previous region (5.70 eV - 6.44 eV) are hot bands $[-2\nu_5^1, -2(\nu_5^1 + \nu^1)]^1$ of the observed transition at 6.53 eV (0-0)[2] we could assign this band system (6.42 - 6.62 eV) to the ^1B_u valence state. However, we are not sure about the existence of such a valence state even if it provides our only explanation for the observed transition.

The next state predicted to occur in this region corresponds to the ^1B_u ($3d_{xy}$) Rydberg state calculated at 6.68 eV. A transition at the same energy observed in the uv spectrum was assigned to a vibronic (ν_3) transition of the 6.53 eV band (0-0).[2] Moving at higher energies we found another Rydberg state at 6.72 eV corresponding to the $2\,^1A_u$ ($3d_{z^2}$) state. This state can be associated with the transition observed at 6.73 eV in the uv spectrum[2] and with the one at 6.75 eV

in the electron-impact spectrum.[5] The next two transitions calculated at ~6.80 eV and ~7.0 eV correspond to the $3\,^1A_u(3d_{\overline{yz}})$ and $4\,^1A_u(3d_{\overline{x}^2-\overline{y}^2})$ Rydberg states, respectively. The transition at 6.80 eV can be correlated to the observed transition at 6.90 eV in the uv spectrum[2] and the one at 6.93 eV in the electron-impact spectrum.[5] Similarly the $4\,^1A_u(3d_{\overline{x}^2-\overline{y}^2})$ state can be correlated with the transition at 7.06 eV (uv)[1] and 7.08 eV (EI).[5]

The last state predicted by our calculations to occur in this region corresponds to the $^1B_u(4d_{\overline{xz}})$ Rydberg state at 7.25 eV. This state could be associated with the bands observed at 7.15 - 7.30 eV in the uv spectrum[2] and with the peak at 7.25 eV of the electron impact spectrum.[5]

A series of medium intense bands starting at ~7.37 eV in the uv spectrum have been tentatively assigned to a $3\,^1B_u$ state.[2] Only one transition at 7.48 eV is observed in the electron-impact spectrum in this region.[5]

A final series of sharp bands starting at ~7.71 eV and extending up to 8.30 eV is observed in the uv spectrum.[2] The associated transitions in the electron-impact spectrum are found at 7.77, 7.93, and 8.06 eV.[5] The analysis of the uv spectrum revealed that these transitions could be fitted in a p_π-type Rydberg series with the principal quantum number in the range n = 5, 12 and quantum defect equal to 0.054.[2]

To understand the nature of these transitions, we examined the various Rydberg series for which our calculations provided the first members. Table XII shows the results of our studies on four Rydberg

series. From Table XII we can see that

a) the quantum defects obtained are in the range expected for each type of series;

b) for $n \geq 4$, the $nd_{\overline{z}^2}$ and nd_{xy} series are practically degenerate and for $n \geq 10$ all the nd series are degenerate. Also, for $n \geq 11$ the four series are pratically degenerate; and

c) these four optically allowed series can account for all the transitions observed in this region.

From the results of our analysis we conclude that the series of bands starting at 7.71 eV and converging for the first IP should correspond to three nd Rydberg series. The first member of the $nd_{\overline{xz}}$ series is more intense than the first members of the other series. This difference in intensity could imply that for large $\hat{n}$ all the transitions should correspond to members of this series ($nd_{\overline{xz}}$). Higher members of the $\hat{n}s$ series are not expected to be observed because the 3s (^1A_u) transition is very weak.

Our assignments for this region are shown in Table XI. The disagreement between our theoretical transitions and the observed transitions for larger values of $\hat{n}$ ($n \geq 9$) is certainly due to the fact that the experimental series[2] converges to a lower IP.

Finally, in the electron-impact spectrum,[5] transitions corresponding to super-exicted states are observed at 9.1 eV, 9.7 eV and 10.5 eV. These transitions can be associated with $\sigma \rightarrow \pi^*$ transitions or with transitions from the inner $\pi(1b_g)$ orbital. The transition at 9.1 eV correlates well with the ^1B_g ($\sigma \rightarrow \pi^*$) state calculated at 9.18 eV. We did not find any transitions that could be correlated with the ones observed at 9.7 eV and 10.5 eV. Those latter states could correspond

either to another ^1B_g ($\sigma \rightarrow \pi^*$) state (the 10.5 eV transition most probably) or to transitions from the inner π ($1b_g$) orbital.

Above 11 eV (energy loss) the electron impact spectra do not show enough resolution to allow for the identification of the ^1A_u ($\sigma \rightarrow \pi^*$) state predicted by our calculation to occur at 11.51 eV.

VII. SUMMARY

In this final section we summarize the main conclusions of our calculations.

A) the spectrum of these polyene molecules can be understood in terms of a few valence states plus a series of Rydberg states;

B) the first dipole-allowed transition ($1\,^1B_u$) which corresponds to the strong and broad band characteristic of these polyenes is most probably a non-vertical transition;

C) while the $2\,^1A_g$ valence states and the non-vertical ^1B_u transition require the inclusion of σ correlation effects to correctly describe them, the remaining valence and Rydberg states can be accurately described at the π-CI level;

D) the effects of σ correlation on these states can be well established using only the subspace of the (C-C) σ orbitals;

E) in the description of the σ Rydberg states the size of the basis set can be considerably reduced without loss of accuracy by using appropriate off-centered basis functions;

F) the super-excited states observed in the electron impact experiments should correspond to $\sigma \rightarrow \pi^*$ states and to transitions from the inner π orbitals ($1a_u$ for butadiene and $1b_g$ for hexatriene). Therefore states occurring below the first IP of these molecules should not be assigned to $\sigma \rightarrow \pi^*$ states.

Appendix A

Improved Virtual Orbitals

In describing the sequence of Rydberg states from excitation out of a particular valence orbital it is convenient to carry out Improved Virtual Oribtal (IVO) calculations. In this procedure all the occupied orbitals of the ground-state $\{\phi_j\}$ are kept fixed and the spectrum of excited orbitals $\{\phi_I\}$ is obtained by diagonalizing the Hamiltonian

$$H_I^{ex} = h + \sum_{j \neq I} (2J_j - K_j) + J_I \pm K_I \qquad \text{(A-1)}$$

subject to the condition that each Φ_I is orthogonal to all occupied $\{\phi_j\}$. In the expression above h is the one-electron part of the hamiltonian, J and K are the coulomb and exchange operators and the positive and negative signs hold for singlet and triplet states, respectively.

We have used IVO's as starting guesses in our calculations of the Rydberg and non-valence states of butadiene and hexatriene. Representing a very good approximation to the excited orbital, they lead to rapid convergence of the self-consistent calculation.

With the IVO orbitals the excitation energy (from the occupied orbital ϕ_j to the IVO ϕ_I) is given by

$$\Delta E_{j \to I} = \epsilon_I - \epsilon_j \qquad \text{(A-2)}$$

where ϵ_I and ϵ_j are the orbital energies from the IVO and SCF calculations. The errors in such a prediction are the same as in using ϵ_j to predict an ionization potential (i.e., using Koopmans theorem). That

is, there is an error due to the fixed shape of the occupied orbitals (making the IP too large) and an error due to the lack of electron correlation effects (making the IP too low). However, for Rydberg states $-\epsilon_I$ is a good approximation to the IP out of the excited state (some electron correlation and orbital readjustment effects are small). Consequently, fairly accurate predictions of the excitation energy to Rydberg states are obtained by replacing (A-2) with

$$\Delta E_{j\to I} = IP_j + \epsilon_I \,, \tag{A-3}$$

where IP_j is the experimental IP corresponding to ionizing out of orbital ϕ_j.

Such IVO calculations are quite useful in determining the proper basis functions for describing the Rydberg states.

ACKNOWLEDGMENT

One of the authors (MACN) acknowledges Conselho Nacional de Pesquisas (BRASIL) for financial support and Universidade Federal do Rio de Janeiro for a leave of absence.

TABLE I: IVO Excitation Energies[a] (in eV) of Butadiene for the $\pi(1b_g) - \sigma,\pi$ Rydberg Transitions for Different Basis Sets

Basis Set Augmentation[b]	Number of diffuse basis functions	Excited Orbital					
a) σ Rydberg states		3s	$3p_{\bar{y}}$	$3p_{\bar{z}}$	$3d_{\bar{z}^2}$	$3d_{\bar{y}\bar{z}}$	$3d_{\bar{x}^2-\bar{z}^2}$
A) one 3s, $3p_y$ and $3p_z$ basis functions on each carbon atom	12	6.55	6.80	7.03	7.64	7.74	7.92
B) one 3s basis function on each carbon atom	4	6.62	7.21	7.83	7.83		
C) four 3s-like basis functions off-center[c]	4	6.55	6.83	7.16	7.80		
D) one 3s, $3p_y$ and $3p_z$ on the midpoint of the C_1-C_2 and C_3-C_4 bonds	6	6.62	6.82	7.09	7.75	7.78	
b) π-Rydberg states		$3p_x$	$4f_{x^3}$	$4f_{xz^2}$	$3d_{xy}$	$3d_{xz}$	$4d_{xy}$
E) one $3p_\pi$ basis function on each carbon atom		6.88	7.82	8.87	7.58	7.97	
F) two $3p_\pi$ basis functions on each carbon atom plus two $3d_{xy}$, $3d_{xz}$ at the midpoints of the C_1-C_2 and C_3-C_4 bonds[d]		6.88	7.69	8.37	7.49	7.72	8.41

[a] Using the relation $\Delta E_I = IP - \epsilon_I$, with IP = 8.45 eV.

[b] In all cases the gaussian exponents are: $\xi_{3s} = 0.023$, $\xi_{3p} = 0.021$.

[c] Floating points at P_1 (0.0, 4.0, -3.125), P_2 (0.0, 3.125, 4.0), P_3 (0.0, -4.0, 3.125), and P_4 (0.0, -3.125, -4.0).

[d] The exponents for the extra basis functions are: $\xi'_{3p} = 0.049$, $\xi_{3d} = 0.049$, $\xi'_{3d} = 0.015$.

TABLE II: Transition Moments and Spatial Extension of the Rydberg Orbitals of Butadiene.

Orbital[a]	Transition Moments (a.u.) $\langle\phi_{IVO}\|r\|\pi_2(1b_g)\rangle$[b]	$\langle S\|r\|X\ ^1A_g\rangle$[c]	Component	Second Moments[d]		
$\pi_1(1a_u)$				2.436	2.277	4.487
$\pi_2(1b_g)$				2.463	3.451	6.721
3s	0.5883	1.0384	⟨xy⟩	15.138	22.057	23.133
	1.2163	2.0701	⟨xz⟩			
$3p_{\bar{y}}$	0.0257	0.0737	⟨x⟩	12.859	33.095	24.371
$3p_{\bar{z}}$	0.3429	0.4684	⟨x⟩	17.315	31.745	47.192
$3p_{\bar{x}}$	0.7863	0.6065	⟨y⟩	27.898	13.827	16.257
	0.7948	0.7590	⟨z⟩			
$3d_{\bar{z}^2}$	0.2180		⟨xy⟩	12.578	29.270	53.010
	0.1566		⟨xz⟩			
$3d_{\overline{yz}}$	0.3284		⟨xy⟩	14.928	55.963	45.454
	0.0925		⟨xz⟩			
$3d_{\bar{x}^2-\bar{z}^2}$	0.7531		⟨xy⟩	18.394	35.346	23.453
	1.3187		⟨xz⟩			
$3d_{\overline{xy}}$	1.4438		⟨yz⟩	30.816	32.224	15.059
$3d_{\overline{xz}}$	0.2717		⟨yz⟩	37.754	13.418	38.540
$4f_{x^3}$	1.0866		⟨y⟩	20.014	8.177	9.434
	0.9729		⟨z⟩			
$4f_{xz^2}$	0.4851		⟨y⟩	32.51	32.630	38.777
	0.4619		⟨z⟩			

[a]Orbitals $\pi_1(1a_u)$ and $\pi_2(1b_g)$ are from ground state wavefunction. Rydberg orbitals are from IVO calculations using basis sets A and E of Table I.

[b]Transition moments using IVO orbitals.

[c]Transition moments using full π-CI wavefunctions.

[d]Second moments from IVO orbitals.

TABLE III: Results of Full π-CI Calculation for the 1,3-*trans*-butadiene Molecule[a]

State	Present Results	Shih *et al.*[b]
$X\,^1A_g$	-154.92796h	-154.9181h
$1\,^1B_g\,(3s)$	6.30 eV	6.24 eV
$2\,^1B_g\,(3d_{\bar{z}^2})$	7.33	7.31
$1\,^1A_u\,(3p_{\bar{y}})$	6.63	6.50
$2\,^1A_u\,(3p_{\bar{z}})$	6.80	6.76
$^1B_u\,(3p_x)$	6.79	6.60
$^1B_u\,(4f_{x^3})$	8.16	7.98
$^1B_u\,(4f_{xz^2})$	9.00	
$3\,^1A_g\,(3d_{xy})$	7.73	7.79
$4\,^1A_g\,(3d_{xz})$	7.84	

[a]Ground state in hartrees. Transition energies in eV.

[b]Reference 25.

TABLE IV: All-Valence CI Results for the Rydberg States of Butadiene[a]

State	Present Results	Buenker et al.[b]
$X\,^1A_g$	-155.01537	-155.1900
$1\,^1B_g\,(3s)$	6.29	6.20
$2\,^1B_g\,(3d_{\bar{z}^2})$	7.29	7.29
$1\,^1A_u\,(3p_{\bar{y}})$	6.61	6.53
$2\,^1A_u\,(3p_{\bar{z}})$	6.78	6.72
$^1B_u\,(3p_x)$	6.67	6.67
$^1B_u\,(4f_{x^3})$	7.97	7.96
$^1B_u\,(4f_{xz^2})$	8.91	
$3\,^1A_g\,(3d_{xy})$	7.68	7.53
$4\,^1A_g\,(3d_{xz})$	7.79	7.78

[a]Ground-state energies in hartrees. Transition energies in eV.

[b]Reference 30.

TABLE V: IVO Excitation Energies[a] (in eV) of Hexatriene for the $\pi(2a_u) \rightarrow$ Rydberg Transitions for Different Basis Sets

Basis Set Augmentation[b]	No. diffuse basis functions	Excited Orbital					
a) σ Rydberg orbitals		3s	$3p_{\bar{y}}$	$3p_{\bar{z}}$	$3d_{\bar{z}^2}$	$3d_{\bar{y}\bar{z}}$	$3d_{x^2-y^2}$
A) one 3s, $3p_y$ and $3p_z$ basis function on each carbon atom	18	6.32	6.37	6.73	7.15	7.26	7.50
B) one 3s, $3p_y$ and $3p_z$ basis function on the midpoints of C_1-C_2, C_3-C_4 and C_5-C_6 bonds	9	6.43	6.42	6.75	7.23	7.30	
b) π Rydberg orbitals		$3p_x$	$4f_{xz^2}$	$4f_{x\bar{y}^2}$	$3d_{xz}$	$3d_{xy}$	$4d_{\bar{x}\bar{z}}$
C) one $3p_\pi$ basis function on each carbon atom	6	6.65	7.34	7.72	6.80	7.15	7.77

[a]Using the relation $E_I = IP-\epsilon_I$ with IP = 8.45 eV.

[b]In all cases the gaussian exponents used are: $\xi_{3s} = 0.023$, $\xi_{3p} = 0.021$.

TABLE VI: Transition Moments and Spacial Extension of the Rydberg Orbitals of Hexatriene

Orbital[a]	Transition Moments (a_u)		Second Moments[c]		
	$\langle\phi_{IVO}\|r^*\|\pi_3(2a_u)\rangle$[b]	Component	$\langle x \rangle$	$\langle y \rangle$	$\langle z^2 \rangle$
$\pi_1(1a_u)$			2.525	3.114	8.010
$\pi_2(1b_g)$			2.566	5.799	17.095
$\pi_3(2a_u)$			2.584	5.789	13.523
3s	0.05597	$\langle x \rangle$	15.924	27.918	23.738
$3p_{\bar{y}}$	0.06012	$\langle xy \rangle$	14.053	40.832	22.196
	0.01468	$\langle xz \rangle$			
$3p_{\bar{z}}$	0.70216	$\langle xy \rangle$	22.045	34.738	66.956
	1.40801	$\langle xz \rangle$			
$3p_x$	0.93646	$\langle yz \rangle$	39.436	16.233	17.812
$3d_{\bar{z}^2}$	0.10274	$\langle x \rangle$	14.998	26.998	82.143
$3d_{\bar{yz}}$	0.15104	$\langle x \rangle$	19.023	68.453	58.839
$3d_{\bar{x}^2-\bar{y}^2}$	0.07412	$\langle x \rangle$	18.707	36.386	28.052
$3d_{\bar{xz}}$	1.54968	$\langle y \rangle$	10.866	14.143	24.439
	1.76578	$\langle z \rangle$			
$3d_{xy}$	0.17917	$\langle y \rangle$	30.972	27.246	18.326
	0.22968	$\langle z \rangle$			
$4f_{\bar{xz}^2}$	2.72703	$\langle yz \rangle$	31.744	41.182	41.616
$4d_{\bar{xz}}$	0.78711	$\langle y \rangle$	31.764	18.300	39.048
	0.81046	$\langle z \rangle$			
$4f_{\bar{xy}^2}$	0.11374	$\langle yz \rangle$	37.315	13.624	59.284

[a]Orbitals π_1, π_2 and π_3 are from ground state wave-function. Rydberg orbitals are from IVO calculations.

[b]Transition moments using IVO orbitals.

[c]Second moments from IVO orbitals.

TABLE VII: Hartree-Fock Transition Energies for the Rydberg States of Trans-hexatriene

State	Transition Energy (eV)
$X\,^1A_g$ (-231.72322 hartrees)	
$1\,^1A_u$ (3s)	5.38
$1\,^1B_g$ ($3p_{\bar{y}}$)	5.29
^1B_u ($3d_{\overline{xz}}$)	5.78

TABLE VIII: CI Transition Energies for the Rydberg States of Trans-hexatriene

State	Transition Energy (eV)
$3s\,(1\,^1A_u)$	5.97
$3p_{\bar{y}}\,(1\,^1B_g)$	6.00
$3p_{\bar{z}}\,(2\,^1B_g)$	6.20
$3p_x\,(3\,^1A_g)$	6.26
$3d_{\overline{xz}}\,(^1B_u)$	6.27
$3d_{xy}\,(^1B_u)$	6.68
$3d_{\bar{z}^2}\,(2\,^1A_u)$	6.72
$3d_{\overline{yz}}\,(3\,^1A_u)$	6.80[a]
$4f_{\overline{xz}}{}^2\,(4\,^1A_g)$	7.19[a]
$4f_{\overline{xy}}{}^2\,(5\,^1A_g)$	7.81[a]

[a]Estimated transition energies. See text for discussion.

TABLE IX. Excited Electronic States of the Butadiene Molecule

State	Theoretical Results[a] (eV)	Experimental Results (eV) McDiarmid[b] uv Absorption	Flicker et al.[c] Electron-Impact	Others
$\tilde{a}\,1\,^3B_u$	3.35		3.22	3.22[d], 3.3[e]
$\tilde{b}\,1\,^3A_g$	5.08		4.91	4.9[f]
$\tilde{A}\,1\,^1B_u$	6.12		5.76, 5.92 (peak), 6.05	(5.75, 5.92, 6.09)[g], (5.71-0.29)[h]
$\tilde{B}\,1\,^1B_g$ (3s)	6.29	6.27		6.26[i]
$\tilde{C}$ ^1B_u ($3p_x$)	6.67	6.66	6.64	
$\tilde{D}\,2\,^1A_u$ ($3p_{\bar{z}}$)	6.78[j]	6.81	6.80	
$\tilde{F}\,2\,^1A_g$	7.06	7.07	7.08	
$\tilde{E}$ $2\,^1B_g$ ($3d_{\bar{z}^2}$)	7.29	7.27, 7.33	7.28	
$\tilde{E}$ $3\,^1B_g$ ($3d_{\bar{y}\bar{z}}$)	7.40[k]	7.47, 7.48	7.48	
$\tilde{E}$ $4\,^1B_g$ (4s)	7.65	7.63, 7.64	7.60	
$\tilde{E}$ $3\,^1A_g$ ($3d_{\bar{x}\bar{y}}$)	7.68			
$\tilde{E}$ ^1B_u ($4p_x$)	7.79	7.79	7.80	
$\tilde{E}$ $4\,^1A_u$ ($4p_{\bar{z}}$)	7.82	7.85		
$\tilde{G}$ ^1B_u ($4f_{x^3}$)	7.97	8.00	8.00	
$\tilde{H}$ ^1B_u ($5p_x$)	8.23	8.18	8.18	
^1A_u ($5p_{\bar{z}}$)	8.26	8.25		
^1B_u ($5f_{x^3}$)	8.33	8.36	8.39	
^1B_u ($6p_x$)	8.45	8.41		
^1A_u ($6p_{\bar{z}}$)	8.48	8.47		
^1B_u ($6f_{x^3}$)	8.52	8.50	8.54	
$7p_x$, $7p_{\bar{z}}$, $7f_{x^3}$	8.60, 8.63	8.65		
$8p_x$, $8p_{\bar{z}}$, $8f_{x^3}$	8.68, 8.70	8.67	8.69	
$9p_x$, $9p_{\bar{z}}$, $9f_{x^3}$	8.74, 8.75	8.77		
$10p_x$, $0p_{\bar{z}}$, $0f_{x^3}$	8.78	8.78		
$11p_x$, $11p_{\bar{z}}$, $11f_{x^3}$	8.80, 8.81	8.85		
$12p_x$, $12p_{\bar{z}}$, $12f_{x^3}$	8.82, 8.83	8.89	8.90	

[a] Results for the valence states from Part I.

[b] Ref. 3.

[c] Ref. 4.

[d] Ref. 35.

[e] H. H. Brongersma, J. A. van der Hart and L. J. Oosterhoff, in Fast Reactions and Primary Processes in Chemical Kinetics, edited by S. Claesson (Interscience, New York, 1967) p. 211.

[f] J. H. Moore, Jr., J. Phys. Chem., 76 (1972) 1130.

[g] Ref. 31.

[h] Ref. 32.

[i] Ref. 7.

[j] The $1\,^1A_u$ ($3p_{\bar{y}}$) state calculated at 6.61 eV is probably not observed (f = 0.0026). See text for discussion.

[k] Estimated from IVO calculations plus CI corrections. See text for discussion.

TABLE X: Rydberg Series for the Butadiene Molecule[a]

n	ns (^1B_g)	np_z (^1A_u)	np_x (^1B_u)	nd_{z^2} (^1A_g)	nf_{x^3} (^1B_u)
	$\delta = 0.76$	$\delta = 0.52$	$\delta = 0.58$	$\delta = 0.18$	$\delta = 0.36$
3	6.29[b]	6.78[b]	6.67[b]	7.29[b]	
4	7.65	7.82	7.79	8.02	7.97[b]
5	8.18	8.26	8.23	8.35	8.33
6	8.44	8.48	8.45	8.53	8.52
7	8.58	8.60	8.60	8.64	8.63
8	8.67	8.68	8.68	8.71	8.70
9	8.73	8.74	8.74	8.75	8.75
10	8.77	8.77	8.77	8.78	8.78
11	8.80	8.80	8.80	8.81	8.81
12	8.82	8.82	8.82	8.83	8.83
∞	8.95	8.95	8.95	8.95	8.95

[a]All energies in eV.

[b]First members of each series represents calculated values. Higher members are predicted values based on the quantum defects.

TABLE XI: Excited Electronic States of the All-trans Hexatriene Molecule

State[a]	Theoretical Results (eV)[b] (present work)	Experimental Results (eV) Gavin and Rice[c]	Flicker et al.[d]	Others
$1\,^3B_u$	2.71		2.61 (1.9-3.5)	2.58[e]
$1\,^3A_g$	4.32		4.11 (3.6-4.6)	4.2[f]
$1\,^1B_u(\pi-\pi^*)$		4.93	4.95, 5.13, 5.5, 5.7	(5.1-5.7)[f]
$2\,^1A_g(\pi-\pi^*)$	5.87			
$1\,^1A_u(3s)$	5.97	5.94 ($2\,^1A_g$, $2\,^1B_u$, $3\,^1A_g$)	6.06	
$1\,^1B_g(3p_{\bar{y}})$	6.0[g]			
$2\,^1B_g(3p_{\bar{z}})$	6.2[g]			
$3\,^1A_g(3p_x)$	6.26			6.23[h]
$^1B_u(3d_{\bar{xz}})$	6.27	6.28 ($2\,^1A_g$, $3\,^1A_g$, $2\,B_u$)	6.25	6.2[f]
$^1B_u(\pi-\pi^*)$ valence	6.56	6.53 ($2\,^1B_u$)	6.57	
$^1B_u(3d_{xy})$	6.68	6.68		
$2\,^1A_u(3d_{\bar{z}^2})$	6.72	6.73 ($2\,^1B_u$, S_2)	6.75	
$3\,^1A_u(3d_{\bar{yz}})$	6.80[i]	6.90 ($2\,^1B_u$, S_1)	6.93	6.9[f]
$4\,^1A_u(3d_{\bar{x}^2-\bar{y}^2})$	7.00[i]	7.06 ($2\,^1B_u$, $\nu_3+\nu_5$)	7.08	
$^1B_u(4d_{\bar{xz}})$	7.26	7.26 ($2\,^1B_u$, $\nu_1+\nu_2+\nu_3$)	7.25	
$^1B_u(4d_{xy})$	7.42	7.37		
$^1A_u(4d_{\bar{z}^2})$	7.44	7.46		
$^1B_u(5d_{\bar{xz}})$	7.68	7.68		
$^1A_u(5d_{\bar{z}^2})$	7.75	7.71 ($5p_x$)[j]	7.77	
$^1B_u(5d_{xy})$	7.76			
$^1B_u(6d_{\bar{xz}})$	7.90	7.88 ($6p_x$)	7.93	
$^1B_u(6d_{xy})$	7.93	7.98 ($7p_x$)		
$^1A_u(6d_{\bar{z}^2})$	7.94			
$^1B_u(7d_{\bar{xz}})$	8.01	8.05 ($8p_x$)	8.06	8.0[f]
$^1B_u(7d_{xy})$, $^1A_u(7d_{\bar{z}^2})$	8.04			
$^1B_u(8d_{\bar{xz}})$	8.09	8.10 ($9p_x$)		
$^1B_u(8d_{xy})$, $^1A_u(8d_{\bar{z}^2})$	8.11			
9d	8.18	8.13 ($10p_x$)		
10d	8.21	8.15 ($11p_x$)		
11d	8.23	8.17 ($12p_x$)		
∞d	8.33	8.27 (∞p_x)		
$^1B_g(\sigma-\pi^*)$	9.18		9.1	9.2[f]
			9.7	9.6[f]
			10.5	10.7[f]
$^1A_u(\sigma-\pi^*)$	11.51			

[a] State assignments based on present calculations, except for the $1\,^1B_u(\pi-\pi^*)$ transition.

[b] Valence states are from part I.

[c] Ref. 2. Assignments in this column from Refs. 2 and 27.

[d] Ref. 5.

[e] Ref. 35.

[f] F. W. E. Knoop and L. J. Oosterhoff, Chem. Phys. Lett., 22 (1973) 247.

[g] These transitions are probably not observed. See text for discussion.

[h] Ref. 8.

[i] These are estimated values from IVO calculations plus CI corrections. See text for discussion.

[j] All members of this series computed using Rydberg formula in Ref. 2.

TABLE XII: Rydberg Series for the Hexatriene Molecule[a]

n	ns (^1A_u), $\delta = 0.6$	nd_{z^2} (^1A_u), $\delta = 0.09$	nd_{xz} (^1B_u), $\delta = 0.43$	nd_{xy} (^1B_u), $\delta = 0.13$
3	5.97[b]	6.72[b]	6.27[b]	6.68[b]
4	7.15	7.44	7.26	7.42
5	7.63	7.76	7.68	7.75
6	7.86	7.94	7.90	7.93
7	7.99	8.04	8.01	8.04
8	8.08	8.11	8.09	8.11
9	8.13	8.16	8.14	8.16
10	8.17	8.19	8.18	8.19
11	8.20	8.21	8.21	8.21
12	8.22	8.23	8.23	8.23
∞	8.33	8.33	8.33	8.33

[a]All energies in eV.

[b]First members of the series are calculated values. Higher members are predicted values based on the quantum defect.

References

(1) B. Honig and T. Ebrey, Annu. Rev. Biophys. Bioeng.,3, 151 (1974); R. A. Morton and G. A. Pitt, Adv. Enzymol. Related Subj. Biochem.,32, 97 (1969); E. W. Abrahamson and S. E. Ostroy, Progr. Biophys. Mol. Biol., 17, 179 (1967).

(2) R. M. Gavin, Jr., and S. A. Rice, J. Chem. Phys., 60, 3231 (1974); R. M. Gavin, Jr., S. Risemberg, and S. A. Rice, ibid., 58, 3160 (1973).

(3) R. McDiarmid, J. Chem. Phys., 64, 514 (1976); K. K. Innes and R. McDiarmid, ibid., 68, 2007 (1978).

(4) O. A. Mosher, W. M. Flicker, and A. Kuppermann, J. Chem. Phys., 59, 6502 (1973); W. M. Flicker, O. A. Mosher, and A. Kuppermann, Chem. Phys., in press.

(5) W. M. Flicker, O. A. Mosher, and A. Kuppermann, Chem. Phys. Lett., 45, 492 (1977).

(6) D. E. Post, Jr., W. M. Hetherington III, and B. Hudson, Chem. Phys. Lett., 35, 259 (1975).

(7) P. J. Johnson, J. Chem. Phys., 64, 4638 (1976).

(8) D. H. Parker, S. J. Sheng, and M. A. El-Sayed, J. Chem. Phys., 65, 5534 (1976).

(9) R. H. Pottier, G. P. Semeluck, and R. D. S. Stevens, Spectrosc. Lett., 2, 369 (1969).

(10) C. Sandorfy, J. Mol. Struct., 19, 183 (1973).

(11) M. B. Robin, "Higher Excited States of Polyatomic Molecules," Vols. I and II, Academic Press, New York, 1975.

(12) K. B. Wiberg, K. S. Peters, G. B. Ellison, and J. L. Dehmer,

J. Chem. Phys., 66, 2224 (1977).

(13) W. M. Hetherington III, B. Hudson, and J. Diamond, Paper MG6, 32nd Symposium on Molecular Spectroscopy, Columbus, Ohio, 1977.

(14) H. Fang and G. E. Leroi, Paper MG9, 32nd Symposium on Molecular Spectroscopy, Columbus, Ohio 1977.

(15) G. B. Ellison, Ph.D. Thesis, Yale University, 1974.

(16) B. S. Hudson and B. E. Kohler, Chem. Phys. Lett., 14, 299 (1972).

(17) M. A. C. Nascimento and W. A. Goddard III, manuscript in preparation.

(18) M. Traetteberg, Acta Chem. Scand., 22, 628 (1968); W. Haugen and M. Traetteberg in "Selected Topics in Structure Chemistry," P. Andresen, O. Bastiansen, and S. Furberg, Eds., Universitetsforlaget, Oslo, Norway, 1967, p. 113.

(19) T. H. Dunning, Jr., J. Chem. Phys., 53, 2823 (1970).

(20) S. Huzinaga, J. Chem. Phys., 42, 1293 (1965).

(21) W. J. Hunt and W. A. Goddard III, Chem. Phys. Lett., 3, 414 (1969).

(22) The GVB calculations were carried out with the Bobrowicz-Wadt-Goddard GVBTWO program. See F. W. Bobrowicz, Ph.D. Thesis, California Institute of Technology, 1974.

(23) The CI calculations were carried out with the Caltech spin-eigenfunction CI program. See ref 22.

(24) M. A. C. Nascimento, Master's Thesis, California Institute of Technology, 1976.

(25) S. Shih, R. J. Buenker, and S. D. Peyerimhoff, Chem. Phys. Lett., 16, 244 (1972).

(26) O. A. Mosher, Ph.D. Thesis, California Institute of Technology, 1975.

(27) M. Karplus, R. M. Gavin, Jr., and S. A. Rice, J. Chem. Phys., 63, 5507 (1975).

(28) M. A. El-Sayed, private communication.

(29) M. A. C. Nascimento, Ph.D. Thesis, California Institute of Technology, 1978.

(30) R. J. Buenker, S. Shih, and S. D. Peyerimhoff, Chem. Phys. Lett., 44, 385 (1976).

(31) L. C. Jones and L. W. Taylor, Anal. Chem., 27, 228 (1955).

(32) This state designation is used by G. Herzberg. See G. Herzberg, "Electronic Spectra and Electronic Structure in Polyatomic Molecules," Van Nostrand-Reinhold Co., New York, 1966, p 656.

(33) A. D. Walsh, J. Phys. Radium, 15, 501 (1954).

(34) F. W. E. Knoop and L. J. Oosterhoff, Chem. Phys. Lett., 22, 247 (1973).

(35) D. F. Evans, J. Chem. Soc. London, 1735 (1960).

(36) K. Shulten and M. Karplus, Chem. Phys. Lett., 14, 305 (1972).

FIGURE CAPTIONS

FIG. 1. 3s and $3p_\sigma$ Rydberg orbitals of butadiene. Orbitals a, c, e using basis set A (Table I). Orbitals b, d, f using basis set C (Table I). Long dashes indicate zero amplitude, solid lines and short dashes indicate positive and negative amplitudes, with a spacing of 0.005 atomic units between the contours.

FIG. 2. $3d_\sigma$ Rydberg orbitals of butadiene using basis set A (Table I). Orbitals a, c, e in the molecular coordinate system. Orbitals b, d, f in the $(\bar{x}, \bar{y}, \bar{z})$ coordinate system indicated in Fig. 1. Same convention as in Fig. 1 is used for the amplitudes.

FIG. 3. $3p_\pi$ and $3d_\pi$ Rydberg orbitals of butadiene using basis set E (Table I). Same convention as in Fig. 1 is used for the amplitudes.

FIG. 4. $4f_\pi$ Rydberg orbitals of butadiene using basis set E (Table I). Same convention as in Fig. 1 is used for the amplitudes.

FIG. 5. Energy of the GVB(1/PP) wavefunction for symmetrically stretched structures. Terminal C-C bonds are stretched but middle C-C bond is kept fixed at (A) 1.34 Å and (B) 1.38 Å.

FIG. 6. Energy of the GVB(1/PP) wavefunction for structures with all C-C bonds equal.

FIG. 7. Energy of the GVB(1/PP) wavefunction for symmetric bent structures. All C-C bonds equal 1.40 Å. (A) Symmetric C_1-C_2 and C_3-C_4 bendings. (B) Terminal $-CH_2$ rockings.

FIG. 8. 3s and $3p_\sigma$ Rydberg orbitals for hexatriene. Orbitals a, c, e using basis set A (Table V). Orbitals b, d, f using basis set B (Table V).

Same convention as in Fig. 1 is used for the amplitudes.

FIG. 9. $3d_{\sigma}$ Rydberg orbitals for hexatriene. Orbitals a, c, e in the molecular coordinate system. Orbitals b, d, f in the $(\bar{x}, \bar{y}, \bar{z})$ coordinate system indicated in Fig. 8. Same convention as in Fig. 1 is used for the amplitudes.

FIG. 10. $3p_{\pi}$ and $3d_{\pi}$ Rydberg orbitals for hexatriene. Orbitals a, c, e in the molecular coordinate system. Orbitals b, d, f in the $(\bar{x}, \bar{y}, \bar{z})$ coordinate system shown in Fig. 8. Same convention as in Fig. 1 is used for the amplitudes.

FIG. 11. $4f_{\pi}$ Rydberg orbitals for hexatriene in the molecular coordinate system (a, c) and in the $(\bar{x}, \bar{y}, \bar{z})$ coordinate system of Fig. 8 (b, d). Same convention as in Fig. 1 is used for the amplitudes.

SIGMA RYDBERG ORBITALS BUTADIENE

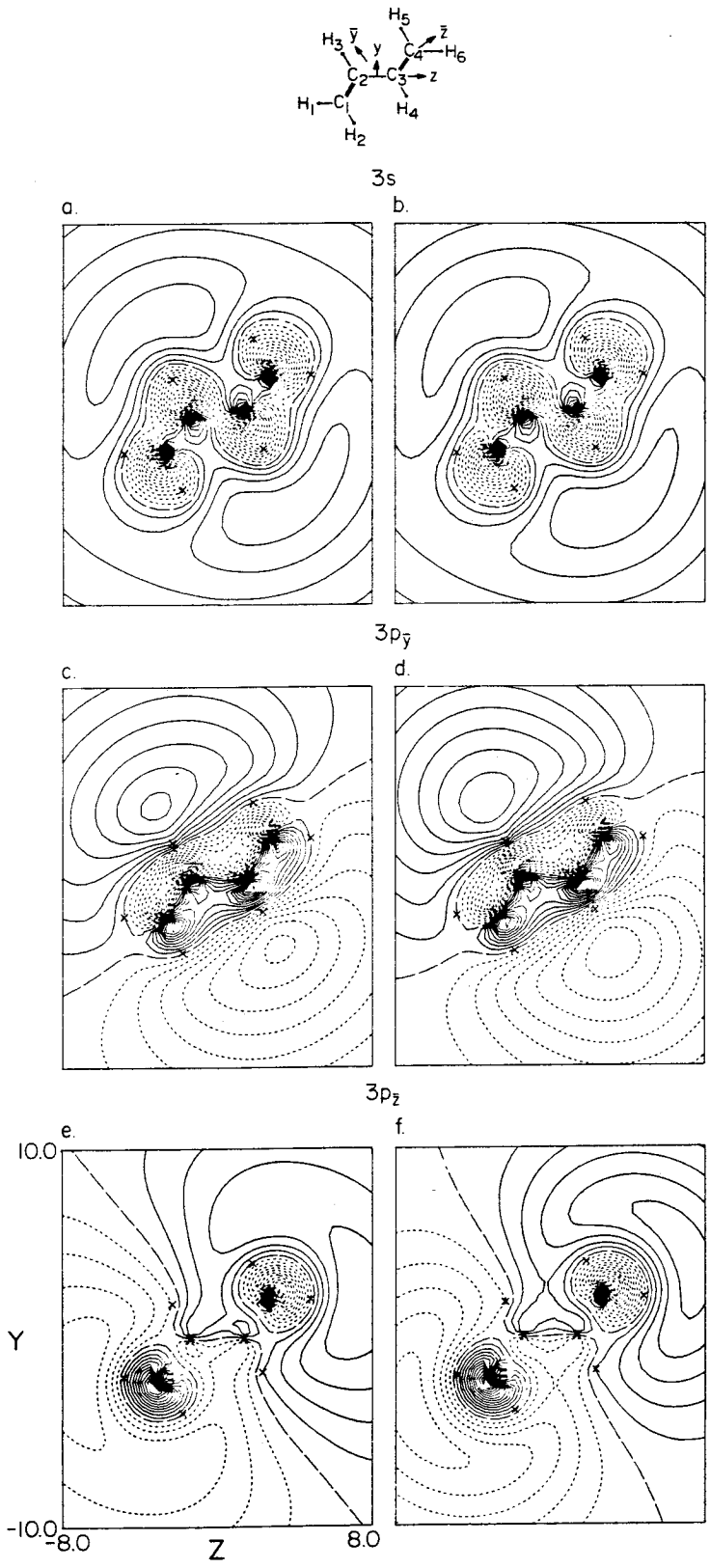

Figure I

SIGMA RYDBERG ORBITALS BUTADIENE

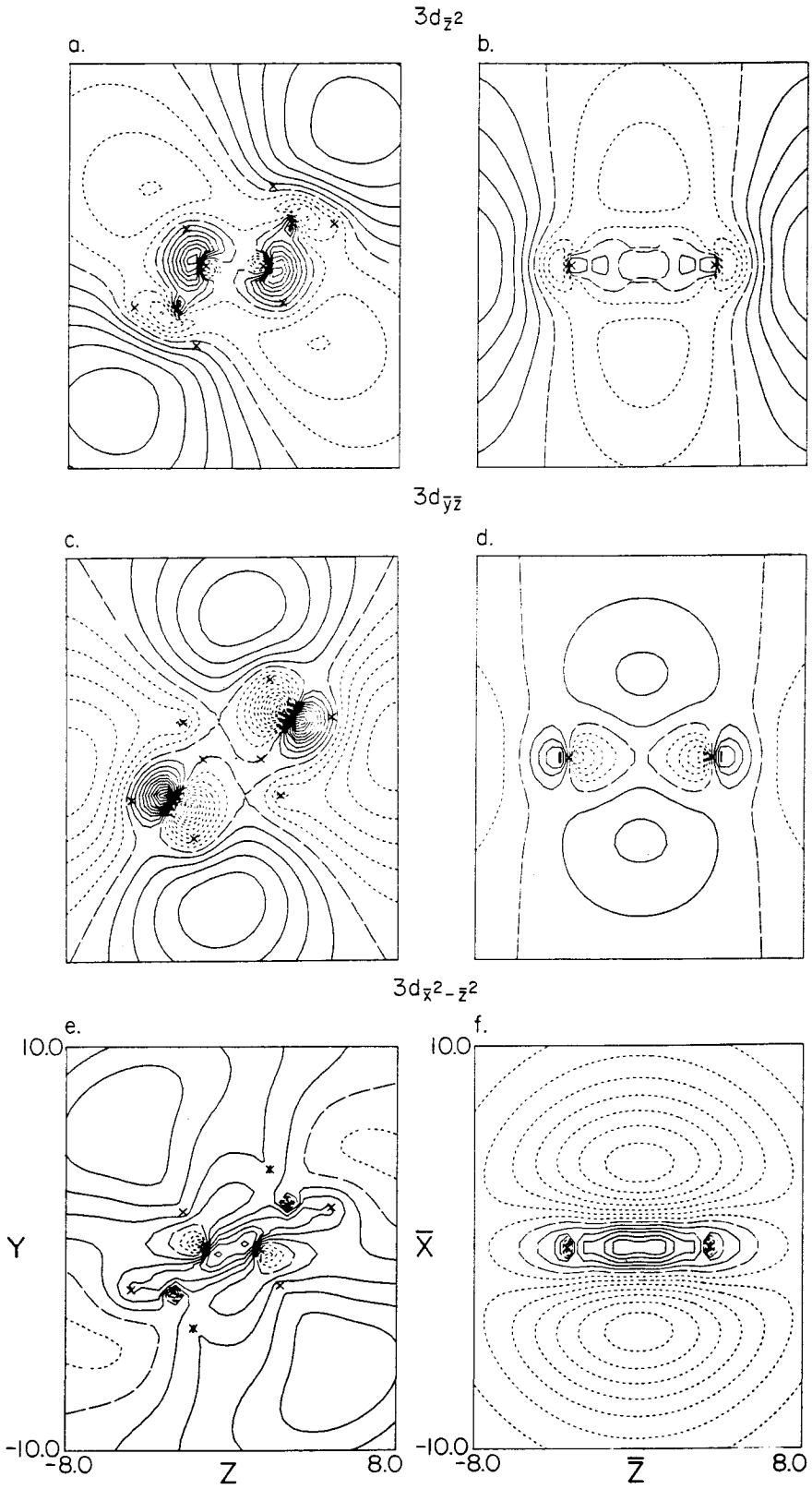

Figure II

PI RYDBERG ORBITALS BUTADIENE

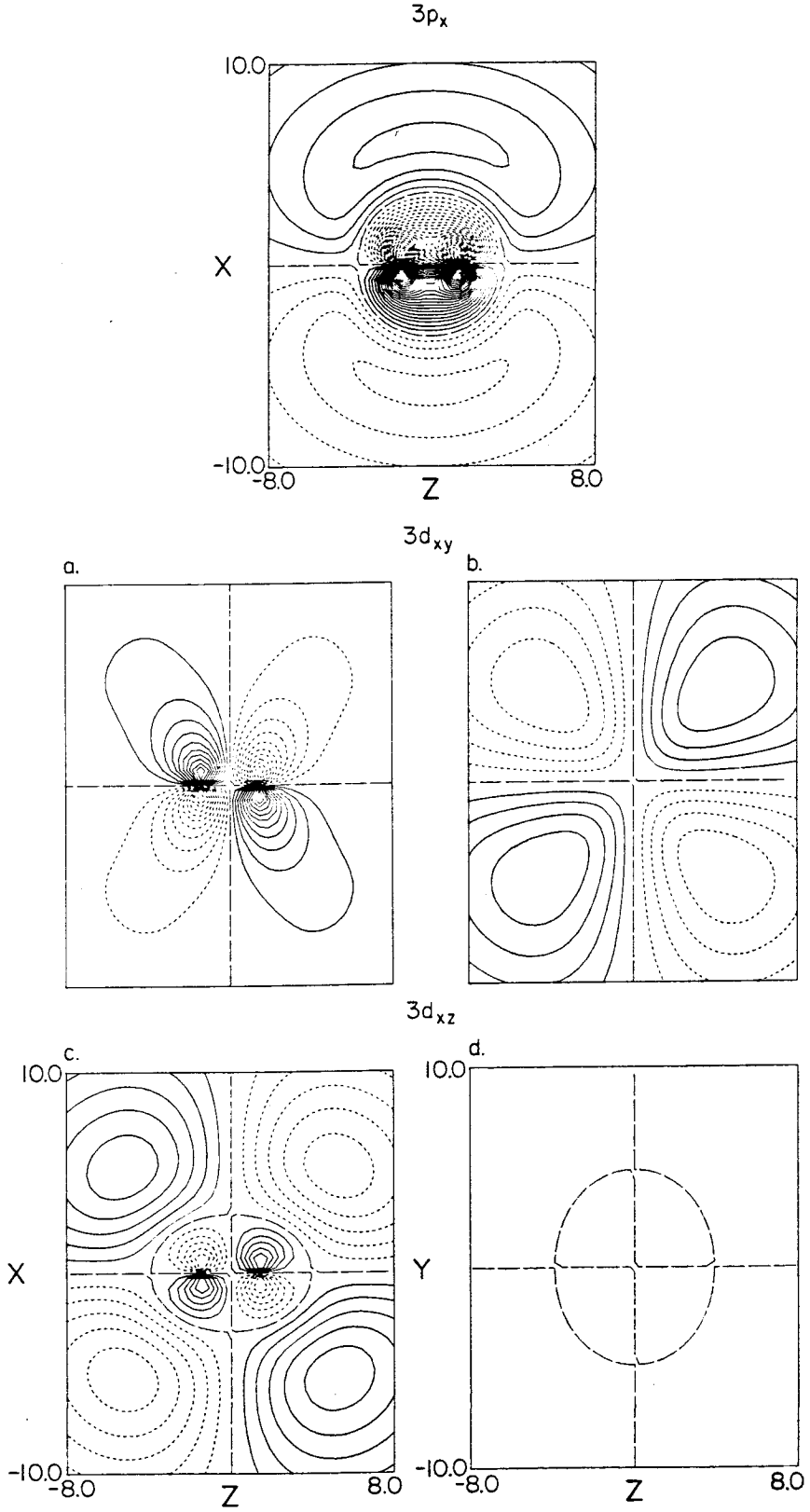

Figure III

PI RYDBERG ORBITALS BUTADIENE

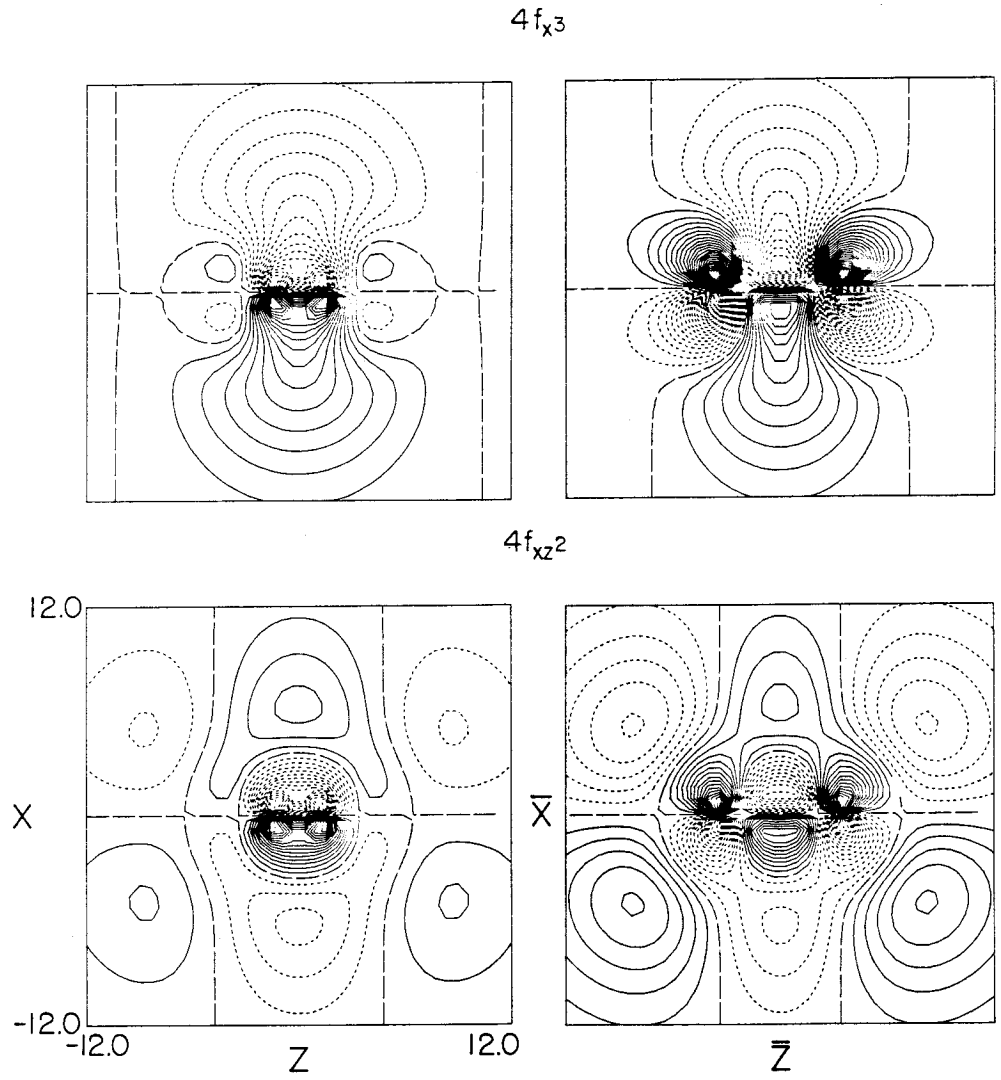

Figure IV

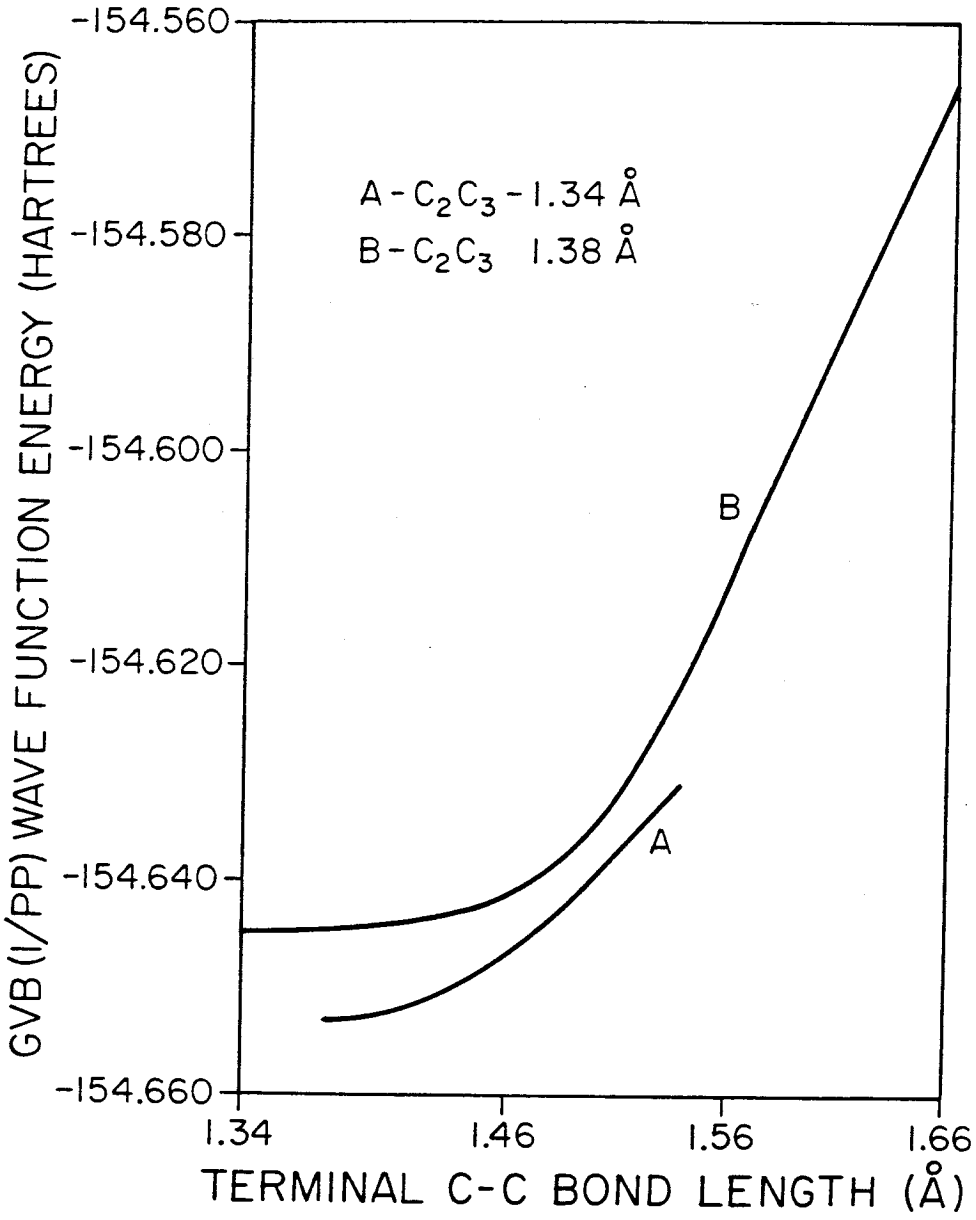
-154.560
-154.580
-154.600
-154.620
-154.640
-154.660
GVB (I/PP) WAVE FUNCTION ENERGY (HARTREES)
A - C_2C_3 - 1.34 Å
B - C_2C_3 1.38 Å
B
A
1.34
1.46
1.56
1.66
TERMINAL C-C BOND LENGTH (Å)

Figure V

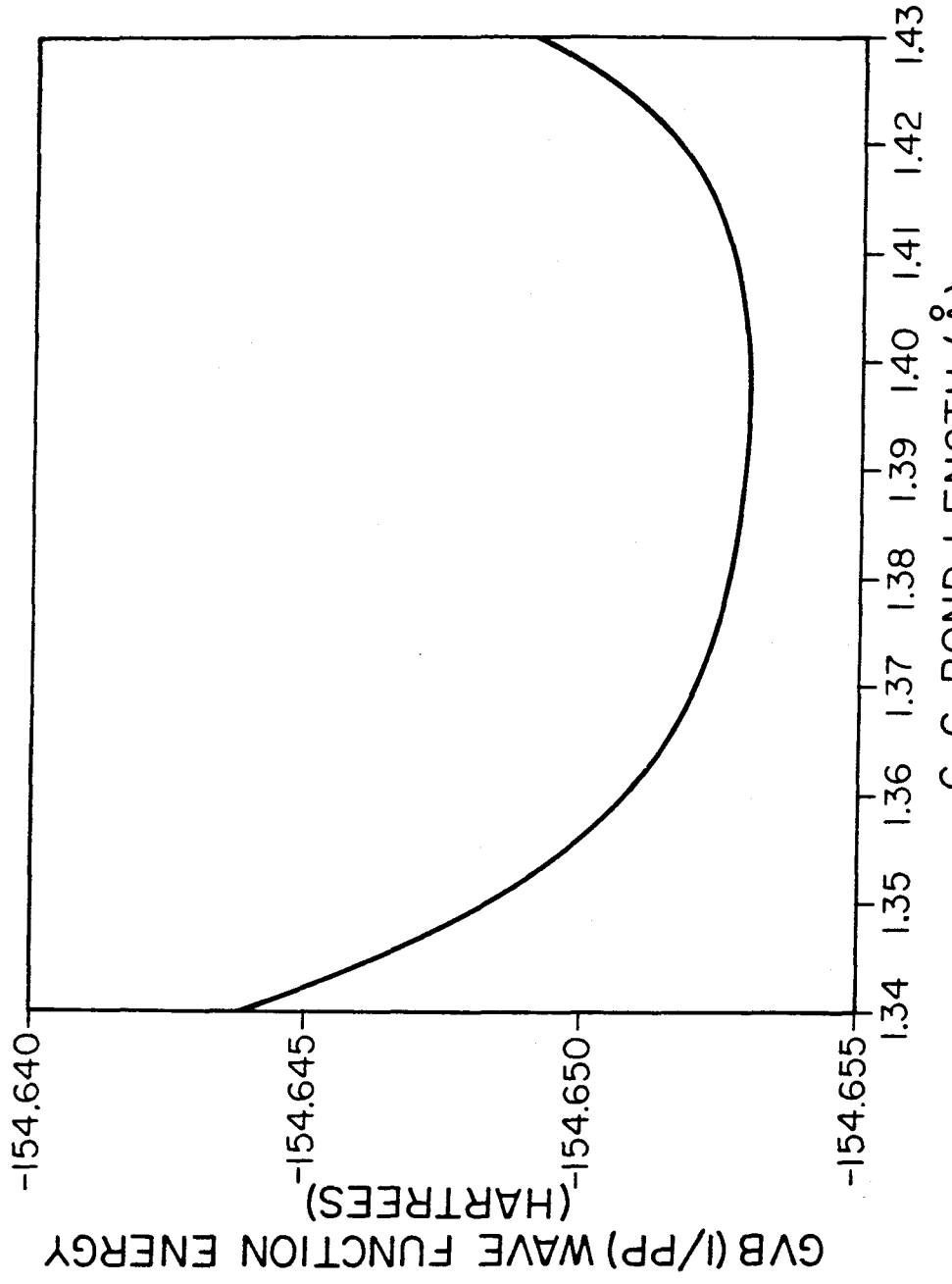
GVB (1/PP) WAVE FUNCTION ENERGY (HARTREES)
-154.640
-154.645
-154.650
-154.655
1.34
1.35
1.36
1.37
1.38
1.39
1.40
1.41
1.42
1.43
C-C BOND LENGTH (Å)

Figure VI

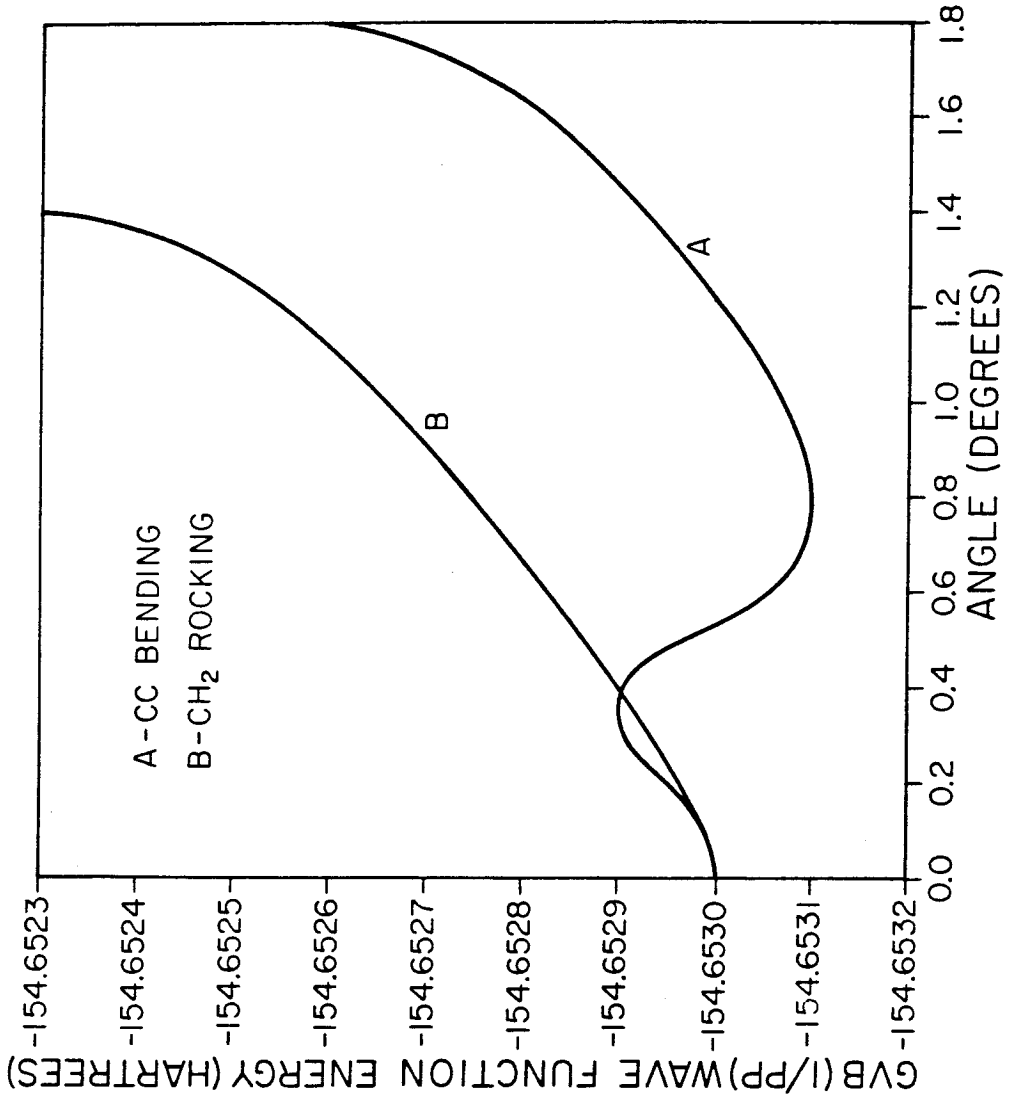
GVB (1/PP) WAVE FUNCTION ENERGY (HARTREES)
-154.6523
-154.6524
-154.6525
-154.6526
-154.6527
-154.6528
-154.6529
-154.6530
-154.6531
-154.6532
0.0
0.2
0.4
0.6
0.8
1.0
1.2
1.4
1.6
1.8
ANGLE (DEGREES)
A - CC BENDING
B - CH2 ROCKING
A
B

Figure VII

SIGMA RYDBERG ORBITALS HEXATRIENE

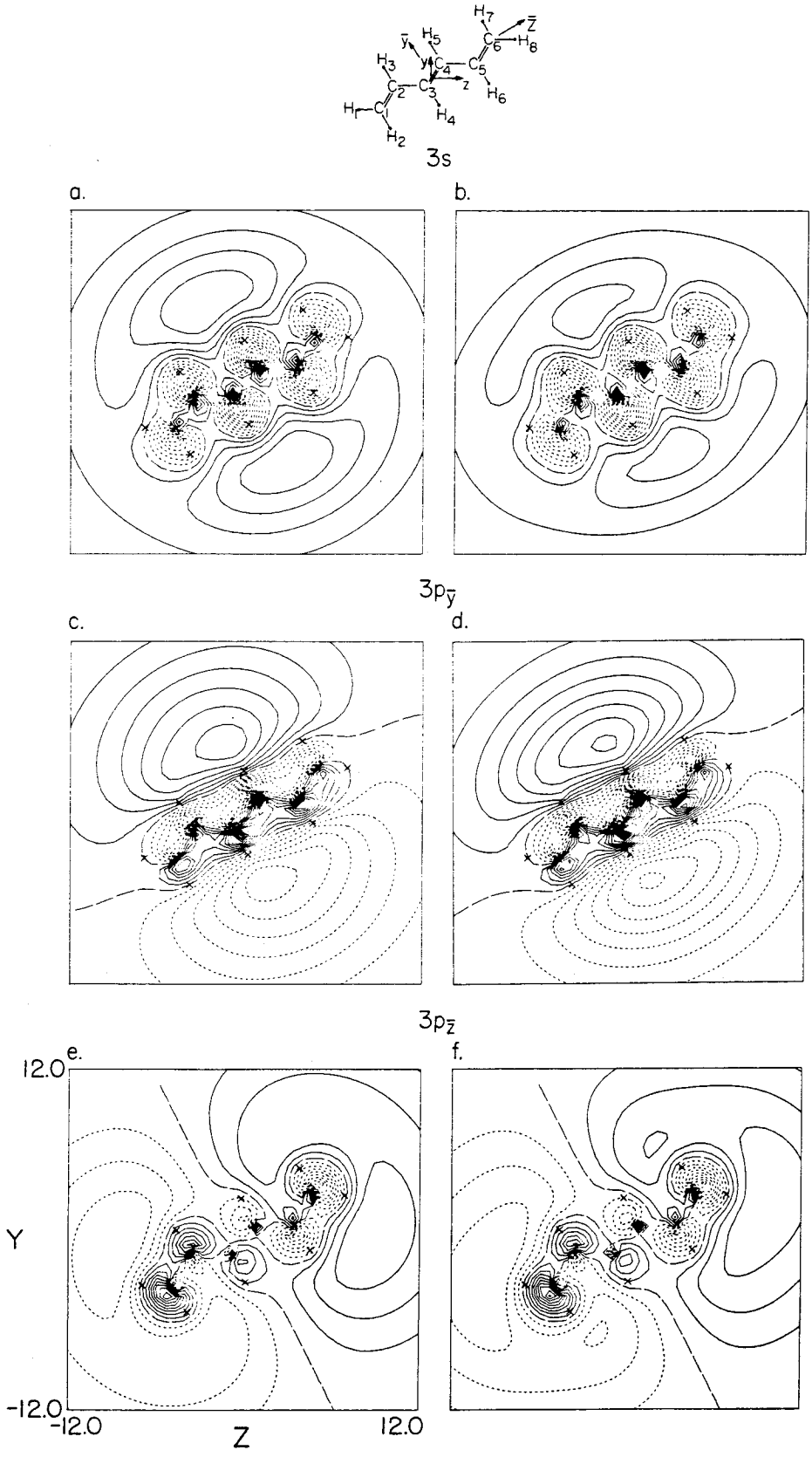

Figure VIII

SIGMA RYDBERG ORBITALS HEXATRIENE

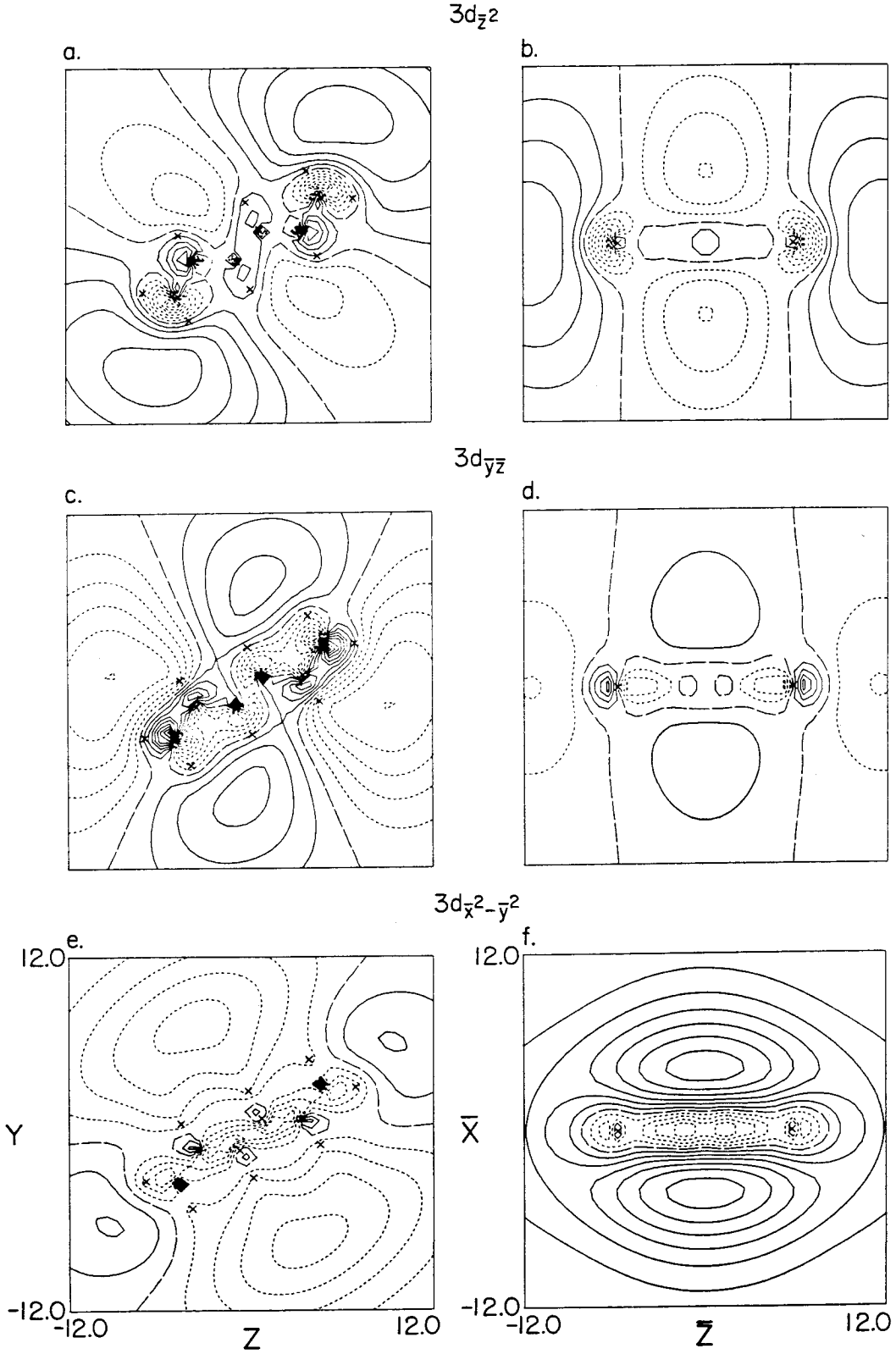

Figure IX

PI RYDBERG ORBITALS HEXATRIENE

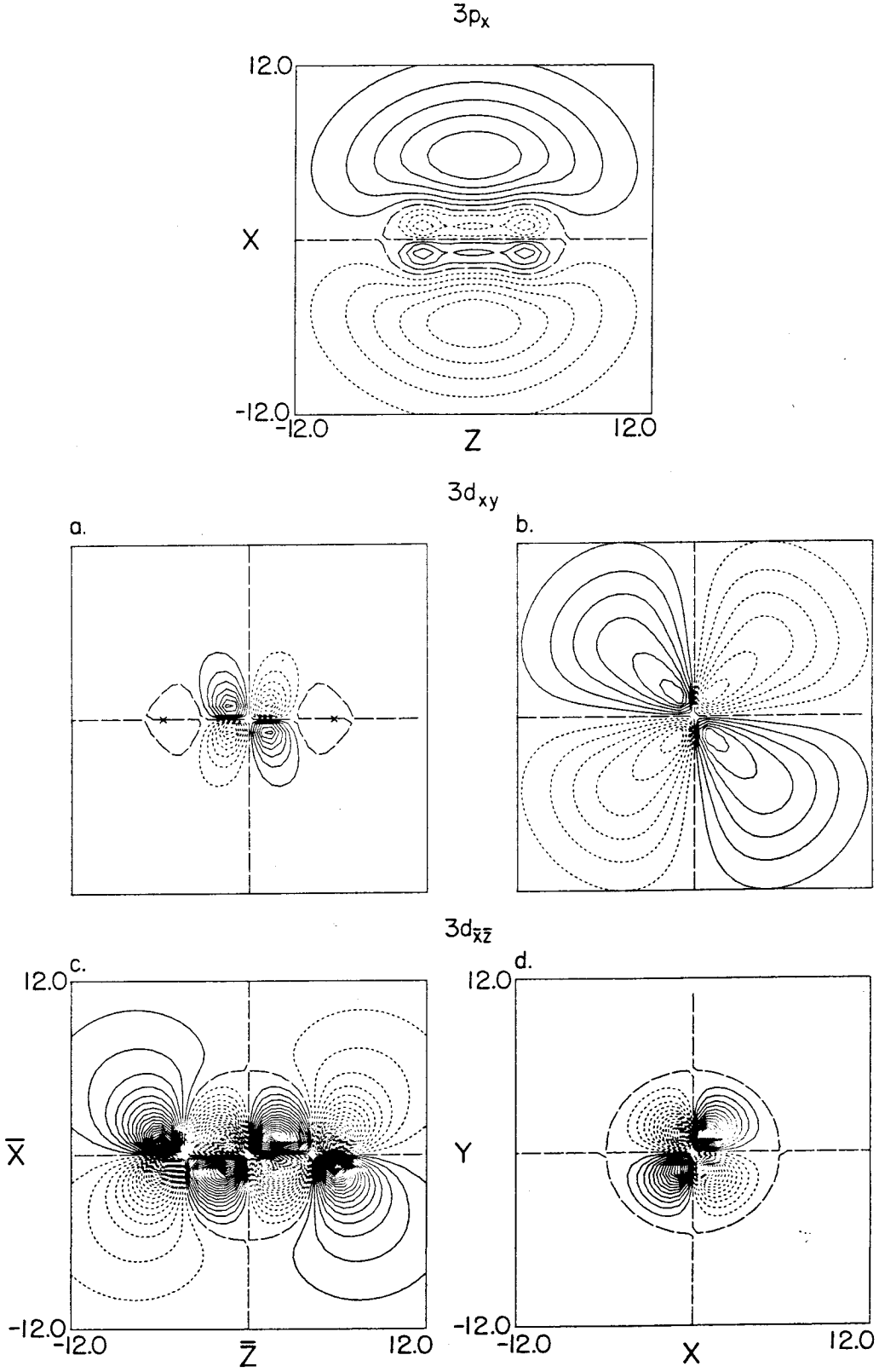

Figure X

PI RYDBERG ORBITALS HEXATRIENE

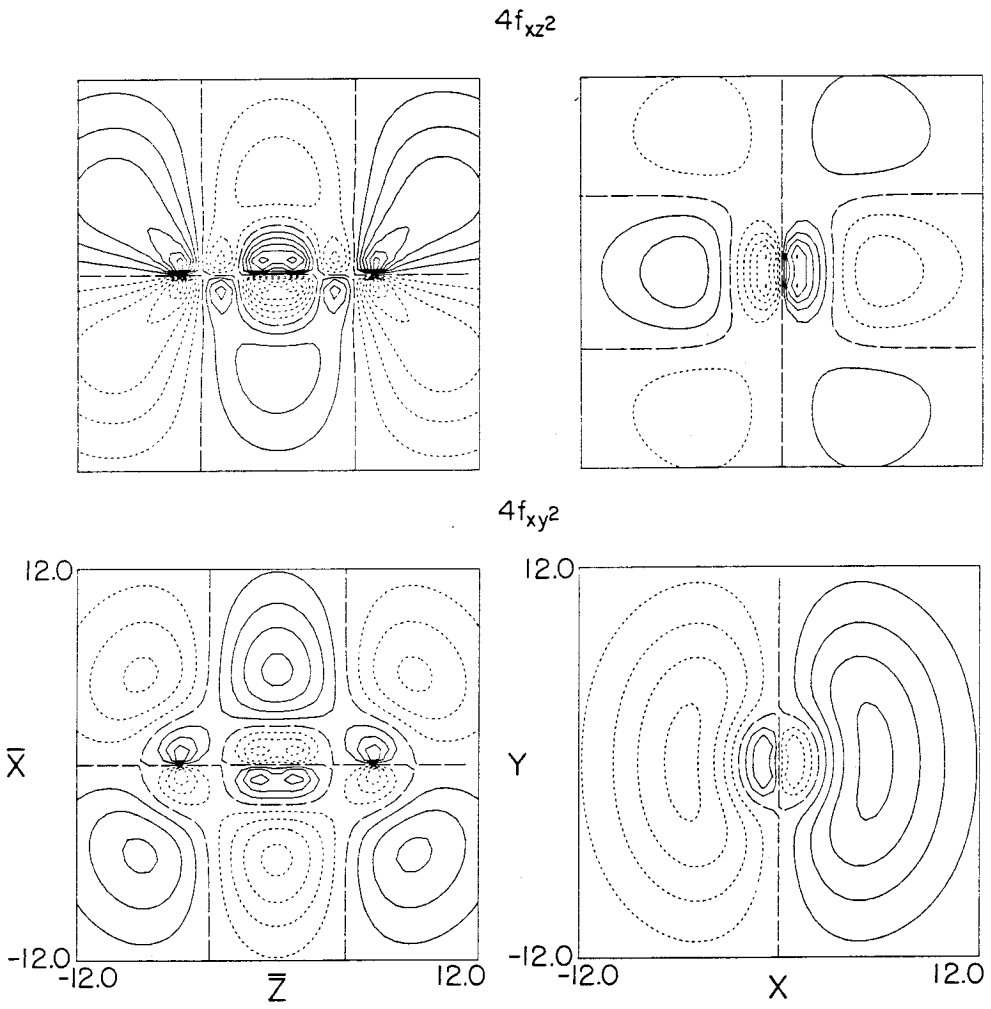

Figure XI